

WSES-FSAR-UNIT-3

4.2 FUEL SYSTEM DESIGN

4.2.1 DESIGN BASES

The bases for fuel system design are discussed in the following subsections. Additional information for the current fuel cycle is discussed in Appendix 4.3A.

4.2.1.1 Fuel Assembly

The fuel assemblies are required to meet design criteria for each design condition listed below to assure that the functional requirements are met. Except where specifically noted, the design bases presented in this section are consistent with those used for previous designs.

a) Condition I: Non-operation and Normal Operation

Condition I situations are those which are planned or expected to occur in the course of handling, initial shipping, storage, reactor servicing and power operation (including maneuvering of the plant). Condition I situations must be accommodated without fuel assembly failure and without any effect which would lead to a restriction on subsequent operation of the fuel assembly. The guidelines stated below are used to determine loads during Condition I situations:

1) Handling and Fresh Fuel Shipping

Loads correspond to the maximum possible axial and lateral loads and accelerations imposed on the fuel assembly by shipping and handling equipment during these periods, assuming that there are no abnormal contact between the fuel assembly and any surface, nor any equipment malfunction. Irradiation effects on material properties are considered when analyzing the effects of handling loads which occur during refueling. Additional information regarding shipping and handling loads is contained in Subsection 4.2.3.1.5.

2) Storage

Loads on both new and irradiated fuel assemblies reflect storage conditions of temperature, chemistry, means of support, and duration of storage.

3) Reactor Servicing

Loads on the fuel assembly reflect those encountered during refueling and reconstitution.

4) Power Operation

Loads are derived from conditions encountered during transient and steady-state operation in the design power range. (Hot operational testing, system startup, hot standby, operator controlled transients within specified rate limits and system shutdown are included in this category.)

WSES-FSAR-UNIT-3

5) Reactor Trip

Loads correspond to those produced in the fuel assembly by control element assembly (CEA) motion and deceleration.

b) Condition II: Upset Condition

Condition II situations are unplanned events which may occur with moderate frequency during the life of the plant. The fuel assembly design should have the capability to withstand any upset condition with margin to mechanical failure and with no permanent effects which would prevent continued normal operation. Incidents classified as upset conditions are listed below:

- 1) Operating basis earthquake (OBE)
- 2) Uncontrolled CEA withdrawal
- 3) Uncontrolled boron dilution
- 4) Partial loss-of-coolant flow
- 5) Idle loop startup (in violation of established operating procedures)
- 6) Loss of load (reactor-turbine load mismatch)
- 7) Loss of normal feedwater
- 8) Loss of offsite power
- 9) Excessive heat removal (feedwater system malfunction)
- 10) CEA drop
- 11) Accidental depressurization of the Reactor Coolant System (RCS)

c) Condition III: Emergency Conditions

Condition III events are unplanned incidents which might occur very infrequently during plant life. Fuel rod mechanical failure must be prevented for any Condition III event in any area not subject to extreme local conditions (e.g., in any fuel rod not immediately adjacent to the impact surface during fuel handling accident).

The Condition III incidents listed below are included as a category to provide assurance that under the occurrence of a Condition III event, rod damage is minimal.

- 1) Complete loss or interruption of primary coolant flow at 100% power, excluding reactor coolant pump locked rotor
- 2) Steam bypass malfunction

WSES-FSAR-UNIT-3

- 3) Minor fuel handling accident (fuel assembly and grapple remain connected)
- 4) Inadvertent loading of fuel assembly into improper position

d) Condition IV: Faulted Conditions

Condition IV incidents are postulated events whose consequences are such that the integrity and operability of the nuclear energy system may be impaired. Mechanical fuel failures are permitted, but they must not impair the operation of the Engineered Safety Features (ESF) systems to mitigate the consequences of the postulated event. Condition IV incidents are listed below:

- 1) Safe shutdown earthquake (SSE)
- 2) Loss-of-coolant accident (LOCA)
- 3) Locked coolant pump rotor
- 4) Major secondary system pipe rupture
- 5) CEA ejection
- 6) Major fuel handling accident (fuel assembly and grapple are disengaged)

→(DRN 03-2058, R14)

See Sections 3.6.2.1.1(d) and 3.6.3 for discussions on pipe break criteria and leak-before-break.

←(DRN 03-2058, R14)

4.2.1.1.1 Fuel Assembly Structural Integrity Criteria

For each of the design conditions, there are criteria which apply to the fuel assembly and components with the exception of fuel rods. These criteria are listed below and give the allowable stresses and functional requirements for each design condition.

a) Design Conditions I and II

$$P_m \leq S_m$$

$$P_m + P_b \leq F_s S_m$$

Under cyclic loading conditions, stresses must be such that the cumulative fatigue damage factor does not exceed 0.8. Cumulative damage factor is defined as the sum of the ratios of the number of cycles at a given cyclic stress (or strain) condition to the maximum number permitted for that condition. The selected limit of 0.8 is used in place of 1.0 (which would correspond to the absolute maximum damage factor permitted) to provide additional margin in the design.

Deflections must be such that the allowable trip time of the control element assemblies is not exceeded.

WSES-FSAR-UNIT-3

b) Design Condition III

$$P_m \leq 1.5 S_m$$

$$P_m + P_b \leq 1.5 F_S S_m$$

Deflections are limited to a value allowing the CEAS to trip, but not necessarily within the prescribed time.

c) Design Condition IV

$$P_m \leq S'_m$$

$$P_m + P_b \leq F_S S'_m$$

where $S'_m =$ smaller value of $2.4 S_m$ or $0.7 S_U$.

- 1) If the equivalent diameter pipe break in the LOCA does not exceed the largest line connected to the main reactor coolant lines, the fuel assembly deformation shall be limited to a value not exceeding the deformation which would preclude satisfactory insertion of the CEAS.
- 2) For pipe breaks larger in equivalent diameter than the largest lines connected to the main reactor coolant lines, deformation of structural components is limited to maintain the fuel in a coolable array. CEA insertion is not required for these events as the appropriate safety analyses do not take credit for CEA insertion.

d) Nomenclature

The symbols used in defining the allowable stress levels are as follows:

$P_m =$ Calculated general primary membrane stress (a)

$P_b =$ Calculated primary bending stress

$S_m =$ Design stress intensity value as defined by Section III, ASME Boiler and Pressure Vessel Code (b)

$S_U =$ Minimum unirradiated ultimate tensile strength

→ (DRN 00-644)

$F_S =$ Shape factor corresponding to the particular cross section being analyzed (c)

← (DRN 00-644)

$S'_m =$ Design stress intensity value for faulted conditions

WSES-FSAR-UNIT-3

The definitions of S' as the lesser value of $2.4 S_m$ and $0.7 S_u$ is contained in the ASME Boiler and Pressure Vessel Code (19/4) Section III, Appendix F-1323.1.

(a) P_m and P_b are defined by Article NB-3000, Section III, ASME Boiler and Pressure Vessel Code, 1971.

(b) With the exception of zirconium base alloys, the design stress intensity values, S_m , of materials not tabulated by the Code are determined in the same manner as the Code. The design stress intensity of zirconium base alloys shall not exceed two-thirds of the unirradiated minimum yield strength at temperature. Basing the design stress intensity on the unirradiated yield strength is conservative because the yield strength of zircaloy increases with irradiation. The use of the two-thirds factor ensures 50% to component yielding in response to primary stresses. This 50% margin together with its application to the minimum unirradiated properties and the general conservatism applied in the establishment of design conditions is sufficient to ensure an adequate design.

(c) The shape factor, F_s , is defined as the ratio of the "plastic" moment (all fibers just at the yield stress) to the initial yield amount (extreme fiber at the yield stress and all other fibers stressed in proportion to their distance from the neutral axis). The capability of cross sections loaded in bending to sustain moments considerably in excess of that required to yield the outermost fibers is discussed in Timoshenko.⁽¹⁾

4.2.1.1.2 Material Selection

→(DRN 02-1538, R12)

The fuel assembly grid cage structure consists of 10 Zircaloy-4 spacer grids, 1 Inconel 625 spacer grid (at the lower end), 5 Zircaloy-4 CEA guide tubes, 2 stainless steel end fittings, and 5 Inconel X-750 coil springs. Beginning with Batch U, some grid cages will have 9 Zircaloy-4 grids and 2 Inconel 625 grids (at the upper and lower ends) Zircaloy-4, selected for fuel rod cladding, guide tubes and spacer grids, has a low neutron absorption cross section, high corrosion resistance to reactor water environment and there is little reaction between the cladding and fuel or fission products. As described in Subsection 4.2.3, Zircaloy-4 has demonstrated its ability as a cladding, CEA guide tube, and spacer grid material.

→(DRN 06-1059, R15)

Beginning with the Region Y fuel assemblies in Cycle 15, ZIRLO™ is introduced as a fuel rod cladding material to provide added corrosion resistance and fuel reliability. ZIRLO™ is a zirconium-based alloy that improves fuel assembly corrosion resistance and dimensional stability under irradiation.

←(DRN 06-1059, R15)

The bottom spacer grid is of Inconel 625 and is welded to the lower end fitting. For the assembly designs with the Inconel 625 top grids, the grid is retained by 10 Zircaloy-4 sleeves that are welded to the Zircaloy-4 guide tubes. In these regions of higher turbulence, Inconel 625 was selected rather than Zircaloy-4 to provide additional strength and relaxation resistance. Inconel 625 is a very strong material with good ductility, corrosion resistance and stability under irradiation at temperatures below 1000°F.

←(DRN 02-1538, R12)

WSES-FSAR-UNIT-3

→(DRN 02-1538, R12, LBDCR 15-025, R309)

The fuel assembly lower end fitting is of cast stainless steel (Grade CF-3) and the upper end fitting assembly consists of two cast stainless steel plates and five Type 304 stainless steel machined alignment posts. This material was selected based on considerations of adequate strength and high-corrosion resistance. Also, Type 304 stainless steel has been used successfully in almost all pressurized water reactor environments, including all currently operating C-E reactors.

←(DRN 02-1538, R12, LBDCR 15-025, R309)

→(EC-9533, R302; LBDCR 13-014, R309)

With the introduction of the Next Generation Fuel (NGF) design in Region Z (Cycle 16), the fuel assembly grid cage structure consists of 13 spacer grids (an Inconel-718 top grid, six vaned Optimized ZIRLO™ mid grids, three unvaned Optimized ZIRLO™ mid grids, two vaned Optimized ZIRLO™ Intermediate Flow Mixing grids (IFMs), and one Inconel-625 bottom grid), five Stress-Relief Annealed (SRA) ZIRLO™ CEA guide tubes, two stainless steel end fittings, and five Inconel X-750 coil springs. Instead of welds, the NGF grid cage structure utilizes bulges to secure the spacer grids to the CEA guide tubes. Similarly, the CEA guide tube flange-to-tube connection is bulged for NGF instead of welded.

←(LBDCR 13-014, R309)

The use of Optimized ZIRLO for the mid grid and IFMs improves the corrosion resistance dimensional stability of the grids, thereby reducing grid growth and improving fretting resistance. Similarly, the use of ZIRLO for the CEA guide tubes improves the corrosion resistance and dimensional stability of the guide tubes.

→(LBDCR 13-014, R309)

The use of Inconel-718 for the top grid maintains the ductility, strength, and stability benefits of the prior Inconel-625 top grid while utilizing a design that is compatible with the NGF rod diameter and basically the same as used in Westinghouse reactors for many years with excellent performance results.

←(LBDCR 13-014, R309)

The NGF fuel rod design utilizes Optimized ZIRLO™ for the cladding and includes several geometric changes (see Section 4.2.2.2 for description of the NGF fuel rod geometry). The use of Optimized ZIRLO™ improves the corrosion resistance of the cladding.

←(EC-9533, R302)

4.2.1.1.3 Control Element Assembly Guide Tubes

All CEA guide tubes are manufactured in accordance with Grade RA-2, ASTM B353, Wrought Zirconium and Zirconium Alloy Seamless and Welded Tubes for Nuclear Service, with the following exceptions and/or additions:

a) Chemical Properties

→(EC-9533, R302)

Chemical analyses are performed for the alloying elements. For Zircaloy-4 guide tubes, the analyses check for tin, iron, chromium, oxygen, and zirconium. For ZIRLO™ guide tubes, the analyses check for tin, iron, niobium, oxygen, and zirconium.

←(EC-9533, R302)

b) Mechanical Properties

→(EC-9533, R302)

The guide tubes are fabricated from Zircaloy-4 or, starting with NGF, ZIRLO™ in the stress-relief annealed (SRA) condition and are tested for yield strength, ultimate strength, and elongation at room temperature and elevated temperature conditions.

←(EC-9533, R302)

c) Dimensional Requirements

	<u>Dimension</u>	<u>Permissible Tolerance (in.)</u>
→(EC-9533, R302)	OD	± 0.003
←(EC-9533, R302)	ID	± 0.005 (thru Batch y) ± 0.002 (Batch Z and beyond)

WSES-FSAR-UNIT-3

4.2.1.1.4 Zircaloy-4 Bar Stock

→(DRN 00-644)

All Zircaloy-4 bar stock is fabricated in accordance with Grade RA-2, ASTM B351, Hot-Rolled and Cold-Finished Zirconium and Zirconium Alloy Bars, Rod and Wire for Nuclear Application, with the following exceptions or additions:

←(DRN 00-644)

a) Chemical Properties

Additional limits are placed on oxygen and silicon content.

b) Metallurgical Properties

1) Grain Size

The maximum average grain size is restricted.

→(EC-9533, R302)

4.2.1.1.5 Zirconium-Based Alloy Strip Stock

←(EC-9533, R302)

→(DRN 00-644)

All Zircaloy-4 strip stock is fabricated in accordance with Grade RA-2, ASTM B352, Zirconium Alloy Sheet, Strip and Plate for Nuclear Application, with the following exceptions or additions:

←(DRN 00-644)

a) Chemical Properties

→(EC-9533, R302)

Chemical analyses are performed for the alloying elements. For Zircaloy-4 strip stock, the analyses check for tin, iron, chromium, oxygen, and zirconium. For Optimized ZIRLO™ strip stock, the analyses check for tin, iron, niobium, oxygen, and zirconium.

←(EC-9533, R302)

b) Metallurgical Properties

(1) Grain Size

The maximum average grain size is restricted.

c) Mechanical Properties

1) Bend

→(DRN 06-895, R15)

Spacer and perimeter strips for spacer grids are to be free of cracks. Strips from each material lot are penetrant inspected in accordance with a quality control plan that ensures, with 95% confidence, that at least 95% of the strips are free of cracks. The method used is capable of detecting known cracks in a standard specimen grid strip. All strips found to have cracks shall be rejected.

←(DRN 06-895, R15)

d) Coefficient of Thermal Expansion

Axial direction - See Reference 2

e) Irradiation Properties:

The yield and tensile strengths are enhanced by irradiation. The stress relaxation with irradiation at operating temperatures proceeds at a rapid rate until nearly complete. The irradiation induced growth is documented.

4.2.1.1.6 Stainless Steel Castings

→(DRN 02-1538, R12, LBDCR 15-025, R309)

Stainless steel castings are fabricated in accordance with Grade CF-3, ASTM A744/A744M, with the following addition:

←(DRN 02-1538, R12)

a) Chemical Properties

Cobalt content is limited.

Starting in 2015, stainless steel end fitting castings are fabricated in accordance with Westinghouse Specification MACASS01. MACASS01 duplicates the requirements of ASTM A744 except for two changes. The required heat treatment (i.e., solution anneal) is not necessary for this application and is not specified. The specification to control delta ferrite level is removed given the relatively low carbon content of the CF-3 cast stainless steel. Casting soundness and casting mechanical properties and other properties affected by the ferrite level are controlled by non-destructive examination and mechanical property measurements of representative samples.

←(LBDCR 15-025, R309)

4.2.1.1.7 Stainless Steel Tubing

→(EC-9533, R302; EC-30663, R307)

Stainless steel tubing is fabricated in accordance with ASTM A269 (with additional requirements) for wear sleeves and the Guardian^{TM1} grid inserts, and in accordance with either ASTM A213 or A249 (both with additional requirements) for the top Inconel grid sleeve.

←(EC-9533, R302; EC-30663, R307)

a) Chemical Properties

Carbon content is limited on tubing to be welded. Cobalt content is limited.

4.2.1.1.8 Inconel X-750 Compression Springs

→(DRN 02-1538, R12; EC-9533, R302)

All Inconel springs are fabricated in accordance with AMS 5699, with the following addition:

←(DRN 02-1538, R12; EC-9533, R302)

a) Chemical Properties

Cobalt content is limited.

→(DRN 02-1538, R12)

4.2.1.1.9 Inconel 625 Spacer Grid Strip Material

→(EC-9533, R302)

Inconel spacer grid strip material is procured in accordance with the specification for nickel-chromium-molybdenum-columbium alloy plate, sheet, and strip (ASTM B443) for Inconel 625 strip and age-hardenable nickel-chromium-iron alloy sheet, strip, and plate (ASTM B670) for Inconel 718, both with the following additional requirements:

←(DRN 02-1538, R12; EC-9533, R302)

a) Chemical Properties

Cobalt content is limited.

b) Special Tests

A check analysis and a bend test are required.

4.2.1.2 Fuel Rod

4.2.1.2.1 Fuel Cladding Design Limits

The fuel cladding is designed to sustain the effects of steady-state and expected transient operating conditions without exceeding acceptable level of stress and strain. Except where specifically noted, the design bases presented in this section are consistent with those used for previous core designs. The fuel rod design accounts for cladding irradiation growth, external pressure, differential expansion of fuel and clad, fuel swelling, clad

¹ **Guardian** is a trademark or registered trademark of Westinghouse Electric Company LLC, its affiliates and/or its subsidiaries in the United States of America and may be registered in other countries throughout the world. All rights reserved. Unauthorized use is strictly prohibited. Other names may be trademarks of their respective owners.

WSES-FSAR-UNIT-3

creep, fission and other gas releases, initial internal helium pressure, thermal stress, pressure and temperature cycling, and flow-induced vibrations. The structural criteria discussed below are based on the following for the normal, upset, and emergency loading combinations identified in Subsection 4.2.1.1. For a discussion of the thermal/hydraulic criteria, see Subsection 4.4.1.

→ (DRN 06-1059, R15; EC-9533, R302)

- a) During normal operating and upset conditions, the maximum primary tensile stress in the Zircaloy, ZIRLO™, or Optimized ZIRLO™ clad shall not exceed two-thirds of the minimum unirradiated yield strength of the material at the applicable temperature. The corresponding limit under emergency conditions is the material yield strength. The use of the unirradiated material yield strength as the basis for allowable stress is conservative because the yield strength of zircaloy increases with irradiation. The use of the two-thirds factor ensures 50 percent margin to component yielding in response to primary stresses. The 50 percent margin, together with its application to the minimum unirradiated properties and the general conservatism applied in the establishment of design conditions, is sufficient to ensure an adequate design.

← (DRN 06-1059, R15)

- b) Net unrecoverable circumferential strain shall not exceed one percent as predicted by computations considering clad creep and fuel clad interaction effects. In addition, the incremental total strain induced during a transient is also limited to one percent, as described in Reference 82 for Zircaloy-4 cladding, Reference 80 for ZIRLO™ cladding, and Reference 84 for the NGF design with Optimized ZIRLO™ cladding.

← (EC-9533, R302)

Data from O'Donnell and Weber were used to determine the present one percent strain limit. (See References 4 & 5.) O'Donnell developed an analytical failure curve for Zircaloy cladding based upon the maximum strain of the material at its point of plastic instability. O'Donnell compared his analytical curve to circumferential strain data obtained on irradiated coextruded Zr-U metal fuel rods tested by Weber. The correlation was good, thus substantiating O'Donnell's instability theory. Since O'Donnell performed his analysis, additional data have been derived at Bettis and AECL. (See References 6, 7, 8, 9 & 10.)

These new data are shown in Figure 4.2-1, along with O'Donnell's curve and Weber's data. This curve was then adjusted because of differences in anisotropy, stress and strain rates; and the design limit was set at one percent.

→ (DRN 06-1059, R15; EC-9533, R302)

The conservatism of the clad strain calculations is provided by the selection of adverse initial conditions and material behavior assumptions, and by the assumed operating history. The acceptability of the 1.0 percent unrecoverable circumferential strain limits is demonstrated by data from irradiated Zircaloy-clad fuel rods which show no cladding failures (due to strain) at or below this level, as illustrated in Figure 4.2-1.

← (DRN 06-1059, R15)

The ductility of ZIRLO™ is expected to be at least equivalent to Zircaloy-4 (Reference 80, Section 5.3.5). Section B.7 of Reference 83 documents that the ductility of Optimized ZIRLO™ and ZIRLO™ are indistinguishable from each other at temperatures above room temperature, so the ductility of Optimized ZIRLO™ is also at least equivalent to that of Zircaloy-4. Ductility is a function of irradiation and hydride formation in the cladding. Since the corrosion rates of ZIRLO™ and Optimized ZIRLO™ are significantly less than that of Zircaloy-4, fewer hydrides will be formed at high burnup levels. Therefore the 1% strain capability limit criterion will continue to be applied and satisfied in Westinghouse fuel mechanical design analysis.

- c) The clad will be initially pressurized with helium to an amount sufficient to prevent gross clad deformation under the combined effects of external pressure and long-term creep. The clad design can rely on the support of fuel pellets (Reference 82) or the holddown spring (Reference 81) to prevent gross deformation.

← (EC-9533, R302)

- d) Cumulative strain cycling usage, defined as the sum of the ratios of the number of cycles in a given effective strain range ($\Delta\epsilon$) to the permitted number (N) at that range, as taken from Figure 4.2-2, will not exceed 0.8.

WSES-FSAR-UNIT-3

→(EC-9533, R302)

The cyclic strain limit design curve shown on Figure 4.2-2, is based upon the Method of Universal Slopes developed by S.S. Manson and has been adjusted to provide a strain cycle margin for the effects of uncertainty and irradiation. The resulting curve has been compared with known data on the cyclic loading of Zircaloy and has been shown to be conservative. (See Reference 11.) Specifically, it encompasses all the data of O'Donnell and Langer. (See Reference 12). The application of the curve to ZIRLO™ is documented in Reference 80 and Appendix B.10 of Reference 83 documents that there is no distinguishable difference in the fatigue characteristics of ZIRLO™ and Optimized ZIRLO™.

←(EC-9533, R302)

As discussed in Subsection 4.2.3.2.5, the fatigue calculation method includes the effect of clad creep to reduce the pellet to clad diametral gap during that portion of operation when the pellet and clad are not in contact. The same model is used for predicting clad fatigue as is used for predicting clad strain. Therefore, the effects of creep and fatigue loadings are considered together in determining end-of-life cumulative fatigue damage factor and the end-of-life cumulative fatigue damage factor and the end-of-life clad strain. Moreover, the current fatigue damage calculation method includes a factor of two which is applied to the calculated strain before determining the allowable number of cycles associated with that strain. This, in combination with the allowable fatigue usage factor of 0.8 ensures a considerable degree of conservatism (see Figure 4.2-2).

- e) There is no specific limit on lateral fuel rod deflection for structural integrity considerations except that which is brought about through application of cladding stress criteria. The absence of a specific limit on rod deflection is justified because it is the fuel assembly structure, and not the individual fuel rod, that is the limiting factor for fuel assembly lateral deflection.
- f) Fuel rod internal pressure increases with increasing burnup and toward end-of-life the total internal pressure, due to the combined effects of the initial helium fill gas and the released fission gas, can approach values comparable to the external coolant pressure. The maximum predicted fuel rod internal pressure will be consistent with the following criteria.

- 1) The primary stress in the cladding resulting from differential pressure will not exceed the stress limits specified earlier in this section.

→(DRN 02-1538, R12)

- 2) The internal pressure will not cause the clad to creep outward from the fuel pellet surface while operating at the design peak linear heat rate for normal operation. In determining compliance with this criterion, internal pressure is calculated for the peak power rod in the reactor, including accounting for the maximum computed fission gas release. In addition, the pellet swelling rate (to which the calculated clad creep rate is compared) is based on the observed swelling rate of "restrained" pellets (i.e., pellets in contact with clad), rather than on the greater observed swelling behavior of pellets which are free to expand.

←(DRN 02-1538, R12)

WSES-FSAR-UNIT-3

→(DRN 03-1821, R13)

The criteria discussed above do not limit fuel rod internal pressure to values less than the primary coolant pressure, and the occurrence of positive differential pressures would not adversely affect normal operation so long as appropriate criteria for cladding stress, strain, and strain rate were satisfied. The fuel rod maximum pressure criterion for allowing fuel rods to operate in reactors with internal hot gas pressure in excess of reactor coolant system pressure is provided in Reference 79.

←(DRN 03-1821, R13)

- g) The design limits of the fuel rod cladding, with respect to vibration considerations, are incorporated within the fuel assembly design. It is a requirement that the spacer grid intervals, in conjunction with the fuel rod stiffness, be such that fuel rod vibration, as a result of mechanical or flow induced excitation, does not result in excessive wear of the fuel rod cladding at the spacer grid contact areas.

4.2.1.2.2 Fuel Rod Cladding Properties

4.2.1.2.2.1 Mechanical Properties

a) Modulus of Elasticity

→(DRN 06-1059, R15; EC-9533, R302)

Young's Modulus $\times 10^6$ = value specified in Reference 13 for Zircaloy-4, in Reference 80 for ZIRLO™, and in Reference 83 for Optimized ZIRLO™.

←(DRN 06-1059, R15; EC-9533, R302)

b) Poisson's Ratio

→(DRN 06-1059, R15; EC-9533, R302)

ν = value specified in Reference 13 for Zircaloy-4, in Reference 80 for ZIRLO™, and in Reference 83 for Optimized ZIRLO™.

←(DRN 06-1059, R15; EC-9533, R302)

c) Thermal Coefficient of Expansion

→(DRN 06-1059, R15; EC-9533, R302)

diametral direction = value specified in Reference 13 for Zircaloy-4, in Reference 80 for ZIRLO™, and in Reference 83 for Optimized ZIRLO™.

←(DRN 06-1059, R15; EC-9533, R302)

d) Yield Strength

→(DRN 06-1059, R15; EC-9533, R302)

Yield strength in the non-irradiated condition is shown in Figure 4.2-20 of Reference 13 for Zircaloy-4, in Section 5.3.7.1 of Reference 80 for ZIRLO™, and in Figure B.7-6 of Reference 83 for Optimized ZIRLO™.

←(DRN 06-1059, R15; EC-9533, R302)

The cladding stress limits identified in Subsection 4.2.1.2.1 are based on values taken from the minimum yield strength curve at the appropriate temperatures. The limits are applied over the entire fuel lifetime, during conditions of reactor heatup and cooldown, steady state operation, and normal power cycling. Under these conditions, cladding temperatures and fast fluences can range from 70° to 750°F and from 0 to 1×10^{22} nvt, respectively.

WSES-FSAR-UNIT-3

e) Ultimate Strength

→(DRN 06-1059, R15; EC-9533, R302)

Ultimate tensile strength in the non-irradiated condition is shown in Figure 4.2-21 of Reference 13 for Zircaloy-4, in Section 5.3.7.2 of Reference 80 for ZIRLO™, and in Figure B7-7 of Reference 83 for Optimized ZIRLO™.

←(DRN 06-1059, R15; EC-9533, R302)

f) Uniform Tensile Strain

→(DRN 02-1538, R12)

Uniform tensile strain in the irradiated condition approaches one percent and remains relatively constant (Subsection 4.2.1.2.1).

→(DRN 06-1059, R15; EC-9533, R302)

Ductility is a function of irradiation and hydride formation in the cladding wall. The ductility of ZIRLO™ and Optimized ZIRLO is expected to be at least equivalent to Zircaloy-4 because the waterside corrosion is significantly lower for ZIRLO™ and Optimized ZIRLO and will result in less hydrogen uptake and less hydride formation. Total strain capability of ZIRLO™ and Optimized ZIRLO is projected to be in excess of 1% at burnup levels of 60 MWD/kgU.

←(DRN 02-1538, R12; 06-1059, R15)

Note: No flare test currently done on production cladding.

g) Hydrostatic Burst Test

Hydrostatic burst tests are conducted on Zircaloy-4 cladding to verify that burst pressure and circumferential elongation exceed prescribed minimum values.

←(EC-9533, R302)

The procedures originally used by CE for the hydrostatic tests were described by D.G. Hardy, J.R. Stewart and A.L. Lowe, Jr., "Development of a Closed End Burst Test Procedure for Zircaloy Cladding," Zirconium in Nuclear Applications, STP-551, ASTM, 1974, pp. 14-30. This information was incorporated into ASTM B353-77. The present procedure for CE cladding is essentially the same procedure as described in B353-77. Typical burst pressures of 35 samples from three lots ranged from 16.6 to 18.8 ksi.

→(EC-9533, R302)

h) Corrosion

→(DRN 03-2058, R14; 06-1059, R15, LBDCR 15-035, R309)

The Zircaloy-water reaction rate correlation used for non-LOCA applications is given in Reference 74. Note that for current analyses, the cladding corrosion rates are described in Reference 82 for Zircaloy-4 and in Reference 85 for ZIRLO™ and in Optimized ZIRLO™.

←(DRN 03-2058, R14; 06-1059, R15; EC-9533, R302, LBDCR 15-035, R309)

→(DRN 06-992, R15)

The maximum allowed fuel rod cladding corrosion will be limited to 100 microns. The corrosion thickness will be calculated using the best estimate models and methods described in CENPD-404-P.

←(DRN 06-992, R15)

4.2.1.2.2.2 Dimensional Requirements

a) Tube straightness is limited to 0.010 in./ft, and inside diameter and wall thickness are tightly controlled.

→(DRN 06-1059, R15; EC-9533, R302)

b) Ovality is measured as the difference between maximum and minimum inside diameters and is acceptable if within the diameter tolerances. Outside diameter is specified as 0.382 ± 0.002 in. Inside diameter is specified as 0.332 ± 0.0015 in. NGF valves are $0.374 \pm .0015$ in. for the outside diameter and $0.329 \pm .0015$ in. for the inside diameter.

←(DRN 06-1059, R15; EC-9533, R302)

WSES-FSAR-UNIT-3

- c) Eccentricity is defined as the difference between maximum and minimum wall thickness at a cross section and is specified as 0.004 inches maximum.

→(EC-9533, R302)

- d) Wall thickness is specified as 0.023 in. minimum (the nominal value reported elsewhere is based on the nominal O.D. and I.D.). Minimum wall thickness specified in NGF is 0.0207 in.

←(EC-9533, R302)

4.2.1.2.2.3 Metallurgical Properties

- a) Hydride Orientation

A restriction is placed on the hydride orientation factor for any third of the tube cross-section (inside, middle, or outside). The hydride orientation factor, defined as the ratio of the number radially oriented hydride platelets to the total number of hydride platelets shall not exceed 0.3. The independent evaluation of three portions of the cross section is included to allow for the possibility that hydride orientation may not be uniform across the entire cross section.

4.2.1.2.2.4 Chemical Properties

→(DRN 02-1538, R12)

All fuel rod cladding is manufactured in accordance with Grade RA-2, ASTM B811, Wrought Zirconium and Zirconium Alloy Seamless and Welded Tubes for Nuclear Service, except additional limits are placed on oxygen, silicon, and iron content.

←(DRN 02-1538, R12)

4.2.1.2.3 Fuel Rod Component Properties

4.2.1.2.3.1 Zircaloy-4 Bar Stock

→(DRN 02-1538, R12)

All Zircaloy-4 bar stock is fabricated in accordance with Grade RA-2, ASTM B351, Hot-Rolled and Cold-Finished Zirconium and Zirconium Alloy Bars, Rod and Wire for Nuclear Application, with the following exceptions and/or additions:

←(DRN 02-1538, R12)

- a) Chemical Properties

Additional limits are placed on oxygen and silicon content.

- b) Metallurgical Properties

- 1) Grain Size

The maximum average grain size is restricted.

4.2.1.2.3.2 Stainless Steel Compression Springs

→(DRN 02-1538, R12)

All stainless steel springs are fabricated in accordance with AMS 5688.

←(DRN 02-1538, R12)

→(DRN 02-1538, R12)

←(DRN 02-1538, R12)

WSES-FSAR-UNIT-3

4.2.1.2.4 UO₂ Fuel Pellet Properties

4.2.1.2.4.1 Chemical Composition

Salient points regarding the structure, composition, and properties of the UO₂ fuel pellets are discussed in the following subsections. Where the effect of irradiation on a specific item is considered to be of sufficient importance to warrant reflection in the design or analyses, that effect is also discussed.

a) Chemical analyses are performed for the following constituents:

- 1) Total Uranium
- 2) Carbon
- 3) Nitrogen
- 4) Fluorine
- 5) Chlorine and Fluorine
- 6) Iron
- 7) Thorium
- 8) Nickel
- 9) Aluminum
- 10) Chromium
- 11) Silicon
- 12) Calcium
- 13) Magnesium
- 14) Erbium

→(DRN 02-1538)

←(DRN 02-1538)

b) Limits are placed on the oxygen-to-uranium ratio.

c) The sum of the calcium + aluminum + silicon contents shall not exceed 300 ppm by weight.

d) The sum of the thermal neutron capture cross-sections of the following impurities shall not exceed a specified equivalent thermal-neutron capture cross-section of natural boron:

- 1) Boron
- 2) Silver
- 3) Cadmium
- 4) Gadolinium
- 5) Europium

WSES-FSAR-UNIT-3

6) Samarium

7) Dysprosium

→(DRN 02-1538)

8) Erbium

←(DRN 02-1538)

e) The total hydrogen content of finished ground pellets is restricted.

f) The nominal enrichment of the fuel pellet will be specified and shall be held within ± 0.05 wt percent U_{235} .

4.2.1.2.4.2 Microstructure

→(DRN 02-1538)

a) Acceptable porosity distribution will be determined by comparison of approved visual standards with photo-micrographs from each pellet lot.

←(DRN 02-1538)

b) The average grain size shall exceed a specified minimum size.

4.2.1.2.4.3 Density

→(DRN 02-1538)

a) The density of the sintered pellet after grinding shall be between 94.0 and 96.5 percent of theoretical density (TD), based on a UO_2 theoretical density of 10.96 g/cm^3 .

b) The in-pile stability of the fuel is ensured by the use of an NRC-approved out-of-pile test during production.

←(DRN 02-1538)

c) The effects of irradiation on the density of sintered UO_2 pellets are discussed in Reference 14.

4.2.1.2.4.4 Thermal Properties

a) Thermal Expansion

The thermal expansion of UO_2 is described by the following temperature dependent equations:⁽¹⁵⁾⁽¹⁶⁾

$$\begin{aligned} \% \quad \text{Linear Expansion} &= (-1.723 \times 10^{-2}) + (6.797 \times 10^{-4}T) \\ &+ (2.896 \times 10^{-7}T^2) \end{aligned}$$

$$(25 \leq T \leq 2200)$$

$$\begin{aligned} \% \quad \text{Linear Expansion} &= 0.204 + (3 \times 10^{-4}T) + (2 \times 10^{-7}T^2) \\ &(10^{-10}T^3) \end{aligned}$$

$$(T > 2200)$$

where T = fuel temperature, degrees Celsius.

WSES-FSAR-UNIT-3

b) Thermal Emissivity

A value of 0.85 is used for the thermal emissivity of UO₂ pellets over the temperature range 800 to 2600K. (See References 17, 18 and 19.)

c) Melting Point and Thermal Conductivity

The fuel temperature required to incur melting is linearly dependent on local burnup as given by:

$$T_{melt} = 5080 - 290 \times \frac{(\text{Burnup})}{50,000}$$

→(DRN 04-1096, R14)

where, T_{melt} is in °F and burnup is in MWD/MTU. This equation T_{melt} is based on UO₂ melt data given by Reference 76. In addition, the fuel melting temperature may be reduced depending on the amount and type of burnable poison in the fuel as described in Reference 78.

←(DRN 04-1096, R14)

The variation of the thermal conductivity of UO₂ with burnup is not explicitly treated, but is implicitly taken from the porosity relationship discussed in Subsection 2.2.5 of Reference 14.

d) Specific Heat of UO₂

The specific heat of UO₂ is described by the following temperature dependent equations.⁽²⁰⁾

→(DRN 04-1096, R14)

$$T \leq 2240^{\circ} F$$

$$C_p = 49.67 + 2.2784 \times 10^{-3} T - \left(\frac{3.2432 \times 10^6}{(T + 460)^2} \right)$$

←(DRN 04-1096, R14)

$$T \leq 2240^{\circ} F$$

$$\geq C_p = -126.07 + (0.2621T) - (1.399 \times 10^{-4} T^2) + (3.1786 \times 10^{-8} T^3) - (2.483 \times 10^{-12} T^4)$$

where:

C_p = specific heat, BTU/lbm-°F

T = fuel temperature, °F

4.2.1.2.4.5 Mechanical Properties

a) Young's Modulus of Elasticity

The Young's modulus of elasticity for UO₂ is used in the analytical model for prediction of the effects of pellet clad interaction. Its value may be found in Reference 21.

Subsection 4.2.3.2.11 discusses the pellet clad interaction model.

WSES-FSAR-UNIT-3

b) Poisson's Ratio

→(DRN 02-1538, R12)

Poisson's ratio = $0.32 - (1.8 \times 10^{-5} (T-25))$ for the range of temperature between 25°C to 1800°C, Poisson's ratio is assumed constant at 0.29 where T = fuel temperature, °C.

←(DRN 02-1538, R12)

c) Yield Stress (not applicable)

d) Ultimate Stress (not applicable)

e) Uniform Ultimate Strain (not applicable)

4.2.1.2.5 Fuel Rod Pressurization

Fuel rods are initially pressurized with helium for two reasons:

- a) Preclude clad collapse during the design life of the fuel. The internal pressurization, by reducing stresses from differential pressure, extends the time required to produce creep collapse beyond the required service life of the fuel.
- b) Improve thermal conductivity of the pellet-to-clad gap within the fuel rod. Helium has a higher coefficient of conductivity than the gaseous fission products.

In unpressurized fuel, the initially good helium conductivity is eventually degraded through the addition of the fission product gases released from the pellets. The initial helium pressurization results in a high helium to fission products ratio over the design life of the fuel with a corresponding increase in the gap conductivity and heat transfer.

The effect of fuel rod power level and pin burnup on fuel rod internal pressure has been studied parametrically. Figures 4.2-3 and 4.2-4 show predicted variation of fuel rod internal pressure with pin burnup and pin peaking factor for minimum pressure rods and maximum pressure rods, respectively, for a full power core.

→(DRN 03-2058, R14; 06-1059, R15; EC-9533, R302)

The initial helium fill pressure will be 395 ± 15 psia for UO₂ and Erbia rods. Due to the design changes associated with the NGF rods, the initial helium fill pressure for UO₂ rods of the NGF design is specified as 275 ± 15 psig at 75F. This initial fill pressure will be sufficient to prevent clad collapse as discussed in Subsection 4.2.3.2.8. The calculational methods employed to generate internal pressure histories are discussed in Reference 14.

←(DRN 03-2058, R14)

The ZrB₂ IFBA rod for both non-NGF and NGF designs is pre-pressurized at a lower helium fill pressure (approximately 150 psig) to prevent an unacceptable maximum pressure due to an increased helium release.

←(DRN 06-1059, R15; EC-9533, R302)

4.2.1.2.5.1 Capacity for Fission Gas Inventory

The greater portion of the gaseous fission products remain either within the lattice or the microporosity of the UO₂ fuel pellets and do not contribute to the fuel rod internal pressure. However, a fraction of the fission gas is released from the pellets by diffusion and pore migration and thereafter contributes to the internal pressure.

→(DRN 06-1059, R15)

The annular pellets provide additional void volume to help control the rod pressure increases due to release of Helium from the thin IFBA coating during the lifetime of such rod.

←(DRN 06-1059, R15)

WSES-FSAR-UNIT-3

The determination of the effect of fission gas generated in and released from the pellet column is discussed in Subsection 4.2.3.2.2. The rod pressure increase which results from the release of a given quantity of gas from the fuel pellets depends upon the amount of open void volume available within the fuel rod and the temperatures associated with the various void volumes. In the fuel rod design, the void volumes considered in computing internal pressure are:

Fuel rod upper end plenum

Fuel-clad annulus

Fuel pellet-end dishes and chamfers

Fuel pellet open porosity

→(DRN 06-1059, R15)

Hollow center of annular pellets

←(DRN 06-1059, R15)

These volumes are not constant during the life of the fuel. The model used for computing the available volume is a function of burnup and power level and accounts for the effects of fuel and clad thermal expansion fuel pellet densification, clad creep, and irradiation induced swelling of the fuel pellets.

4.2.1.2.5.2 Fuel Rod Plenum Design

The fuel rod upper end plenum is required to serve the following functions:

- a) Provide space for axial thermal expansion and burnup swelling of the pellet column.
- b) Contain the pellet column hold-down spring.
- c) Act as a plenum region to ensure an acceptable range of fuel rod internal pressures.

→(DRN 02-1538, R12)

Of these functions, listing c is expected to be the most limiting constraint on plenum length selection, since the range of temperatures in fuel rod, together with the effects of swelling, thermal expansion, and fission gas release, can produce a wide range of internal pressure during the life of the fuel. The fuel rod plenum pressure will be consistent with the pressurization and clad collapse criteria specified in Subsection 4.2.1.2.1.

←(DRN 02-1538, R12)

4.2.1.2.5.3 Outline of Procedure Used to Size the Fuel Rod Plenum

- a) A parametric study of the effects of plenum length on maximum and minimum rod internal pressure is performed. Because the criteria pertaining to maximum and minimum rod internal pressure differ, the study is divided into two sections:

WSES-FSAR-UNIT-3

1) Maximum Internal Pressure Calculation

Maximum rod pressure is limited by the stress criteria. Maximum end-of-life pressure is determined for each plenum length by including the fission gas released, selecting conservative values for components dimensions and properties, and accounting for burnup effects on component dimensions. The primary cladding stress produced by each maximum pressure is then compared to the stress limits to find the margin available with each plenum length. Stress limits are listed in Subsection 4.2.1.2.1.

2) Minimum Internal Pressure/Collapse Calculation

Minimum rod pressure is limited by the criterion that no rod will be subject to collapse during the design lifetime. The minimum pressure history for each plenum length is determined by neglecting fission gas release, selecting a conservative combination of component dimensions and properties, and accounting for dimension changes during irradiation. Each minimum pressure history is input to the cladding collapse model to establish the acceptability of the associated plenum length (see Reference 22).

- b) For each plenum length, there is a resultant range of acceptable initial fill pressures. The optimum plenum length is generally considered to be the shortest which satisfies all criteria related to maximum and minimum rod internal pressure including a range sufficient to accommodate a reasonable manufacturing tolerance on initial fill pressure.

→(LBDCR 13-014, R309)

- c) Additional information on those factors which have a bearing on determination of the plenum length are discussed below:

- 1) Creep and dimensional stability of the fuel rod assembly influence the fission gas release model and internal pressure calculations, and are accounted for in the procedure of sizing the fuel rod plenum length. Creep in the cladding is accounted for in a change in clad inside diameter, which in turn influences the fuel/clad gap. The gap change varies the gap conductance in the FATES computer code with resulting change in annulus temperature, internal pressure, and fission gas release (see Reference 14). In addition, the change in clad inside diameter causes a change in the internal volume, with its resulting effect on temperature and pressure. Dimensional stability considerations affect the internal volume of the fuel rod, causing changes in internal pressure and temperature. Fuel pellet densification reduces the stack height and pellet diameter. Irradiation-induced radial and axial swelling of the fuel pellets decreases the internal volume within the fuel rod. In-pile growth of the fuel rod cladding contributes to the internal volume. Axial and radial elastic deformation calculations for the cladding are based on the differential pressure the cladding is exposed to, resulting in internal volume changes. Thermal relocation, as well as differential thermal expansion of the fuel rod materials also affect the internal volume of the fuel rods.

←(LBDCR 13-014, R309)

WSES-FSAR-UNIT-3

→(DRN 02-1538, R12; 04-1096, R14)

- 2) The maximum expected fission gas release in the peak power rod is calculated using the FATES computer code. Rod power history input to the code is consistent with the design limit for peak linear heat rate set by LOCA considerations, and therefore the gas release used to size the plenum represents an upper limit. Because of time-varying gap conductance, fuel depletion, and expected fuel management, the release rate varies as a function of burnup.

←(DRN 02-1538, R12; 04-1096, R14)

4.2.1.2.6 Fuel Rod Performance

Steady state fuel temperatures are determined by the FATES computer program. The calculational procedure considers the effect of linear heat rate, fuel relocation, fuel swelling, densification, thermal expansion, fission gas release, and clad deformations. The model for predicting fuel thermal performance including the specific effects of fuel densification on increased linear heat generation rate (LHGR) and stored energy is discussed in detail in Reference 14.

→(DRN 02-1538, R12)

Significant parameters such as cold pellet and clad diameters, gas pressure and composition, burnup and void volumes are calculated and used as initial conditions for subsequent calculations for stored energy during the ECCS analysis. The coupling mechanism between FATES calculations and the ECCS analysis is described in detail in Reference 23.

←(DRN 02-1538, R12)

Discussions of uncertainties associated with the model, and of comparative analytical and experimental results, are also included in Reference 14.

→(DRN 02-1538, R12; EC-9533, R302)

The methodology for modeling the NGF design is described in the CE 16x16 Next Generation Fuel Topical Report, Reference 84.

←(EC-9533, R302)

4.2.1.2.7 Fuel Rod with Erbium (Er_2O_3) Addition

Some fuel rods in the fuel assembly may contain pellets which incorporate erbium (Er_2O_3) as a burnable absorber into the central portion of the pellet column. These fuel rods are analyzed by the same methods and subject to the same design criteria as fuel rods containing only uranium pellets.

The uranium-erbium pellets are fabricated by mechanically blending erbium powder with uranium powder to produce a homogeneous mixture, followed by pressing and sintering. These fuel pellets may contain up to 2.5 weight percent erbium.

←(DRN 02-1538, R12)

→(DRN 04-1096, R14)

The addition of erbium to uranium fuel pellets may influence the thermal properties of the fuel. Of particular importance are the properties that are used in fuel performance analyses. These properties are: 1) solidus temperature, 2) specific heat, 3) density, 4) thermal expansion, and 5) thermal conductivity. The effect of erbium addition on these properties of uranium is discussed in detail in Section 2.2 of Reference 78.

←(DRN 04-1096, R14)

→(DRN 06-1059, R15)

4.2.1.2.8 Fuel Rod with IFBA (ZrB_2 coated) Pellets

The Zirconium Diboride (ZrB_2) integral fuel burnable absorber (IFBA) fuel design commences with Batch Y for Cycle 15. The ZrB_2 is applied as a very thin uniform coating on the outer surface only of the solid UO_2 pellet stack prior to loading into the fuel rod cladding tube. The coating is applied over the center of the UO_2 pellet stack length, consistent with positioning of the Erbium (Er_2O_3 - UO_2) burnable absorber pellets in the prior batches present in Cycle 15 (T, U, W and X) and does not extend to either end of the fuel rod (see Figure 4.2-11A). Pellets at the ends of the pellet stack (cutback zones) are of an annular design.

→(EC-9533, R302)

The annular pellets have the same pellet outside diameter (.3250 inch for pre-NGF batches and .3225 inch for NGF batches) and pellet edge chamfer as the corresponding enriched solid fuel pellets, but have no dish on the pellet ends. The annular pellets are also longer

←(DRN 06-1059, R15; EC-9533, R302)

→(DRN 06-1059, R15; EC-9533, R302)

than the solid fuel pellets (.500 inch versus .390 inch for pre-NGF batches and 0.387 inch for NGF batches). The diameter of the annulus is 0.1625 inches (pre-NGF) or 0.1550 inches (NGF) which results in about 25% annular volume to accommodate gas release in the IFBA rods. The fully-enriched annular pellets in the IFBA rods increase the void volume for gas accommodation within the fuel rod compared to the previous burnable absorber fuel rod design (Erbia), thereby providing sufficient margin to meet the rod internal pressure criterion. Also, to compensate for the additional helium released from the ZrB_2 coating, the initial fill gas pressure, designed to reduce pressure differences across the cladding, is reduced as compared to non-IFBA rods.

←(EC-9533, R302)

Introduction of the ZrB_2 IFBA fuel rod design has influenced fuel rod pressurization as discussed in the Topical Report, Reference 81. During irradiation, the B-10 isotope absorbs a neutron and fissions into Helium and Lithium. Much of the Helium may be released from the thin coating into the fuel rod void by the time complete burnout is attained, thus additionally increasing the rod internal pressure at end of life. The released Helium compensates for the initial reduction in helium fill gas and mitigates the potential impact of less helium fill gas on the thermal heat transfer from the fuel pellets to the cladding and into the coolant. Thus, the IFBA coating and corresponding Helium release have no significant impact on the heat transfer characteristic of the fuel rod.

←(DRN 06-1059, R15)

4.2.1.3 Burnable Poison Rod

→(DRN 06-1059, R15)

The earlier cycles poison rods containing the Al_2O_3 burnable poison pellets were replaced by fuel rods with Erbium ($Er_2O_3 - UO_2$) burnable absorber pellets (Section 4.2.1.2.7) during the late 1990's. Most recently, the ZrB_2 IFBA fuel rod design (Section 4.2.1.2.8) is being introduced beginning with Batch Y in Cycle 15, such that the current core design uses only Erbium or IFBA burnable absorbers rods as poison rods. Hence, the previous design of the poison rods containing the Al_2O_3 burnable poison pellets, as presented in subsections 4.2.1.3.1 through 4.2.1.3.3, is only relevant to those poison rods, if any, that are being kept in long term storage outside of the current core.

←(DRN 06-1059, R15)

4.2.1.3.1 Burnable Poison Rod Cladding Design Limits

The burnable poison rod design accounts for external pressure, differential expansion of pellets and clad, pellet swelling, clad creep, helium gas release, initial internal helium pressure, thermal stress, and flow-induced vibrations. Except where specifically noted, the design bases presented in this section are consistent with those used for previous designs. The structural criteria for the normal, upset and emergency loading combinations identified in Subsection 4.2.1.1. are as follows:

- a) During normal operating and upset conditions, the maximum primary tensile stress in the Zircaloy clad shall not exceed two-thirds of the minimum unirradiated yield strength of the material at the applicable temperature. The corresponding limit under emergency conditions is the material yield strength.
- b) Net unrecoverable circumferential strain shall not exceed one percent as predicted by computations considering clad creep and poison pellet swelling effects.
- c) The clad will be initially pressurized with helium to an amount sufficient to prevent gross clad deformation under the combined effects of external pressure and long-term creep. The clad design will not rely on the support of pellets or the hold-down spring to prevent gross deformation.

4.2.1.3.2 Burnable Poison Rod Cladding Properties

Cladding tubes for burnable poison rods are purchased under the specification for fuel rod cladding tubes. Therefore, the mechanical metallurgical chemical, and dimensional properties of the cladding are as discussed in Subsection 4.2.1.2.2.

→(DRN 03-2058, R14)

4.2.1.3.3 Al_2O_3 - B_4C Burnable Poison Pellet Properties

→(DRN 02-1538, R12)

The Al_2O_3 - B_4C burnable poison pellets used in C-E designed reactors consist of a relatively small volume fraction of fine B_4C particles dispersed in a continuous Al_2O_3 matrix. The boron loading is varied by adjusting the B_4C concentration in the range from 0.7 to 4.0 w/o (1 to 6.0 v/o). Typical pellets have a bulk density of about 90 percent of theoretical. Many properties of the two-phase Al_2O_3 - B_4C mixture, such as thermal expansion, thermal conductivity, and specific heat are very similar to the properties of the Al_2O_3 major constituent. In contrast, properties such as swelling, helium release, melting point and corrosion are dependent on the presence of B_4C . The operating centerline temperature of burnable poison is less than 1100°F, with maximum surface temperatures close to 750°F.

←(DRN 02-1538, R12)

4.2.1.3.3.1 Thermal-Physical Properties

a) Thermal Expansion

The mean thermal expansion coefficients of Al_2O_3 and B_4C from 0 to 1850°F are 4.9 and 2.5 in/in.-°F x 10⁻⁶, respectively (see References 24 and 25). The thermal expansion of the Al_2O_3 - B_4C two-phase mixture can be considered to be essentially the same as the value for the continuous Al_2O_3 matrix, as the dispersed B_4C phase has a lower expansion coefficient and occupies no more than 6 v/o of the available volume. The low temperature (80 to 250°F) thermal expansion coefficient of Al_2O_3 irradiated at 480, 900, and 1300°F does not change as a result of irradiation (see Reference 26). The expansion of a similar material, beryllium oxide, up to 1900°F has also been reported to be relatively unchanged by irradiation (see Reference 27). It is therefore appropriate to use the values of thermal expansion measured for Al_2O_3 for the burnable poison pellets:

←(DRN 03-2058, R14)

Temperature Range (°F)	Linear Expansion (percent)
400	0.12
600	0.23
800	0.30
1000	0.40

b) Melting Point

→(DRN 03-2058, R14)

The melting points of Al_2O_3 (3710°F) and B_4C (4440°F) are higher than the melting point of the Zr-4 cladding (see References 28 and 29). No reactions have been reported between the component which would lower the melting point of the pellets to any significant extent. As the B_4C burns up, the lithium atoms formed occupy interstitial sites randomly distributed within the B_4C lattice, rather than forming a lithium-rich phase (see Reference 30). The solid solution of lithium in B_4C should not appreciably influence the melting point of the Al_2O_3 - B_4C pellets, as only a small quantity of lithium compounds (0.5 w/o) forms during irradiation. It is concluded that the melting point of Al_2O_3 - B_4C will remain considerably above the maximum 1100°F operating temperature.

←(DRN 03-2058, R14)

WSES-FSAR-UNIT-3

→(DRN 03-2058, R14)

c) Thermal Conductivity

The thermal conductivity of $Al_2O_3-B_4C$ was calculated from the measured values for Al_2O_3 and B_4C using the Maxwell-Buckan relationship for a continuous matrix phase (Al_2O_3) with spherical dispersed phase (B_4C) particles (see Reference 31). Because of the high Al_2O_3 content of these mixtures and the similarity in thermal conductivity, the resultant values for $Al_2O_3-B_4C$ were essentially the same as the values for Al_2O_3 . The measured, unirradiated values of thermal conductivity at 750°F are 0.06 cal/sec-cm-°K for B_4C and 0.05 cal/sec-cm-°K for Al_2O_3 .

The thermal conductivity of Al_2O_3 after irradiation decreases rapidly as a function of burnup to values of about one-third the unirradiated values (see Reference 26). The irradiated values of $Al_2O_3-B_4C$ calculated from the above relationships are given below as a function of temperature (see References 26 and 32).

←(DRN 03-2058, R14)

Temperature (°F)	Thermal Conductivity (cal/sec-cm-°K)
400	0.015
600	0.013
800	0.010
1000	0.008

d) Specific Heat

→(DRN 03-2058, R14)

The specific heat of the $Al_2O_3-B_4C$ mixture can be taken to be essentially the same as pure Al_2O_3 since the concentration of B_4C is low (6.0 v/o maximum). In addition, the effect of irradiation on specific heat is expected to be small based on experimental evidence from similar materials which do not sustain transmutations as a function of neutron exposure.

←(DRN 03-2058, R14)

→(DRN 03-2058, R14)

The values for Al_2O_3 measured on unirradiated samples (32)(33) are given below:

Temperature (°F)	Specific Heat (cal/gm-°F)
250	0.12
450	0.13
800	0.14
1000 and above	0.15

←(DRN 03-2058, R14)

→(DRN 03-2058, R14)

4.2.1.3.3.2 Irradiation Properties

a) Swelling

$A\ell_2O_3$ - B_4C consists of B_4C particles dispersed in a continuous $A\ell_2O_3$ matrix, which occupies more than 94 percent of the poison pellet. The swelling of $A\ell_2O_3$ - B_4C depends primarily upon the neutron fluence on the continuous $A\ell_2O_3$ matrix and, secondarily, on the B^{10} burnup of the dispersed B_4C phase. Recent measurements performed on material containing about two w/o B_4C irradiated in a C-E PWR to 100 percent B^{10} burnup at a fluence of 2.4×10^{21} nvt ($E > 0.8$ MeV) revealed a diametral swelling of about one percent. Pellets similar to the burnable poison used in C-E reactors with up to 3 w/o B_4C also sustained about 100 percent B^{10} burnup. Experimental data⁽³⁴⁾ on $A\ell_2O_3$ reveal a diametral swelling of about 0.7 percent at a fluence of 2.4×10^{21} nvt ($E > 0.8$ MeV). Swelling of $A\ell_2O_3$ increases linearly with fluence to 1.8 percent diametral after an exposure of 6×10^{21} nvt ($E > 0.8$ MeV).

These data show that $A\ell_2O_3$ - B_4C swells somewhat more than $A\ell_2O_3$ up to a burnup of 100 percent B_4C (about 2×10^{21} nvt, $E > 0.8$ MeV).

The C-E design value of $A\ell_2O_3$ - B_4C swelling rate for fluences less than 2×10^{21} is greater than the swelling rate of $A\ell_2O_3$, while after 100 percent B^{10} burnup the swelling rate for $A\ell_2O_3$ - B_4C is considered equal to that of $A\ell_2O_3$.

The data and considerations presented above result in best-estimate diametral swelling values at end-of-life (7×10^{21} nvt, $E > 0.8$ MeV) of about two percent for $A\ell_2O_3$ and from two to three percent for $A\ell_2O_3$ - B_4C depending on B_4C .

b) Helium Release

Experimental measurements reveal that less than five percent of the helium formed during irradiation will be released.⁽³⁵⁾ These measurements were performed on $A\ell_2O_3$ - B_4C pellets irradiated at temperatures to 500°F and, subsequently, annealed at 1000°F for five days. The helium release in a burnable poison rod which operated for

←(DRN 03-2058, R14)

one cycle in a ABB CE PWR was calculated from internal pressure measurements to be less than five percent. The design is based on a release of three to ten percent of the helium generated. The design of the burnable poison rod will not be limited by helium pressure despite the conservative use of 10 percent release.

4.2.1.3.3.3 Chemical Properties

→(DRN 03-2058, R14)

a) $A\ell_2O_3$ - B_4C Coolant Reactions

→(DRN 02-1538, R12)

The stability of $A\ell_2O_3$ - B_4C in contact with reactor coolant has been investigated before and after irradiation. Prior to irradiation no significant boron loss was observed after testing for hundreds of hours at 650°F in borated water at 2250 psig. Visual and metallographic evaluations showed no erosion of the $A\ell_2O_3$ matrix. In addition, pellet measurements showed no change in diameter or length as a result of exposure to the borated water.

←(DRN 02-1538, R12; 03-2058, R14)

→(DRN 03-2058, R14)

A series of tests were performed to assess the compatibility of irradiated $A\ell_2O_3$ - B_4C with reactor coolant. The results of these tests show that $A\ell_2O_3$ - B_4C pellets irradiated to 100 percent B_{10} burnup retain their mechanical integrity after 350 hours in 650°F, 2250 psig water. Visual and metallographic observations indicate that the $A\ell_2O_3$ matrix does not sustain significant erosion or micro-cracking, although the B_4C particles are leached out of portions of the pellet. No diameter or length changes were noted in the pellets. The amount of B_4C loss is primarily dependent upon the accessibility of the B_4C particles to the reactor coolant, and the time of exposure. B_4C particles that are completely enclosed in the $A\ell_2O_3$ matrix do not corrode, as the $A\ell_2O_3$ matrix material has relatively good corrosion resistance.

Should irradiated B_4C particles be exposed to reactor coolant, the primary corrosion products that would be produced are H_3BO_3 and Li_2O , which are soluble in water, and free carbon. The presence of these products in the reactor coolant would not be detrimental to the operation of the plant.

b) Chemical Compatibility

Chemical compatibility between the $A\ell_2O_3$ - B_4C pellets and the burnable poison rod cladding during long-term normal operations has been demonstrated by examinations of a burnable poison rod from the Maine Yankee Reactor. The rod had been exposed to an axial average fluence in excess of 2×10^{21} nvt (>0.821 MeV). No evidence of a chemical reaction was observed on the cladding I.D.

Short term chemical compatibility during upset and emergency conditions is demonstrated by the fact that conditions favorable to a chemical reaction between B_4C and $A\ell_2O_3$ are not present at temperatures below 1300°F⁽³⁶⁾. This temperature is higher than that which will occur at burnable poison pellet surfaces during Condition II and III occurrences (Subsection 4.2.1.1). The action between Zr-4 and $A\ell_2O_3$ described by Idaho Nuclear⁽³⁷⁾ was observed to occur rapidly only at temperatures in excess of 2500°F, well above the peak Condition IV Zr-4 temperatures in the higher energy fuel rods described in Chapter 15.

←(DRN 03-2058, R14)

4.2.1.4 Control Element Assembly

Except where specifically noted, the design bases presented in this section are consistent with those used for previous designs.

The mechanical design of the control element assemblies is based on compliance with the following functional requirements and criteria:

- a) To provide for or initiate short term reactivity control under all normal and adverse conditions experienced during reactor start-up, normal operation, shutdown, and accident conditions.
- b) Mechanical clearances of the CEA within the fuel and reactor internals are such that the requirements for CEA positioning and reactor trip are attained under the most adverse accumulation of tolerances.
- c) Structural material characteristics are such that radiation induced changes to the CEA materials will not impair the functions of the reactivity control system.

WSES-FSAR-UNIT-3

4.2.1.4.1 Thermal-Physical Properties of Absorber Material

→ (DRN 00-644; 01-1103, R12)

The primary control rod absorber materials consist of boron carbide pellets (B_4C) and silver-indium-cadmium bars (Ag-In-Cd). Refer to Figures 4.2-5, 4.2-6, and 4.2-7 for the specific application and orientation of the absorber materials. The significant thermal and physical properties used in mechanical analysis of the absorber materials are listed below:

← (DRN 00-644; 01-1103, R12)

a)	Boron Carbide (B_4C)	
	Configuration	Right cylinder
	Outside diameter in.	0.737 ± 0.001
	Pellet length, in. nominal	2
	End chamber	0.03 in. by 45°
	Density gm/cc	1.84
	w/o boron, minimum	77.5
	Percent open porosity in pellet	27
	Ultimate tensile strength, psi	N/A
	Yield strength, psi	N/A
	Elongation, percent	N/A
	Young's modulus, psi	N/A
	Thermal conductivity (cal/sec-cm- $^\circ C$):	<u>Irradiated</u> <u>Unirradiated</u>
	800 $^\circ F$	8.3×10^{-3} 28×10^{-3}
	1000 $^\circ F$	7.9×10^{-3} 24×10^{-3}
	Melting point, $^\circ F$	4400
	Percent thermal linear expansion	0.23% @ 1000 $^\circ F$
b)	Silver-Indium-Cadmium (Ag-In-Cd)	
	Configuration	Cylindrical bars with central hole
	Outside diameter, in.	0.734 ± 0.003
	Inside diameter, in.	1/4

WSES-FSAR-UNIT-3

Length of bar, in. nominal	12.5 (for 5 element CEAs), 5 (for 4 element CEAs)	
Density, lb/in. ³	0.367	
Ultimate tensile strength, psi	N/A	
Yield strength, psi	N/A	
Elongation, percent	N/A	
Young's modulus, psi	N/A	
Thermal conductivity (cal/sec-cm-°C):	<u>Irradiated</u>	<u>Unirradiated</u>
at 300°C	0.14	0.182
at 400°C	0.148	0.196
Melting point, °F	1,470	
Linear thermal expansion (in./in.-°F)	12.5 x 10 ⁻⁶	
c) Inconel Alloy 625 (Ni-Cr-Fe)		
Configuration (as absorber)	Cylindrical bar	
Outside diameter, in.	0.816 ± 0.002	
Inside diameter, in.	Solid	
Length of cylinder, in.	See Figures 4.2-5, 4.2-6, 4.2-7	
Density, lb/in. ³	0.305	
Ultimate tensile Strength, psi	120-150	
Specified minimum yield strength @ 650°F, ksi	65	
Elongation in two in., percent	30	
Young's modulus, psi		
at 70°F	29.7 x 10 ⁶	
at 650°F	27.0 x 10 ⁶	
Thermal conductivity (Btu/hr-ft-°F):		

WSES-FSAR-UNIT-3

	70°F	5.7
	600°F	8.2
→(DRN 00-644)	Linear thermal expansion (in./in.-°F)	7.4×10^{-6} (70 to 600°F)
←(DRN 00-644)		

4.2.1.4.2 Compatibility of Absorber and Cladding Materials

The cladding material used for the control elements is Inconel Alloy 625. The selection of this material for use as cladding is based on considerations of strength, creep resistance, corrosion resistance, and dimensional stability under irradiation and also upon the acceptable performance of this material for this application in other ABB CE reactors currently in operation.

a) B₄C/Inconel 625 Compatibility

Studies have been conducted by HEDL(38) on the compatibility of Type 316 stainless steel with B₄C under irradiation for thousands of hours at temperatures between 1300 and 1600°F. Carbide formation to a depth of about 0.004 in. in the Type 316 stainless steel was measured after 4400 hours at 1300°F. Similar compound formation depths were observed after ex-reactor bench testing. After testing at 1000°F, only 0.0001 in/yr of penetration was measured. Since Inconel 625 is more resistant to carbide formation than 316 stainless steel, and the expected pellet/clad interfacial temperature in the Waterford 3 design is below 800°F, it is concluded that B₄C is compatible with Inconel.

4.2.1.4.3 Cladding Stress-Strain Limits

The stress limits for the Inconel Alloy 625 cladding are as follows:

Design Conditions I and II (Non Operation, Normal Operation, and Upset Conditions)

$$P_m \leq S_m$$

$$P_m + P_b \leq F_s S_m$$

Design Condition III (Emergency Conditions)

$$P_m \leq 1.5 S_m$$

$$P_m + P_b \leq 1.5 F_s S_m$$

Design Condition IV (Faulted Conditions)

$$P_m \leq S'_m$$

$$P_m + P_b \leq F_s S'_m$$

where S'_m is the smaller of $2.4S_m$ or $0.7S_u$

For definition of P_m , P_b , S_m , S'_m , S_u , and F_s see Subsection 4.2.1.1.1. For the Inconel 625 CEA cladding, the value of S_m is two-thirds of the minimum specified yield strength at temperature.

For Inconel 625, the specified minimum yield strength is 65,000 psi at 650°F.

WSES-FSAR-UNIT-3

$F_s = M_p/M_y$ where M_p is the bending moment required to produce a fully plastic section and M_y is the bending moment which first produces yielding at the extreme fibers of the cross section. The capability of cross-sections loaded in bending to sustain moments considerably in excess of that required to yield the outermost fiber is discussed in Reference 1. For the CEA cladding dimensions, $F_s = 1.33$.

The strain of the cladding is limited to a value which will permit the CEAs to trip within the allowable time and which is less than the irradiated uniform elongation of the material.

The values of uniform and total elongation of Inconel Alloy 625 cladding are as follows:

Fluence (E>1 MeV), nvt	1×10^{22}	3×10^{22}
Uniform elongation, percent	3	1
Total elongation, percent	6	3

4.2.1.4.4 Irradiation Behavior of Absorber Materials

a) Boron Carbide Properties

- 1) Swelling. The linear swelling of B_4C increases with burnup according to the relationship:

$$\% \Delta L = (0.1) B_{10} \text{ Burnup, a/o}$$

→ (DRN 00-644; 06-895, R15)

This relationship was obtained from experimental irradiations on high density (90 percent theoretical density) wafers⁽³⁹⁾ and pellets with densities ranging between 71 and 98 percent TD.⁽³⁸⁾⁽⁴⁰⁾ Dimensional changes were measured as a function of burnup, after irradiating at temperatures expected in the Waterford 3 design.

← (DRN 00-644; 06-895, R15)

- 2) Thermal Conductivity. The thermal conductivity of unirradiated 73 percent dense B_4C decreases linearly with temperatures from 300 to 1600°F, according to the relationship:

$$\lambda = \frac{1 \text{ cal / cm}^\circ\text{K} \cdot \text{sec}}{2.17(6.87 + 0.017 T)}$$

This relationship was obtained from measurements performed on pellets ranging from 70 to 98 percent TD.⁽⁴¹⁾

The relationship between the thermal conductivity of irradiated 73 percent TD B_4C pellets and temperature given below was derived from measured values⁽⁴¹⁾ on higher density pellets irradiated to fluences out to 3×10^{22} nvt (E > 1 MeV).

$$\lambda = \frac{1 \text{ cal / cm}^\circ\text{K} \cdot \text{sec}}{2.17(38 + 0.025 T)}$$

where T = temperature, °K

Thermal conductivity measurements of 17 B_4C specimens with densities ranging from 83 to 98 percent TD, irradiated at temperatures from 930 to 1600°F showed that thermal conductivity decreased significantly after irradiation. The rate of decrease is high at the lower irradiation temperatures, but saturates rapidly with exposure.

WSES-FSAR-UNIT-3

- 3) Helium Release. Helium is formed in B₄C as B₁₀ burnup proceeds. The fraction of helium released from the pellets is important for determining rod internal gas pressure. The relationship between helium release and irradiation temperature given below was developed at ORNL⁽⁴²⁾ to fit experimental data obtained from thermal reactor irradiations.

→(DRN 00-644)

$$\% \text{ He release} = e(A - 1.85D)e^{-\frac{Q}{RT}} + 5$$

←(DRN 00-644)

where:

A = Constant, 6.69 for ABB CE pellets

D = Fractional density, 0.73 for ABB CE pellets

Q = Activation energy constant, 3600 cal/mole

→(DRN 06-895, R15)

R = Gas constant, 1.98 cal/mole -°K

←(DRN 06-895, R15)

T = Pellet temperature, °K

This expression becomes

$$\% \text{ He release} = 208e^{-\frac{1820}{T}} + 5$$

when the above parameters are substituted. In this form, design values for helium release as a function of temperature are generated. The five percent helium release allowance (the last term in the expression) was added to ensure that design values lie above all reported helium release data. Calculated values of helium release obtained from the recommended design expression lie above all experimental data points⁽³⁸⁾⁽⁴³⁾⁽⁴⁴⁾ obtained on B₄C pellet specimens irradiated in thermal reactors.

- 4) Pellet Porosity. Experimental evidence is available⁽⁴⁵⁾ which shows that for pellet densities below 90 percent, essentially all porosity is open at beginning-of-life. Irradiation induced swelling does not change the characteristics of the porosity, but only changes the bulk volume of the specimens. Therefore, the amount of porosity available at end-of-life is the same as that present at beginning-of-life.

b) Silver-Indium-Cadmium Properties

- 1) Swelling. Measurements performed on Ag-In-Cd rods irradiated at fluences up to 6.2×10^{21} nvt (E>0.6 eV) were employed to develop the following expression to predict the volumetric swelling for silver-indium-cadmium alloy:

$$\% \Delta V = \frac{0.3\phi}{10^{21}}$$

where ϕ = fluence, nvt (E>0.6 eV).

WSES-FSAR-UNIT-3

Linear swelling is approximately one-third of the volumetric swelling.

- 2) Thermal Conductivity. The increase in cadmium content from five to perhaps 10 w/o, and the formation of two to three w/o tin as a result of long-term exposures, is expected to decrease the thermal conductivity from the accepted⁽⁴⁶⁾ unirradiated values. Published data for unirradiated Ag-Cd binary alloys shows that thermal conductivity was decreased by about 20 percent by increasing the cadmium content from 5.0 to 10.0 w/o.⁽⁴⁶⁾ Since irradiated Ag-In-Cd is expected to perform in much the same fashion, the unirradiated values of thermal conductivity are decreased by 25 percent to account for irradiation.
 - 3) Linear Thermal Expansion. The coefficient of linear thermal expansion for unirradiated Ag-In-Cd material is 12.5×10^{-6} in./in.-°F over the temperature range of 70 to 930°F⁽⁴⁷⁾ Published data on unirradiated⁽⁴⁶⁾ Ag-Cd binary alloys reveal that a cadmium increase of five percent will result in about a five percent increase in thermal expansion coefficient. The small changes in indium and tin content do not influence the thermal coefficient appreciably. For simplicity, the irradiated value of 13.1×10^{-6} in./in.-°F is used in all design calculations.
 - 4) Melting Point. The melting point of unirradiated Ag-In-Cd has been measured as $1470 \pm 30^\circ\text{F}$ ⁽⁴⁶⁾ ($800 \pm 17^\circ\text{C}$). The formation of three w/o tin due to the transmutation of indium and the increase in cadmium content to about 10 w/o due to the transmutation of silver may result in a small decrease in the melting point.
- c) Inconel 625 Properties
- 1) Swelling. Available information indicates that Inconel 625 is highly resistant to radiation swelling. Exposure of Inconel 625 to a fluence of 3×10^{22} nvt ($E > 0.1$ MeV) at a temperature of 400°C (752°F) showed no visible cavities in metallographic examinations⁽⁴⁸⁾ so that swelling, if any, would be very minor. Direct measurements made after exposure of Inconel 625 to fluence of 5×10^{22} nvt ($E > 0.1$ MeV) at LMFBR conditions showed no evidence, of swelling.⁽⁴⁹⁾ Thus, Inconel 625 after fluences of 3×10^{22} nvt (> 0.1 MeV) is not expected to swell.
 - 2) Ductility. The ductility of Inconel 625 decreases after irradiation. Extrapolation of lower fluence data on Inconel 625 and 500 indicates that the values of uniform and total elongation of Inconel 625 after 1×10^{22} nvt ($E > 1$ MeV) are three and six percent, respectively.

WSES-FSAR-UNIT-3

4.2.1.5 Surveillance Program

4.2.1.5.1 Requirements for Surveillance and Testing of Irradiated Fuel Rods

→(DRN 02-1538)

High burnup performance experience, as described in Subsection 4.2.2 has provided evidence that the fuel will perform satisfactorily under the design conditions. The current core design bases do not include a specific requirement for testing of irradiated fuel rods. However, the fuel assembly design allows disassembly and reassembly to facilitate such inspections, should the need arise.

←(DRN 02-1538)

A fuel rod irradiation program has been developed to evaluate the performance of the fuel rods designed for use in the 16 x 16 fuel assembly. The program includes the irradiation of six standard 16 x 16 assemblies, two each for one, two, and three cycles, respectively, in the Arkansas Nuclear One Unit 2 reactor (ANO-2). Each assembly will contain a minimum of 50 precharacterized, removable rods distributed within the assembly to obtain a spectrum of exposure levels for evaluation purposes in interim and terminal examinations. Interim examination of all six assemblies is planned during refueling shutdowns after each cycle.

→(DRN 02-1538)

The ANO-2 fuel rods and specific components of the fuel rods will receive detailed precharacterizations. The program calls for substantial cladding characterization to include mechanical properties, texture, hydride orientation and out-of-reactor low strain rate behavior. In addition to the ID and OD dimensional data normally obtained on the clad tubing material, a minimum of 300 fuel rods will be profiled to obtain as-loaded dimensions. Sufficient fuel rods will be profiled to obtain diameter and quality measurements such that changes in these parameters can be tracked by similar measurements during interim inspections. Also, a random selection of approximately 100 UO₂ pellets from each lot per batch used will be characterized dimensionally and the density distribution will be determined. About one-half of these pellets will be placed in known axial locations in selected fuel rods while the remainder will be set aside as archives.

A poolside non-destructive examination will be made during each of the first three refuelings at ANO-2. The six 16 x 16 assemblies with characterized rods will be removed from the reactor at each refueling and moved to the spent fuel pool for leak testing (if failed fuel is in the core) and for visual inspection. The length of the assembly and peripheral rods will be measured. During the shutdown, a target of 20 precharacterized rods per batch will be scheduled for examination and measurement. At some time after the refueling outage, pre-characterized rods retained in discharged assemblies will be measured. A target of 100 rods will be eddy current tested after each shutdown.

←(DRN 02-1538)

A post irradiation fuel surveillance program for Waterford 3 is planned. This program shall consist of a visual inspection of a minimum of six irradiated assemblies prior to replacement of the Reactor Vessel Head at each of the first three refueling outages. The six assemblies inspected shall consist of two assemblies of each fuel type and will be from core locations which are non-adjacent. Visual inspections shall consist of viewing the top and sides of each fuel assembly via an underwater TV camera or periscope.

WSES-FSAR-UNIT-3

The visual inspection will include observation with special attention to gross problems involving cladding defects, spacer grid damage and other major structural abnormalities. No special measurement devices for these effects are intended to be provided for this visual inspection.

If major abnormalities are detected during this visual inspection or if plant instrumentation indicates gross fuel failures, the fuel vendor will be informed and further inspections shall be performed. Depending on the nature of the observed condition, further examination could include fuel sipping, single rod examination and other examinations. The 16 x 16 fuel design enables reconstitution. Individual fuel rods and other structural components may be examined and replaced, if required. Under unusual circumstances, destructive examination of a fuel rod may be required but this would not be accomplished on site or during the refueling outage.

The NRC shall be contacted regarding gross fuel failure detected by plant instrumentation or major abnormalities observed during the post irradiation inspections described above.

→(DRN 02-1538)

The post fuel irradiation fuel surveillance program shall be continued following the first three cycles of operation of Waterford 3. Six assemblies shall be visually inspected during each refueling outage, not necessarily prior to replacement of the reactor vessel head. The visual inspection shall consist of viewing the tops and sides of each fuel assembly via an underwater TV camera or periscope. The visual inspection will include observation with special attention to gross problems involving cladding defects, spacer grid damage, and other major structural abnormalities. The NRC will be notified of major abnormalities noted as a result of these inspection activities.

←(DRN 02-1538)

4.2.2 DESCRIPTION AND DESIGN DRAWINGS

This subsection summarizes the mechanical design characteristics of the fuel system and discusses the design parameters which are of significance to the performance of the reactor. A summary of mechanical design parameters is presented in Table 4.2-1. These data are intended to be descriptive of the design; limiting values of these and other parameters will be discussed in the appropriate sections.

4.2.2.1 Fuel Assembly

The fuel assembly (Figure 4.2-8) consists of 236 fuel and poison rods, five control element assembly guide tubes, 11 fuel rod spacer grids, upper and lower end fittings, and a hold-down device. The outer guide tubes, spacer grids, and end fittings form the structural frame of the assembly.

→(DRN 02-1538)

The fuel spacer grids (Figure 4.2-9) maintain the fuel rod array by providing positive lateral restraint to the fuel rod but only frictional restraint to axial fuel rod motion. The grids are fabricated from pre-formed Zircaloy or Inconel strips (the bottom, and in some cases the top, spacer grid material is Inconel) interlocked in an egg crate fashion and welded together. Each cell of the spacer grid contains two leaf springs and four arches. The leaf springs press the rod against the arches to restrict relative motion between the grids and the fuel rods. The perimeter strips contain features designed to prevent hangup of grids during a refueling operation.

←(DRN 02-1538)

WSES-FSAR-UNIT-3

→(DRN 02-1538, R12; 04-502, R13)

The Zircaloy-4 spacer grids are fastened to the Zircaloy-4 guide tubes by welding, and each grid is welded to each guide tube at eight locations, four on the upper face of the grid and four on the lower face of the grid, where the spacer strips contact the guide tube surface. The lowest spacer grid (Inconel) is not welded to the guide tubes due to material differences. It is supported by an Inconel 625 skirt which is welded to the spacer grid and to the perimeter of the lower end fitting. For the assembly design with an Inconel top spacer grid, the grid is retained by ten Zircaloy-4 sleeves (five above and five below the grid) that are welded to the guide tubes at four locations per sleeve.

←(DRN 02-1538, R12; 04-502, R13)

→(LBDCR 15-025, R309)

The upper end fitting is an assembly consisting of two cast stainless steel plates, five machined posts and five helical Inconel X-750 springs, which attaches to the guide tubes to serve as an alignment and locating device for each fuel assembly and has features to permit lifting of the fuel assembly. The lower cast plate locates the top ends of the guide tubes and is designed to prevent excessive axial motion of the fuel rods.

←(LBDCR 15-025, R309)

The Inconel X-750 springs are of conventional coil design having a coil diameter of 1.844 in., a wire diameter of 0.299 in., and approximately 14 active coils. Inconel X-750 was selected for this application because of its previous use for coil springs and good resistance to relaxation during operation.

→(DRN 02-1538, R12)

The upper cast plate of the assembly, called the hold-down plate, together with the helical compression springs, comprise the hold-down device. The hold-down plate is movable, acts on the underside of the fuel alignment plate, and is loaded by the compression springs. Since the springs are located at the upper end of the assembly, the spring load combines with the fuel assembly weight to counteract upward hydraulic forces. The determination of upward hydraulic forces includes factors accounting for flow maldistribution, fuel assembly component tolerances, crud buildup, drag coefficient, and bypass flow. The springs are sized and the spring preload selected such that a net downward force will be maintained for all normal and anticipated transient flow and temperature conditions. The design criteria limit the maximum stress under the most adverse tolerance conditions to below yield strength of the spring material. The maximum stress occurs during cold conditions and decreases as the reactor heats up. The reduction in stress is due to a decrease in spring deflection resulting from differential thermal expansion between the Zircaloy fuel bundles and the stainless steel internals.

←(DRN 02-1538, R12)

During normal operation, a spring will never be compressed to its solid height. However, if the fuel assembly were loaded in an abnormal manner such that a spring were compressed to its solid height, the spring would continue to serve its function when the loading condition returned to normal.

The lower end fitting is a single piece stainless steel casting consisting of a plate with flow holes and four support legs which also serve as alignment posts. Precision drilled holes in the support legs mate with four core support plate alignment pins, thereby properly locating the lower end of the fuel assembly.

WSES-FSAR-UNIT-3

→(DRN 02-1538, R12)

The four outer guide tubes have a widened region at the upper end which contains an internal thread. Connection with the upper end fitting is made by passing the male threaded end of the guide posts through holes in the lower cast flow plate and into the guide tubes. When assembled, the flow plate is secured between flanges on the guide tubes and on the guide posts. The connection with the upper end fitting is locked with a mechanical crimp. Each outer guide tube has, at its lower end, a welded Zircaloy-4 fitting. This fitting has a female threaded portion which accepts a stainless steel bolt, which passes through a hole in the lower end fitting, to secure it. This joint is secured with a stainless steel locking ring tack welded to the lower end fitting in four places.

←(DRN 02-1538, R12)

The central guide tube inserts into a socket in the upper end fittings and is thus retained laterally by the relatively small clearance. The upper end fitting socket is created by the center guide tube post which is threaded into the lower cast flow plate and tack welded in two places.

→(EC-9533, R302)

The NGF design incorporates many of the same features and geometry as the standard fuel assembly, but incorporates a full complement of innovative components to improve fuel reliability, fuel cycle economics, fuel duty, manufacturability, burnup capability, and thermal performance. The major differences between the two designs are the following:

- The NGF assembly uses bulged joints to build the grid cage versus welded joints and uses a pull rod loading process versus the current push loading process. These process changes were selected for NGF to improve the fabricability of the design while preserving the rigidity of the fuel assembly structure.
- The guide thimbles are made of SRA Zircaloy-4 in the prior designs and SRA ZIRLO™ in the NGF design. This change was made because of ZIRLO™'s improved corrosion resistance and dimensional stability under irradiation.
- The NGF guide tube flange, which includes an anti-rotation feature to prevent the transmission of torque to the grids during post installation/removal, is connected to the guide tube by bulging instead of by welding as in the standard design. The bulged flange to guide tube connection retains adequate strength and is necessary to compensate for the axial shrinkage of the guide tubes due to bulging.
- The NGF top grid is made of Inconel-718 and has vertical springs and horizontal dimples. Stainless steel sleeves are brazed into the grid at guide tube locations and are bulged with the guide tubes during cage fabrication to secure the grid to the guide tubes. The design is comparable to others that have an extensive history of successful operation in Westinghouse NSSS nuclear power plants.

→(LBDCR 15-035, R309)

- The standard design Mid grids (HID-1L, Figure 4.2-5) are made using wavy strap Zircaloy-4, while the NGF Mid grids use straight strap Optimized ZIRLO™. The material change was made because of Optimized ZIRLO™'s improved corrosion resistance and dimensional stability under irradiation. The straight straps allow the incorporation of the "I-spring" design and mixing vanes for improved fretting and thermal performance, respectively. Sleeves fabricated from Optimized ZIRLO™ are laser-welded into the guide tube openings and secured to the guide tubes by bulges both above and below the grid.

←(LBDCR 15-035, R309)

- Two IFM grids are included to improve thermal performance in two critical grid spans near the top for active core. These grids are short, non-structural grids that are made from straight strap Optimized ZIRLO™ with side-supported mixing vanes and opposing dimples with small grid-to-rod gaps in lieu of an active (preloaded spring-dimple) support system. The IFM grids have sleeves that are similar to the Mid grid sleeves, except the protrusion of the sleeve above the IFM grids is less than above the Mid grids because the IFM sleeves are only bulged to the guide tubes below the grid.

←(EC-9533, R302)

→(EC-9533, R302; EC-30663, R307)

- The lower portion of the NGF assembly includes several changes to accommodate rod push loading. In lieu of welding, the NGF Guardian™ grid is retained by inserts that are laser-welded to the four outer guide tube openings and then clamped between the bottom of the guide tube and the lower end fitting. To facilitate the installation of the lower end fitting after the rods have been pulled into the grid cage, a small gap remains between the bottoms of the NGF fuel rods and the bottom nozzle. This gap, in combination with associated changes to the lower end cap design, result in the bottom of the active fuel column being 0.165 inches higher than the prior design. The head of the NGF bolt has a skirted region that is crimped into recesses in the lower end fitting to secure the bolt, rather than using a separate locking disc that is welded to the lower end fitting to secure the bolt. The NGF bolt also includes a hole through the center of the bolt to allow water to drain out of the guide tubes after washing the fuel assemblies during fabrication, or prior to the installation of the fuel assemblies in dry casks for spent fuel storage.

←(EC-30663, R307)

- The NGF fuel rod design includes several changes relative to the standard fuel rod design, the most significant of which are the reduced diameter/thickness of the cladding, a modified pellet geometry, the use of Optimized ZIRLO™ cladding, and an increase in the overall rod length. These changes, as well as the other design changes associated with the NGF fuel rods, are detailed in Section 4.2.2.2.

←(EC-9533, R302)

The five guide tubes have the effect of ensuring that bowing or excessive swelling of the adjacent fuel rods cannot result in obstruction of the control element pathway. This is so because:

- a) There is sufficient clearance between the fuel rods and the guide tube surface to allow an adjacent fuel rod to reach rupture strain without contacting the guide tube surface.
- b) The guide tube, having considerably greater diameter and wall thickness (and also being at a lower temperature) than the fuel rod, is considerably stiffer than the fuel rod and would, therefore, remain straight, rather than be deflected by contact with the surface of an adjacent fuel rod.

Therefore, the bowing or swelling of fuel rods would not result in obstruction of the control element channels such as could hinder CEA movement.

The fuel assembly design enables reconstitution, i.e., removal and replacement of fuel and poison rods, of an irradiated fuel assembly. The fuel and poison rod lower end caps are conically shaped to ensure proper insertion within the fuel assembly grid cage structure; the upper end caps are designed to enable grappling of the fuel and poison rod for purposes of removal and handling. Threaded joints which mechanically attach the upper end fitting to the control element guide tubes will be properly torqued and locked during service, but may be removed to provide access to the fuel and poison rods.

Loading and movement of the fuel assemblies is conducted in accordance with strictly monitored administrative procedures and, at the completion of fuel loading, an independent check as to the location and orientation of each fuel assembly in the core is required.

→(DRN 00-644; 02-1538, R12)

Markings provided on the fuel assembly upper end fitting enable verification of fuel enrichment and orientation of the fuel assembly. Identical markings are provided on the lower end fitting to ensure preservation of fuel assembly identity in the event of upper end fitting removal. Additional markings are provided on each fuel rod during the manufacturing process to distinguish between fuel enrichments and burnable poison rods, if present.

←(DRN 00-644; 02-1538, R12)

→(DRN 00-644; 02-1538, R12)

During the manufacturing process, each fuel rod is marked in order to facilitate a means of maintaining a record of pellet enrichment, pellet lot and fuel stack weight. In addition, a quality control program specification requires that measures be established for the identification and control of materials, components, and partially fabricated subassemblies. These means provide assurance that only acceptable items are used and also provide a method of relating an item or assembly from initial receipt through fabrication, installation, repair, or modification to an applicable drawing, specification, or other pertinent technical document.

←(DRN 00-644; 02-1538, R12)

4.2.2.2 Fuel Rod

→(DRN 02-1538, R12; 06-1059, R15)

The fuel rods consist of slightly-enriched UO_2 cylindrical ceramic pellets, a round wire Type 302 stainless steel compression spring, and an alumina spacer disc located at each end of the fuel column, all encapsulated within a Zircaloy-4 tube seal welded with Zircaloy-4 end caps. The upper alumina disc was removed in the Batch S rod assemblies, and both spacers were removed from the Batch U and subsequent reload fuel. Beginning with Batch U, a Tungsten Inert Gas (TIG) welding is utilized, using a friction fit of the cladding on a reduced diameter pedestal section of the end cap. Beginning with Batch Y, the ZIRLO™ cladding tubes are used and are TIG welded with the Zircaloy-4 end caps. The fuel rods are internally pressurized with helium during assembly. Figure 4.2-10 depicts the fuel rod design.

←(DRN 02-1538, R12; 06-1059, R15)

Each fuel rod assembly includes a unique serial number. The serial number ensures traceability of the fabrication history of each fuel rod component. Finished fuel rods, prior to being loaded into bundles, are processed through a rod scanner to check pellet enrichment.

→(EC-9533, R302)

The fuel cladding is cold-worked and stress relief annealed Zircaloy-4 tubing 0.025 in. thick. The actual tube forming process consists of a series of cold working and annealing operations, the details of which are selected to provide the combination of properties discussed in Subsection 4.2.1.2.2.

←(EC-9533, R302)

The UO_2 pellets are dished at both ends in order to better accommodate thermal expansion and fuel swelling. The initial density of the UO_2 pellets is 10.44 g/cm^3 , which corresponds to 95.25 percent of the 10.96 g/cm^3 theoretical density (TD) of UO_2 . However, because the pellet dishes and chamfers constitute about three percent of the volume of the pellet stack, the average density of the pellet stack is reduced to 10.11 g/cm^3 . This number is referred to as the "stack density."

→(DRN 06-1059, R15)

Note that the initial pellet density and stack density for Erbia pellets used in Erbia fuel rods (see Section 4.2.2.3) are slightly lower (respectively 10.41 and 10.09 g/cm^3) due to Erbia content. These densities for the ZrB_2 coated UO_2 (IFBA) pellets that were first introduced in Batch Y for Cycle 15 are consistent with those for the solid UO_2 pellets. However, the pellet stack density for the annular pellets used in the cutback zones of the pellet stack is lowered to 7.80 g/cm^3 (due to hollow center of 0.1625" diameter).

←(DRN 06-1059, R15)

→(DRN 02-1538, R12)

The compression spring located at the top of the fuel pellet column maintains the column in its proper position during handling and shipping. The fuel rod plenum, which is located above the pellet column, provides space for axial thermal differential expansion of the fuel column and accommodates the initial helium loading and evolved fission gases. (See Subsection 4.2.1.2.5.1 and 4.2.1.2.5.2). The specific manner in which these factors are taken into account, including the calculation of temperatures for the gas contained within the various types of rod internal void volume, is discussed in Reference 14.

→(EC-9533, R302)

Starting with Batch U, fuel rod fabrication was moved from Hematite, MO, to the Columbia, SC, facility. Figure 4.2-10A compares the Hematite and Columbia production uranium rod assembly features. Figure 4.2-11A compares the corresponding erbia rod assemblies.

←(DRN 02-1538, R12; EC-9533, R302)

→(EC-9533, R302)

The basic configuration of the NGF fuel rod (Figure 4.2-10B) and IFBA rod (Figure 4.2-11B) are comparable to the prior rod designs, but there are significant differences in the detailed design of the rods.

- The NGF rods have a smaller outside diameter than prior designs (0.374" versus 0.382") to compensate for some of the pressure drop increase associated with the NGF spacer grids. The 0.374" diameter rod is the same as the standard Westinghouse 17x17 design, which precipitated the use of the 17x17 cladding dimensions and pellet geometry for the NGF design. Therefore, the cladding outside/inside diameters are 0.374" and 0.329", while the fuel and IFBA pellets have a diameter of 0.3225", a length of 0.387", and a spherical dish at each end instead of a truncated dish. The blanket pellet associated with the IFBA rod has a diameter of 0.3225", a length of 0.500", and a central hole of 0.155". The corresponding stack densities for these pellet configurations are 10.31 g/cc for the fuel and IFBA pellets, and 8.00 g/cc for the blanket pellets.

→(LBDCR 15-035, R309)

- Optimized ZIRLO™ fuel cladding has been used to replace the ZIRLO™ fuel cladding. The topical report, Reference 83, summarizes the material properties as they pertain to fuel rod cladding, design and licensing activities. The difference between Optimized ZIRLO™ fuel cladding and ZIRLO™ cladding is that Optimized ZIRLO™ has a slight reduction in Tin content for improved corrosion resistance (0.6% minimum for Optimized ZIRLO™ versus 0.8% minimum for ZIRLO™). Reference 85 updates the cladding corrosion model.

←(LBDCR 15-035, R309)

- The overall length of the NGF fuel rod is increased by 0.7" to minimize the loss of void volume associated with the diameter reduction of the rod. To further offset the effect of the diameter reduction, the initial fill gas pressure of the fuel rods has been reduced to approximately 275 psig.

→(EC-13881, R304)

- The nominal active length remains 150" for both the fuel and IFBA rods. The fuel rod stack continues to exclude any cutback/blanket pellets, while the IFBA rod stack has a cutback/blanket zone at each end of the center pellet column (See Fig. 4.3A-19b).

←(EC-13881, R304)

- The bottom end cap has been modified to accommodate a recess in the bottom end that is necessary for pull-loading the rods into the fuel assemblies. The length of the upper end cap has been reduced and the "acorn" removed to allow as large an increase as possible to the plenum to facilitate the accommodation of fission gas release.

4.2.2.3 Burnable Poison Rod

→(DRN 02-1477, R12)

Fixed burnable neutron absorber (poison) rods, Figure 4.2-11, will be included in selected fuel assemblies to reduce the beginning-of-life moderator coefficient. They will replace fuel rods at selected locations. The poison rods will be mechanically similar to fuel rods. The poison material will be alumina with uniformly-dispersed boron carbide particles. The balance of the column will consist of two Zircaloy-4 spacers with the total column length the same as the column length in fuel rods. The burnable poison rod plenum spring is designed to produce a smaller preload on the pellet column than that in a fuel rod because of the lighter material in the poison pellets.

←(DRN 02-1477, R12; EC-9533, R302)

Each burnable poison rod assembly includes a unique serial number. The serial number is used to record fabrication information for each component in the rod assembly.

→(DRN 02-1477, R12; 06-1059, R15; EC-9533, R302)

←(DRN 02-1477, R12; 06-1059, R15; EC-9533, R302)

4.2.2.4 Control Element Assembly Description and Design Drawings

→(DRN 01-1103, R12; 02-1477, R12)

The Waterford 3 reactor contains a total of 87 CEAs. These are distributed among the fuel assemblies as shown in Figure 4.2-12. The CEA is shown in Figure 4.2-5. CEAs have four control elements arranged in a 4.050-in. square array plus one element at the center of the array. Each CEA interfaces with the guide tubes of one fuel assembly.

←(DRN 01-1103, R12; 02-1477, R12)

→(DRN 02-1477, R12)

←(DRN 02-1477, R12)

→(DRN 02-1477, R12)

The control elements of a CEA consist of an Inconel 625 tube loaded with a stack of cylindrical absorber pellets. The absorber material consists of 73 percent TD boron carbide (B_4C) pellets, with the exception of the lower portion of the elements, which contain silver-indium-cadmium (Ag-In-Cd) alloy cylinders.

←(DRN 02-1477, R12)

Two design objectives are realized by the use of Ag-In-Cd in the element tip zones:

a) CEA Cladding Dimensional Stability

Because of its high ductility and low strength, the Ag-In-Cd will not deform the CEA cladding. Buffering of the CEA following scram, which occurs when the corner element tips enter a reduced diameter portion of the fuel assembly guide tubes, is not degraded with long term exposure of the CEA to reactor operating conditions.

b) Adequate CEA Worth

Although some reduction in CEA worth arises because of the substitution of B_4C with Ag-In-Cd, the effect is small and is accounted for.

During normal powered operation, most of the CEAs are expected to be in the fully withdrawn position.

Above the poison column is a plenum which provides expansion volume for helium released from the B_4C . The plenum volume contains a Type 302 stainless steel hold-down spring, which restrains the absorber material against longitudinal shifting with respect to the clad while allowing for differential expansion between the absorber and the clad. The spring develops a load sufficient to maintain the position of the absorber material during shipping and handling.

→(DRN 02-1477, R12)

Each control element is sealed by welds which join the tube to an Inconel 625 nose cap at the bottom, and an Inconel 625 end fitting at the top. The end fittings, in turn, are threaded and pinned to the spider structure which provides rigid lateral and axial support for the control elements. The spider hub bore is specially machined to provide a point of attachment for the CEA extension shaft.

←(DRN 02-1477, R12)

→(DRN 01-1103, R12)

←(DRN 01-1103, R12)

→(DRN 00-644; 01-1103, R12; 02-1477, R12)

Each CEA is positioned by a magnetic jack control element drive mechanism (CEDM) mounted on the reactor vessel closure head. The extension shaft joins with the CEA spider and connects the CEA to the CEDM. CEAs may be connected to any extension shaft depending on control requirements. Mechanical reactivity control is achieved by positioning groups of CEAs by the CEDMs.

←(DRN 00-644; 02-1477, R12)

In the outlet plenum region, all CEAs are enclosed in CEA shrouds which provide guidance and protect the CEA and extension shaft from coolant cross flow. Within the core, each element travels in a Zircaloy guide tube. The guide tubes are part of the fuel assembly structure and ensure proper orientation of the control elements with respect to the fuel rods.

←(DRN 01-1103, R12)

When the extension shaft is released by the CEDM, the combined weight of the shaft and CEA causes the CEA to insert into the fuel assembly.

→(DRN 01-1103, R12; 02-1477, R12)

The lower ends of the four outer fuel assembly guide tubes are tapered gradually to form a region of reduced diameter which, in conjunction with the outer control element on the CEA, constitutes an effective hydraulic buffer for reducing the deceleration loads at the end of a trip stroke. This purely hydraulic damping action is augmented by a spring and plunger arrangement on the CEA spider. When fully inserted, CEAs rest on the central post of the fuel assembly upper end fitting.

←(DRN 01-1103, R12; 02-1477, R12)

The capability of the CEAs to scram within the allowable time is demonstrated as part of the flow testing discussed in Subsection 4.2.4.4.

4.2.3 DESIGN EVALUATION

4.2.3.1 Fuel Assembly

4.2.3.1.1. Vibration Analyses

Three sources of periodic excitation are recognized in evaluating the fuel assembly susceptibility to vibration damage. These sources are as follows:

a) Reactor Coolant Pump Blade Passing Frequency

Precritical vibration monitoring on previous C-E reactors indicates the peak pressure pulses are expected at the pump blade passing frequency, and a lesser but still pronounced peak at twice this frequency.

b) Core Support Plate Motion

Experience with earlier C-E reactors indicates that random lateral motion of the core support plate is expected to occur with an amplitude of 0.001 to 0.002-in. and a frequency range of between 2 and 10 Hz.

c) Flow-induced vibration resulting from coolant flow through the fuel assembly.

The capability of the Waterford 3 16 x 16 fuel assembly to sustain the effects of flow-induced vibration without adverse effects has been demonstrated in a dynamic flow test performed in CE's TF-2 flow test facility. The test utilized prototypical 16 X 16 reactor components consisting of a 16 X 16 type fuel assembly, a CEA shroud, control element drive mechanism, and a simulation of surrounding core internal support components and was performed under extreme flow and temperature conditions. The success of this test, similar previous tests of 16 X 16 fuel assemblies and the operation of CE's ANO-2 plant, demonstrate that flow-induced vibration will have no adverse effects on the Waterford 3 fuel assemblies.

→(EC-9533, R302)

The NGF fuel assembly design was designed to have a lateral stiffness comparable to the prior designs that have operated successfully in the Waterford plant. In addition, the NGF configuration was tested to confirm the hydraulic stability of the fuel assembly design and to demonstrate the acceptability of the fretting performance of the fuel assembly design. The testing included full scale single and dual bundle tests with both the NGF design and the standard design. The single bundle tests demonstrated the hydraulic stability of both designs over the expected range of flow rates. The dual bundle test was an endurance test that provided additional confirmation of the hydraulic stability of the designs and showed a significant improvement in the fretting performance of the NGF design compared to the standard design. These results indicate that the NGF design is even less susceptible to any vibration effects than the prior designs.

←(EC-9533, R302)

These sources of periodic motion are not expected to have an adverse effect on the performance of the Waterford 3 fuel assembly.

4.2.3.1.2 CEA Guide Tube

The CEA guide tubes were evaluated for structural adequacy using the criteria given in Subsection 4.2.1.1 in the following areas:

- a) Steady axial load due to the combined effects of axial hydraulic forces and upper end fitting holddown forces.

For normal operating conditions, the resultant guide tube stress levels satisfy the criteria given in Subsection 4.2.1.1.1.

- b) Short-term axial load due to the impact of the spring loaded CEA spider against the top of the fuel assembly at the end of a CEA trip.

For trips occurring during normal power operation, solid impact is not predicted to occur due to the kinetic energy of the CEA being dissipated in the hydraulic buffer and by the CEA spring.

- c) Short-term differential pressure load occurring in the hydraulic buffer regions of the outer guide tubes at the end of each trip stroke.

The buffer region slows the CEA during the last few inches of the trip stroke. The resultant differential pressure across the guide tube in this region is predicted to be 300 psi, and this gives rise to circumferential stresses of 3300 psi, which is less than one quarter of the yield stress, for a very short term. The trip is assumed to be repeated daily. However the resultant stress is too small to have a significant effect on fatigue usage.

For conditions other than normal operation, the additional mechanical loads imposed on the fuel assembly by an OBE (equivalent to one-half SSE), SSE, and large break LOCA and their resultant effect on the control element guide tubes are discussed in the following paragraphs:

4.2.3.1.2.1 Operating Basis Earthquake

During the postulated OBE, the fuel assembly is subjected to lateral and axial accelerations which, in turn, cause the fuel assembly to deflect from its normal shape. The method of calculating these deflections is described in Subsection 3.7.3.14. The magnitude of the lateral deflections and resultant stresses are evaluated for acceptability. The method for calculating stresses from deflected shapes is described in Reference 50. The results of the stress analysis demonstrate that the equipment stresses are less than the allowable values discussed in Subsection 4.2.1.1.

4.2.3.1.2.2 Safe Shutdown Earthquake

The axial and lateral loads and deformation sustained by the fuel assembly during a postulated SSE have the same origin as those discussed above for the OBE, but they arise from initial ground accelerations twice those used for the OBE. The analytical methods used for the SSE are identical to those used for the OBE. The predicted component stresses were less than the allowable values discussed in Reference 50.

4.2.3.1.2.3 Loss-of-Coolant Accident

→(DRN 03-2058, R14)

In the event of a large break LOCA, there will occur rapid changes in pressure and flow within the reactor vessel. Associated with the transient are relatively large axial and lateral loads on the fuel assemblies.

←(DRN 03-2058, R14)

→(DRN 03-2058, R14)

The response of a fuel assembly to the mechanical loads produced by a LOCA is considered acceptable if the fuel rods are maintained in a coolable array, i.e., acceptably low grid crushing. The methods used for analysis of combined seismic and LOCA loads and stresses is described in Reference 50. See Sections 3.6.2.1.1.1(d) and 3.6.3 for discussions on pipe break criteria and leak-before-break.

→(DRN 00-644)

←(DRN 03-2058, R14)

To qualify the complete fuel assembly, full-scale hot loop testing has been conducted. The tests were designed to evaluate fretting and wear of components, refueling procedures, fuel assembly uplift forces, holddown performance and compatibility of the fuel assembly with interfacing reactor internals, CEAs and CEDMs under conditions of reactor water chemistry, flow velocity, temperature, and pressure. Additional information on the test is given in Subsection 4.2.3.2.4.2. The test was run for approximately 2000 hours and was completed in 1976.

←(DRN 00-644)

Mechanical testing of the fuel assembly and its components has been performed to support analytical means of defining the assembly's structural characteristics. The test program consisted of static and dynamic tests of spacer grids and static and vibratory tests of a full size fuel assembly.

4.2.3.1.2.4 Combined SSE and LOCA

It is not considered appropriate to combine the stresses resulting from the SSE and LOCA events. Nevertheless for purposes of demonstrating margin in the design, the maximum stress intensities for each individual event were combined by a square root of the sum of the squares (SRSS) method. This was performed as a function of fuel assembly elevation and position, e.g., the maximum stress intensities for the center guide tube at the upper grid elevation (as determined in the analysis discussed in Subsections 4.2.3.1.2.2 and 4.2.3.1.2.3) were combined by the SRSS method. The results demonstrated that the allowable stresses described in Reference 50 were not exceeded for any position along the fuel assembly, even under the added conservatism provided by this load combination.

4.2.3.1.3 Spacer Grid Evaluation

As discussed in Subsection 4.2.2.1 the function of the spacer grids is to provide lateral support to fuel and burnable poison rods in such a manner that the axial forces are not sufficient to buckle or bow the rods and that the wear resulting at the grid-to-clad contact points will be limited to acceptably small amounts. It is also a criterion that the grid be capable of withstanding the lateral loads imposed during the postulated seismic and LOCA events.

→(DRN 02-1538, R12)

With respect to the design criterion that the axial restraint offered by the grids during initial assembly be such that the axial forces on a fuel rod are not sufficient to cause the rod to bow or buckle, it is currently understood that the observed instances of fuel rod bowing have occurred because the axial restraint of the spacer grids on the fuel rods was such that relative motion between the fuel rods and the grids (e.g., differential thermal expansion) could not occur except at axial forces high enough to cause slight bowing of the fuel rods. Fuel assemblies, however, are designed such that the combination of fuel rod rigidity, grid spacing, and grid preload will not cause significant fuel rod deformation under axial loads. The long-term effects of clad creep (reduction in clad OD), the reduction of grid stiffness with temperature, and the partial relaxation of the grid material during operation ensure that this criterion is also satisfied during all operating conditions. Moreover, visual inspection of irradiated fuel assemblies from the Maine Yankee (14 x 14), Palisades (15 x 15) and Fort Calhoun (14 x 14) reactors has not shown any significant bowing of the fuel rods. In view of these factors and the similarity of these designs to the Waterford 3 design, it is concluded that the axial forces applied by the grids on the cladding will not result in a significant degree of fuel rod bow. Additional discussion of the causes and effects of fuel rod bowing are contained in Subsection 4.2.3.2.6 and in References 53 and 75.

←(DRN 02-1538, R12)

→(EC-9533, R302)

The capability of the grids to support the clad without excessive clad wear has been demonstrated by out-of-pile flow testing, and by the results of post-irradiation examination of grid-to-clad contact points in Maine Yankee fuel assemblies which showed only negligible clad wear⁽⁵¹⁾. An extensive flow test program was conducted to support the implementation of the NGF design. A full scale dual bundle test with a NGF fuel assembly and a standard fuel assembly was run to demonstrate the acceptability of the fretting performance of the NGF assembly design. The dual bundle test was an endurance test that provided confirmation of the hydraulic stability of the designs and showed a significant improvement in the fretting performance of the NGF design compared to the standard design.

←(EC-9533, R302)

→(DRN 00-644)

The capability of the grid to withstand the lateral loads produced during the postulated seismic and LOCA events is demonstrated by impact testing of the reference grid design and comparing the test results with the analytical predictions of the seismic and LOCA loads. The test methods are discussed in Reference 50.

←(DRN 00-644)

→(DRN 03-2058, R14)

For the original fuel design, the results of the load comparison were that under seismic loading no spacer grids in the core were subjected to loadings in excess of their capability based on test results. However, under LOCA conditions some fuel assemblies in the periphery of the core had spacer grids with predicted loads which exceeded the capability defined by testing. An ECCS analysis was performed for the core locations occupied by these fuel assemblies, and the results confirmed that the ECCS acceptance criteria (10CFR50.46) were still satisfied. The methods used in the ECCS evaluation were the same as used in previous analyses (Reference 77). In order to demonstrate margin in the design, spacer grid loadings from the SSE and LOCA events were combined by a square root of the sum of squares (SRSS) method, and no additional fuel assemblies were found to have grids which exceeded the capability defined by testing.

With the introduction of the HID-1L grid design, the grid strengths increased above those of the original fuel design such that the grid strengths exceeded the maximum grid impact loads. There was therefore no further need to perform the ECCS analysis to show that the HID-1L grid design was acceptable.

For the power uprate condition, updated LOCA loadings were determined which included a combination of power uprate and Leak-Before-Break effects. Seismic loadings remained unchanged. Because the loadings used in the analyses performed for the original fuel design are conservative and bounding with respect to the uprate loadings, there was no need to reevaluate the fuel assemblies.

←(DRN 03-2058, R14)

→(EC-9533, R302)

The NGF design utilizes straight-strip mid grids that have a higher spacer grid stiffness than the HID-1L spacer grids of the prior fuel designs. Due to this increased grid stiffness, the seismic and LOCA analyses were reevaluated for the mixed core and all NGF core cases. The results showed that the documented strengths of the NGF and HID-1L spacer grids exceeded predicted impact loads, but that the loading history simulated in the determination of the HID-1L grid strength did not bound the predicted loading history in some peripheral core locations. Instead of retesting the HID-1L grids with the predicted mixed core loading history, an ECCS evaluation was performed to demonstrate compliance with the ECCS acceptance criteria.

The Zircaloy-4 spacer grid material is of the same composition as the fuel rods and guide tubes with which it is in contact, thereby obviating any problem of chemical incompatibility with those components. For the same reason, adequate resistance to corrosion from the coolant is assured (see Subsection 4.2.3.2.3, for additional information relative to the corrosion resistance of Zircaloy-4 in the primary coolant environment). Similarly, the NGF design is not susceptible to chemical incompatibility since it utilizes Optimized ZIRLO™ spacer grids and Optimized ZIRLO™ cladding. In addition, the use of Optimized ZIRLO™ for the spacer grids offers improved corrosion resistance relative to the Zircaloy-4 spacer grids.

←(EC-9533, R302)

→(DRN 02-1538, R12; 06-1059, R15, LBDCR 15-025, R309)

The Inconel-625 material used for the lowest, and in some cases the uppermost, spacer grid is in contact with the coolant, the stainless steel lower end fitting (to which it is welded), the Zircaloy-4 or ZIRLO™ fuel and poison rods, and the Zircaloy-4 guide tubes. The mutual chemical compatibility of these materials in a reactor environment has been demonstrated by the use of these materials in fuel assemblies that have been operated in other C-E reactors and for which post irradiation examination has yielded no evidence of chemical reaction between these components. In addition, experiments have also been performed at C-E on Inconel type alloys and Zircaloy-4 which showed the eutectic reactions did not occur below 2200°F, a temperature far in excess of that anticipated at the lower grid location in the event of a LOCA.

←(DRN 02-1538, R12; 06-1059, R15, LBDCR 15-025, R309)

→(EC-9533, R302)

The Inconel-718 material used for the top spacer grid in the NGF design has similar material characteristics to the Inconel-625 material and has operated successfully in Westinghouse plants for many years with ZIRLO™ clad fuel rods. The slight reduction in tin content of the Optimized ZIRLO™ cladding compared to the ZIRLO™ cladding does not impact its compatibility with Inconel-718, as evidenced by the successful operation of the NGF lead fuel assemblies in Waterford and in other Westinghouse reactors.

←(EC-9533, R302)

The only dissimilarity, between the fuel for which post-irradiation examination data are presently available and the Waterford 3 design (other than dimensional variations), is that the Inconel-625 is used as a spacer grid for Waterford 3 and was used originally as a retention grid. However, the effect that such a change might have on fretting behavior has been evaluated in out-of-pile flow test programs (see Subsection 4.2.3.2.4.2).

→(EC-9533, R302)

4.2.3.1.4

Dimensional Stability of Zirconium-Based Alloys

→(DRN 06-1059, R15)

Zircaloy components are designed to allow for dimensional changes resulting from irradiation-induced growth. Extension analyses of in-pile growth data have been performed to formulate a comprehensive model of in-pile growth. The in-pile growth equations are used to determine the minimum axial differential growth allowance which must be included in the axial gap between the fuel rods and the upper end fitting. For determining the necessary fuel rod growth allowance, the growth correlations for fuel rod and guide tube growth are combined statistically such that the minimum initial gap is adequate to accommodate the upper 95 percent confidence level of differential growth between fuel rods and guide tubes in the peak burnup assembly for Zircaloy, ZIRLO™, and Optimized ZIRLO™ clad rods. For the purpose of predicting axial and lateral growth of the fuel assembly structure (thereby establishing the minimum initial clearance with interfacing components), the equations are used in a conservative manner to ensure adequate margins to interference are maintained.

←(DRN 06-1059, R15; EC-9533, R302)

→(DRN 02-1538, R12)

Inspection of fuel assemblies after two cycles of operation at the Arkansas Nuclear One, Unit 2 reactor has shown higher rates of gap closure than predicted by the method described in Reference (3). Closure rates predicted by Reference (3) may remain valid for the Waterford 3 fuel assemblies because of differences in the Waterford and Arkansas designs. Nonetheless, additional shoulder gap has been provided in those fuel assemblies scheduled for three cycles of operation.

←(DRN 02-1538, R12)

The additional gap was selected to provide the maximum shoulder gap without violating other design criteria. Based on the shoulder gap reduction observed at ANO-2 at EOC2, the additional shoulder gap is expected to provide three cycle operation capability.

→(EC-9533, R302)

The NGF design incorporates material changes that improve the dimensional stability of the CEA guide tubes and the fuel rod cladding. These improvements allow a reduction in the NGF shoulder gap while still providing adequate space to accommodate rod burnups above 60,000 MWd/MTU.

←(EC-9533, R302)

4.2.3.1.5 Fuel Handling and Shipping Design Loads

Three specific design bases have been established for shipping and handling loads. These are as follows:

- a) The fuel assembly, when supported in the new fuel shipping container, shall be capable of sustaining the effects of five g axial, lateral or vertical acceleration without sustaining stress levels in excess of those allowed for normal operation. The five g criterion was originally established experimentally, and its adequacy is continually confirmed by the presence of impact recorders as described in the following paragraph.

Impact recorders are included with each shipment which indicate if loadings in excess of five g are sustained. A record of shipping loads in excess of five g indicates an unusual shipping occurrence in which case the fuel assembly is inspected for damage prior to releasing it for use.

The axial shipping load path is through either end fitting to the guide tubes. A five g axial load produces a compressive stress level in the guide tubes less than the two-thirds yield stress limit that is allowed for normal condition events. The fuel assembly is prevented from buckling by being clamped at grid locations. For lateral or vertical shipping loads, the grid spring tabs have an initial preload which exceeds five times the fuel rod weight. Therefore, the spring tabs see no additional deflection as a result of five g lateral or vertical acceleration of the shipping container. In addition, the side load on the grid faces produced by a five g lateral or vertical acceleration is less than the measured impact strength of the grids.

- b) The fuel assembly shall be capable of sustaining a 5000 pound axial load applied at the upper end fitting by the refueling grapple (and resisted by an equal load at the lower end fitting) without sustaining stress levels in excess of those allowed for normal operation. The 5000 pound load was chosen in order to provide adequate lift capability should an assembly become lodged. This load criterion is greater than any lift load that has been encountered in-service.
- c) The fuel assembly shall be capable of withstanding a 0.125 in. deflection in any direction whenever the fuel assembly is raised or lowered from a horizontal position without sustaining a permanent deformation beyond the fuel assembly inspection envelope.

Fuel handling procedures require the use of a strongback to limit the fuel assembly deflection to a maximum of 0.125 in. in any direction whenever the fuel assembly is raised or lowered to a horizontal position. This limits the stress and strain imposed upon the fuel assembly to values well below the limits set for normal operating conditions. The adequacy of the 0.125 in. criterion is based on the inclusion of this limitation in specifications and procedures for fuel handling equipment, which is thereby constrained to provide support that lateral deflection is limited to 0.125 in.

4.2.3.2 Fuel Rod Design Evaluation

The evaluations discussed in this section are based on assumed fuel rod operation within certain linear heat rate limits related to avoiding excessive fuel clad temperatures. Information concerning the bases for these limits is contained in Section 4.4.

4.2.3.2.1 Results of Vibration Analyses

Three sources of periodic excitation are recognized in evaluating the fuel rod susceptibility to vibration damage. These sources are as described in Subsection 4.2.3.1.1.

These sources of periodic motion are not expected to have an adverse effect on the performance of the fuel rod. Subsection 4.2.3.2.4 includes additional information on fuel rod response to the sources.

4.2.3.2.2 Fuel Rod Internal Pressure and Stress Analysis

→(DRN 02-1538, R12)

A fuel rod cladding stress analysis is conducted to determine the circumferential stress and strain resulting from normal, upset, and emergency conditions. The analysis includes the calculation of cladding temperatures and rod internal pressures during each of the occurrences listed in Subsection 4.2.1.1. The design criteria to be used to evaluate the analytical results are specified in Subsection 4.2.1.2.1. Fuel rod stresses resulting from seismic events are calculated, using the methodology described in Reference 50.

←(DRN 02-1538, R12)

4.2.3.2.3 Potential for Chemical Reaction

a) Corrosion

Corrosion tests of Zircaloy-4 fuel rod tubing which were conducted in excess of 4000 hours exposure include 600 and 650°F autoclave tests and 600°F loop tests with borated lithium hydroxide additives to the water chemistry. The test results agree with long term corrosion tests in lithium hydroxide reported by Bettis.⁽⁵²⁾ No deleterious effects have occurred.

→(DRN 02-1538, R12)

Experience at both Shippingport and Saxton Core I have shown under PWR conditions (hydrogen overpressure and chemical additives) that in reactor behavior with low heat flux was similar to autoclave behavior. Experience at the Saxton reactor in Cores II and III, however, have shown that with severe nucleate boiling, some accelerated corrosion was encountered. Similar accelerated corrosion with high crud deposits was also reported at KWO, but was terminated by using hydrogen overpressure and chemical additives.

→(DRN 00-644; 06-1141, R15; EC-9533, R302, LBDCR 15-035, R309)

Batch Y fuel rods were fabricated with ZIRLO™ cladding to improve the corrosion resistance of the fuel. Section 4.5 of Reference 80 presents corrosion data at high burnup for both Zircaloy-4 cladding and ZIRLO™ cladding and concludes that the ZIRLO™ cladding offers a significant improvement in the corrosion resistance of the cladding. NGF fuel rods are fabricated with Optimized ZIRLO™ cladding that has a slightly reduced tin content compared to ZIRLO™ specifically to improve its corrosion resistance. Autoclave steam testing demonstrated almost a 20% corrosion resistance improvement of Optimized ZIRLO™ compared to ZIRLO™. Reference 85 presents additional cladding corrosion data and provides updated cladding corrosion models for both ZIRLO™ and Optimized ZIRLO™ cladding.

←(EC-9533, R302, LBDCR 15-035, R309)

Coolant chemistry parameters have been specified that minimize corrosion product release rates and their mobility in the primary system. Specifically, the precore hot functional environment is controlled (ph and oxygen) to provide a thin, tenacious, adherent, protective oxide film. This approach minimizes corrosion product release and associated inventory on initial startup and subsequent operation. During operation, the specified lithium concentration range (0.2-3.5 ppm) effects a chemical potential gradient or driving force between hot and cooler surfaces (refuel cladding and steam generator tubing, respectively) such that soluble iron and nickel species will preferentially deposit on the steam generator surfaces. The associated ph also minimizes general corrosion product release rates from primary system surfaces. Moreover, the specified hydrogen concentration range (10-50 cm³/kg STP) ensures; reducing conditions in the core thereby avoiding low solubility Fe³⁺. Additionally, dissolved hydrogen promotes rapid recombination of oxidizing species. Oxidizing species and a fast neutron flux are synergistic prerequisites to accelerated Zircaloy-4 corrosion.

←(DRN 00-644; 02-1538, R12; 06-1141, R15)

During operations lithium, dissolved oxygen, and dissolved hydrogen will be monitored at a frequency consistent with maintaining these parameters within their specifications.

→(EC-9533, R302)

Post-operational examinations of fuel cladding that has operated within these specifications, has shown no significant chemical or corrosive attack of the Zircaloy cladding. ZIRLO™ cladding and Optimized ZIRLO™ cladding are less sensitive to chemical or corrosive attack due to their better corrosion resistance.

←(EC-9533, R302)

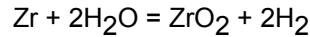
b) External Hydriding

→(EC-9533, R302)

During operation of the reactor with exposure to high temperature, high pressure water, Zirconium-based cladding will react to form a protective oxide film in accordance with the following equation.

←(EC-9533, R302)

→(DRN 00-644)



←(DRN 00-644)

Approximately 20 percent of the hydrogen is adsorbed by the Zircaloy. Based on data described in WAPD-MRP-107, the cladding would be expected to contain up to 250 ppm of hydrogen following three years of exposure.

A series of 600°F burst tests was performed on Zircaloy-4 tubes containing to 200 to 250 and 400 ppm of hydrogen precipitated as hydride platelets in various orientations from radial to circumferential. Additional burst tests have shown similar effects at 725°F. Little difference in burst test ductility was evident. Therefore, hydrogen normally adsorbed in Zr-4 tubing will not prove deleterious to the cladding integrity.

→(EC-9533, R302, LBDRCR 15-035, R309)

The impact of hydrides and hydride reorientation in ZIRLO™ cladding is discussed in Section 4.4.2.5 of Reference 80, where it is concluded that the performance of the ZIRLO™ cladding will be similar to that of the Zircaloy-4 cladding since the hydride reorientation is primarily a function of the tensile stresses and temperatures in the cladding. Due to the similarity of the material composition of Optimized ZIRLO™ and ZIRLO™, the same conclusion applies for Optimized ZIRLO™ cladding. Reference 85 provides updated data and models for ZIRLO™ and Optimized ZIRLO™ cladding.

←(EC-9533, R302, LBDRCR 15-035, R309)

c) Internal Hydriding

A number of reported fuel rod failures have resulted from excessive moisture available in the fuel. Under operation, this moisture would flash to steam and oxidize the Zircaloy.

The hydrogen, which was not absorbed during normal oxidation, would then be absorbed into the Zircaloy through a scratch in the oxide film. This localized hydrogen absorption by the cladding would shortly result in a localized fuel rod failure. Work performed at the Institt for Atomenergi, Halden, Norway, of which C-E is a member, demonstrated that a threshold value of water moisture is required for hydride sunbursts to occur. Through a series of in-pile experiments, the level of this threshold value was established. The allowable hydrogen limit in the fuel complies with this requirement, ensuring that hydride sunbursts will not occur.

d) Crud

The slow general corrosion of out-of-core plant surfaces will release corrosion products to reactor coolant, some of which will deposit on core surfaces as "crud". The major constituents of crud are iron and nickel, with lesser amounts of chromium and traces of manganese and cobalt, all present as oxides. Crud is essentially a nickel ferrite ($\text{Ni}_x\text{Fe}_{3-x}\text{O}_4$) with "x" in the range 0.45-0.75. Chromium appears to enter the inverse spinel substantially to give a composition $\text{CR}_y\text{Ni}_x\text{Fe}_{3-x-y}\text{O}_4$ (Reference 69). The porosity of core crud deposits is typically given as 80 to 85 percent (density ~ 1.2 g/cm³.)

Although there are significant efforts underway within the industry to develop mathematical models for crud transport in reactor coolant systems (e.g., see Reference 70), at present there are not analytical techniques available for estimating crud buildup on fuel surfaces.

Although heavy crud deposits have been observed in older plants (see Reference 71), measurements made on modern pressurized water reactors indicate that crud buildup is low, ranging from < 0.02 mils up to a few tenths of a mil (see Reference 72). As discussed in Subsection 4.2.3.2.3 a) above, coolant chemistry parameters have been specified to minimize crud deposition. Visual inspection of fuel removed from CE's Calvert Cliffs I plant, which operated under these specifications, revealed relatively light crud deposits, such that clad surface features from fabrication could be discerned (see Reference 73). Similar behavior is anticipated for the Waterford 3 core.

Enhanced corrosion of Zircaloy cladding should not occur under light deposits of porous crud. Water is free to flow through porosity in the crud, providing heat transfer through convection. Even heavy crud found in Yankee Rowe (Reference 71) was non-insulating because of its porosity.

e) Fuel-Cladding Chemical Reaction

An in-depth Post Irradiation Examination has been conducted wherein fuel-cladding chemical reactions were among those items studied. This study concluded that early unpressurized elements containing unstable fuel were more susceptible to stress corrosion attack than are those of the current design that utilizes stable fuel and pressurized cladding. Since stress corrosion attack is the result of a combination of stress imposed by the fuel on the cladding and the corrosive chemical species available to the cladding, irradiation programs are being pursued to define the conditions under which pellet-clad interaction will damage the cladding. These programs are currently underway both at Halden and in the Pathfinder test program being conducted jointly with KWU in the Obrigheim and Petten reactors.

4.2.3.2.4 Fretting Corrosion

The phenomenon of fretting corrosion, particularly in Zircaloy clad fuel rods supported by Zircaloy spacer grids, has been extensively investigated. Since irradiation-induced stress relaxation causes a reduction in grid spring load, spacer grids must be designed for end-of-life conditions as well as beginning-of-life conditions to prevent fretting caused by flow - induced tube vibrations. To ensure this, out-of-pile fretting tests have been performed concentrating on the more severe end-of-life conditions. Two testing approaches have been used; i.e., autoclave vibration tests and dynamic flow tests.

4.2.3.2.4.1 Autoclave Vibration Tests

The autoclave tests were performed by vibrating a fuel rod sample supported by two rigidly held spacer grid sections. Test conditions matched reactor coolant chemistry, temperature, and pressure. Variable parameters provided data to evaluate the effects of:

- a) Frequency of tube vibration
- b) Spacer grid spring load (preset)
- c) Axial tube movement (simulating reactor load following characteristics)

Data from such tests have indicated that wear starts with a brief break-in period and then proceeds at a negligible rate. Changes in frequency, spring preset (including zero preset) and amplitude within representative limits do not significantly alter fretting characteristics. At no time under any conditions was fretting significant.

4.2.3.2.4.2 Dynamic Flow Tests

Dynamic flow tests have been performed on four x four rod arrays (16 fuel rods) and on full size fuel assemblies. The four x four rod array testing was conducted under the following conditions:

- a) Flow velocities ranged from 14 ft/sec to 25 ft/sec
- b) Coolant temperature was 590°F
- c) Coolant pressure was 2150 psia

In addition, the four x four rod arrays were subjected to cross-flow and a mechanically induced forced vibration of the lower end of the rod array at a frequency of 15 Hz and an amplitude of five mils (representing vibratory forces imparted by the reactor internals). The four x four rod array testing also included rod arrays with preset spacer grid springs ranging from approximately 10 mils interference to gaps of up to five mils, simulating both tightly held and loose rods. The four x four rod arrays were tested for intervals from 1000 hours up to 3182 hours for a total accumulated test time of 18,000 hours.

The fuel rods in the four x four assemblies were either of a 0.413 in. diameter on a 0.550 in. pitch or of a 0.440 in. diameter on a 0.580 in. pitch, which are representative of a 15 x 15 and 14 x 14 fuel array, respectively. All fuel rods were visually inspected at each spacer grid interface. The depth of wear marks was accurately determined using an optical micrometer. The maximum depth of wear noted for the conditions above was less than 1/2 mil. In a special test where a fuel rod was completely unsupported at its lower end for a distance of 15 in., a depth of wear of three mils was noted after 2000 hours of flow at 25 ft/sec. This test was not representative of any design condition, but was performed to demonstrate the need for supporting the lower end of the fuel rod. Based on test results of four x four assemblies which follow the same trend as found in the autoclave vibration test, the maximum expected clad wear at end-of-life will be less than three mils.

Separate full scale flow tests at or exceeding reactor flow conditions were run with an array of four full-size prototypical 15 x 15 fuel assemblies, four full size 14 x 14 fuel assemblies of which two were prototypical and two contained stainless steel fuel rods, several tests of individual full size 14 x 14 fuel assemblies and a prototype 16 x 16 fuel assembly. The test conditions were as follows:

- a) Flow velocities ranged from 16 ft/sec for 15 x 15 fuel assemblies up to 23.7 ft/sec for some of the 14 x 14 fuel assemblies, and 22 ft/sec for the 16 x 16 fuel assembly. In all cases, the flow test velocities exceeded the maximum calculated velocity at operating conditions for fuel assemblies in each particular reactor.
- b) A large number of fuel rods (in some cases all rods within a fuel assembly) were tested with zero preset Zircaloy spacer grid spring loads to conservatively represent end-of-life spacer grid conditions. A number of fuel rods were also loosely supported at various spacer grid locations, and, in some cases, over the entire length of the rod.
- c) Test time accumulated exceeded 13,500 hours, with the longest single test 4000 hours in length.

The results of these tests are similar to those of the four x four fuel assemblies with a few exceptions. On the 14 x 14 fuel assemblies subjected to 4000 hours of continuous testing at 23.7 ft/sec and 1000 hours at 19.1 ft/sec, the maximum depth of wear on one assembly was 1.7 mils, while on the other assembly, one wear mark was found to be 2.2 mils deep and a few others ranged from 1.6 to 1.8 mils. The only incidence of significant wear on a full size fuel assembly occurred in special test of an off-design condition where the lower end of the fuel assembly was essentially unrestrained laterally. In this test, the depth of wear of one fuel rod was 10.9 mils after only 1188 hours of testing at 23.7 ft/sec. Again, this test, as in the case of the cantilevered fuel rod test in a four x four fuel assembly, showed the need for laterally restraining the lower end of the fuel assembly.

→(EC-9533, R302)

Results for the 16 x 16 fuel assembly test, where the Zircaloy spacer grid springs were preset to zero interference and the Inconel grid springs were preset to a small interference with the fuel rods, showed no evidence of fretting on any fuel rod after 1000 hours of testing.

An extensive flow test program was conducted to support the implementation of the NGF design. The NGF configuration was tested to confirm the hydraulic stability of the fuel assembly design and to demonstrate the acceptability of the fretting performance of the fuel assembly design. These tests included full scale single bundle tests of the NGF and standard designs, a full scale dual bundle test with a NGF fuel assembly and a standard fuel assembly, and a full cross-section/short length bundle test of the NGF design. The single bundle tests were run to evaluate the hydraulic stability of the fuel assemblies. The tests demonstrated the hydraulic stability of both designs over the expected range of flow rates. The dual bundle test was an endurance test to evaluate fretting performance of the two designs. This test provided additional confirmation of the hydraulic stability of the designs and showed a significant improvement in the fretting performance of the NGF design compared to the standard design. The short length bundle test was run to confirm the absence of flow-induced strip vibration within the spacer grids, which it did. The successful results of the flow test program demonstrate that the hydraulic performance of the NGF design is acceptable and superior to that of the prior designs.

←(EC-9533, R302)

4.2.3.2.5 Cycling and Fatigue

A fatigue analysis is performed to determine the cumulative fatigue damage of fuel rods exposed to lifetime power cycling conditions. The fatigue cycle is determined by considering combinations of normally anticipated events that would produce conservative estimates of strain in the clad. Some of the major conservative assumptions are as follows:

- a) Hot spot fuel radii are used in the calculations
- b) The most adverse tolerance conditions on the fuel and cladding dimensions are chosen to produce maximum interactions and hence maximum clad strains.

The chosen fatigue cycle represents daily operation at both full and reduced power. Clad strains are calculated from the primary creep rate of the clad and used to calculate the effective strain ranges. The cumulative fatigue damage fraction is determined by summing the ratios of the number of cycles at a given effective strain range to the permitted number at that range as taken from the fatigue curve presented in Figure 4.2-2.

4.2.3.2.6 Fuel Rod Bowing

Analysis of bowing data has shown that the bowing expected in the 16 x 16 design will have no effect on the margin to DNB beyond the allowance provided by the pitch, bowing and clad diameter enthalpy rise factor given in Table 4.4-1 and discussed in Section 4.4. A more complete discussion of the cause and effects of rod bowing is presented in References 53 and 75.

4.2.3.2.7 Irradiation Stability of Fuel Rod Cladding

The combined effects of fast flux and cladding temperature are considered in three ways as discussed below:

- a) Cladding Creep Rate

→(EC-9533, R302)

The in-pile creep performance of Zircaloy-4, ZIRLO™, and Optimized ZIRLO™ are dependent upon both the local material temperature and the local fast neutron flux. The functional form of the dependencies for Zircaloy-4 cladding is presented in Reference 14 for gap conductance calculations, and in Reference 22 for cladding collapse time predictions. The corresponding functional form of the dependencies is presented in Reference 80 for ZIRLO™ cladding, while Reference 83 documents that the similarities between the ZIRLO™ cladding and the Optimized ZIRLO™ cladding result in the same correlation for the two materials.

←(EC-9533, R302)

b) Cladding Mechanical Properties

The yield strength, ultimate strength, and ductility of Zircaloy-4 are dependent upon temperature and accumulated fast neutron fluence. The temperature and fluence dependence is discussed in Subsection 4.2.1.2.2.1. Unirradiated or irradiated properties were used depending upon which is more restrictive for the phenomenon being evaluated.

c) Irradiation Induced Dimensional Changes

→(EC-9533, R302)

Zirconium-based alloys have been shown to sustain dimensional changes (in the unstressed condition) as a function of the accumulated fast fluence. These changes are considered in the appropriate clearances between the various core components. The irradiation induced growth correlation method is discussed in Reference 3 (see Subsection 4.2.3.1.4), with the rod growth correlations specified in Reference 82 for Zircloy-4 cladding, Reference 80 for ZIRLO™ cladding, and Reference 84 for Optimized ZIRLO™ cladding.

Zircaloy-4 fuel cladding has been utilized in pressurized water reactors at temperatures and burnups anticipated in current designs with no failures attributable to radiation damage. Mechanical property tests on Zircaloy-4 cladding exposed to neutron irradiation of 4.7×10^{21} nvt (estimated) have revealed that the cladding retains a significant amount of ductility (in excess of four percent elongation). Typical results are shown in Table 4.2-2. It is believed that the fluence of 4.7×10^{21} nvt is at saturation so that continued exposure to irradiation will not change these properties.⁽⁵⁴⁾ Similar performance has been experienced with ZIRLO™ cladding and Optimized ZIRLO™ cladding, as detailed in Reference 80 and 83, respectively.

←(EC-9533, R302)

4.2.3.2.8 Cladding Collapse Analysis

→(DRN 02-1538, R12)

A cladding collapse analysis is performed to ensure that no fuel rod in the core will collapse during its design lifetime. The clad collapse calculation method⁽²²⁾ itself does not include arbitrary safety factors. However, the calculation inputs are deliberately selected to produce a conservative result. For example, the as-built clad dimensional data are chosen to be worst case combinations which result in 95 percent confidence in minimum predicted collapse time; the internal pressure history is based on minimum fill pressure with no assistance from released fission gas; and the flux and temperature histories are based on conservative assumptions. The combined effect of using conservative inputs in the clad buckling analysis method is to produce computed collapse time in excess of three cycles of operation.

←(DRN 02-1538, R12)

4.2.3.2.9 Fuel Dimensional Stability

Fuel swelling due to irradiation (accumulation of solid and gaseous fission products) and thermal expansion results in an increase in the fuel pellet diameter. The design makes provision for accommodating both forms of pellet growth. The fuel-clad diametral gap is more than sufficient to accommodate the thermal expansion of the fuel. To accommodate irradiation-induced swelling, it is conservatively assumed that the fuel-clad gap is reduced by the thermal expansion and that only the volume due to fuel porosity and the dishes on each end of the pellets are available. Thermal and irradiation induced creep of the restrained fuel results in redistribution of fuel so that the swelling due to irradiation is accommodated by the free volume (eight percent of the fuel volume).

→(DRN 00-644)

For such restrained pellets, and at a total fission-product-induced swelling rate of 0.7 percent $\Delta V/V$ per 10^{20} fissions/cm³, 0.54 percent would be accommodated by the fuel porosity and dished pellet ends through fuel creep, and 0.16 percent would increase the fuel diameter. Assuming peak burnup, this would correspond to using up a void volume equal to approximately 7.4 percent of the fuel volume and increasing the fuel rod diameter by a maximum of < 0.0025 in. (< 0.7 percent clad strain). When these numbers were compared to the minimum available volume and the maximum allowable strain, it was concluded that sufficient accommodation volume has been provided even under the most adverse burnup and tolerance conditions.

Demonstration of the margin which exists is seen in the large seed blanket reactor (LSBR) irradiation. Two rods which operated in the B-4 loop of the MTR offer an interesting simulation for current PWR design.^{(6) (7) (55)}

Both rods were comprised of 95 percent theoretical density pellets with dished ends and clad in Zircaloy. The first of these, No. 79-21, was operated successfully to a burnup of 12.41×10^{20} fissions/cm³ (>48,000 MWd/MTU). The second fuel pin, No. 79-25, operated successfully to 15.26×10^{20} fissions/cm³ (>60,000 MWd/MTU). The linear heat rating ranged from 7.1 to 16.0 KW/ft. The wall thickness for the latter pin was 0.028 in. as compared with 0.016 in. for the former. All other parameters were essentially identical. The two rods were assembled by shrinking the cladding onto the fuel. The maximum diametral increase measured at the ridge heights for rod 79-21 was 0.005 in., while it was less than 0.002 in. for rod 79-25. From post-irradiation examination, it was concluded that approximately 84 percent of the total fuel swelling was accommodated by the porosity and dishes, while 16 percent caused diametral expansion of the clad and ridging at pellet interfaces. These results indicate that a comparable irradiation of the fuel elements for Waterford 3 (cold diametral gap 0.007 in., wall thickness of 0.025 in., density 94.75 percent TD) would allow adequate margin for swelling accommodation.

The successful combined VBWR-Dresden irradiation of Zircaloy-clad uranium dioxide pellets provides additional confidence with respect to the design conditions for the fuel rods for this core.⁽⁵⁶⁾⁽⁵⁷⁾ Ninety-eight rods which had been irradiated in VBWR to an average burnup of about 10,700 MWd/MTU were assembled in fuel bundles and irradiated in Dresden to a peak burnup greater than 48,000 MWd/MTU. The reported maximum heat rating for these rods is 17.3 KW/ft which occurred in VBWR. Post-irradiation examination⁽⁵⁸⁾ revealed that diametral increases in the fuel rods ranged from 0.001 to 0.003 in. maximum. The maximum diametral change corresponds to 1.42 percent $\Delta V/V$, (or 0.12 percent $\Delta V/V$ per 10^{20} fission/cm³) for these 0.424 in. diameter rods. The relevant fuel parameters are listed below for the above test and the Waterford 3 design.

←(DRN 00-644)

	Fuel Density %TD	Cold Diametral Gap (in.)	Peak Burnup (MWd/MTU)
VBWR-Dresden	95	0.004 to 0.008	>48,000
LSBR-MTR	95	0.001	50,000; 61,000
Waterford 3	94.75	0.007	55,000

A comparison of the design parameters above, relative to the test results, provides a demonstration of the clad strains resulting from swelling of fuel.

4.2.3.2.10 Potential for Waterlogging Rupture and Chemical Interaction

The potential for waterlogging rupture is considered remote. Basically, the necessary factor or combination of factors, include the presence of a small opening in the cladding, time to permit filling of the fuel rod with water, and finally a rapid power transient. The size of the opening necessary to cause a problem falls within a fairly narrow band. Above a certain defect size, the rod can fill rapidly, but during a

power increase it also expels water or steam readily without a large pressure buildup. Defects which could result in an opening in cladding are scrupulously checked for during the fuel rod manufacturing process by both ultrasonic and helium leak testing. Clad defects which could develop during reactor operation due to hydriding are also controlled by limiting those factors (e.g., hydrogen content of fuel pellets) which contribute to hydriding.

The most likely time for a waterlogging rupture incident would be after an abnormally long shutdown period. After this time, however, the startup rate is controlled so that even if a fuel rod were filled with coolant, it would "bake out", thus minimizing the possibility of additional cladding rupture. The combination of control and inspection during the manufacturing process and the limits on the rate of power change restrict the potential for waterlogging rupture to a very small number of fuel rods.

The UO₂ fuel pellets are highly resistant to attack by reactor coolant in the event cladding defects should occur. Extensive experimental work and operating experience have shown that the design parameters chosen conservatively account for changes in thermal performance during operation and that coolant activity buildup resulting from cladding rupture is limited by the ability of uranium dioxide to retain solid and gaseous fission products.

4.2.3.2.11 Fuel-Cladding Interaction

An analytical model to evaluate cladding response to pellet-clad interaction has been developed⁽²¹⁾. This analysis which is based on an advanced version of the FATES computer code, considers generalized plane-strain of a unit section of fuel and clad. All of the physical phenomena calculational methods and input variables of the present FATES program⁽¹⁴⁾ are included in the new version; and in addition, models are included for elastic and plastic stresses and strains in the clad and fuel, and fuel creep. A compatible interface modeled between the fuel and clad ensures that interaction is accurately accounted for.

The treatment of power history, axial power shapes and other operating parameters is handled similar to the current FATES version with the exception that power ramp rates and cycling can be considered. The response of the fuel and clad is calculated through an interactive process, and the interaction between the fuel and clad is established.

The resulting analytical predictions of temperatures, stresses, strains and geometric configuration are thus made available for use in conjunction with operating experience and irradiation test results in demonstrating the acceptability of the various operating conditions to which the fuel may be subjected. A detailed discussion of the methods and capabilities of the pellet-clad interaction model is contained Reference 21.

4.2.3.2.12 Fuel Burnup Experience

→(EC-9533, R302)

Design bases for the Zircaloy-4, ZIRLO™, and Optimized ZIRLO™ cladding have been established which are conservative with respect to the reported data. Evidence currently available indicates that these claddings and UO₂ fuel performance is satisfactory to exposures in excess of 60,000 MWd/MTU.

←(EC-9533, R302)

a) High Linear Heat Rating Irradiation Experience

→(DRN 00-644)

The determination of the effect of linear heat rating and fuel cladding gap on the performance of Zircaloy-clad UO₂ fuel rods was the object of two experimental capsule irradiation programs conducted in the Westinghouse Test Reactor (WTR).⁽⁵⁹⁾ In the first program, 18 rods containing 94 percent theoretical density UO₂ pellets were irradiated at 11, 16, 18, and 25 kW/ft with cold diametral gaps of 0.006 in., 0.012 in., and 0.025 in. The wall thickness to diameter ratio (t/OD) of the Zircaloy cladding was 0.064 which is comparable to the 0.066 value in this design. Although

←(DRN 00-644)

these irradiations were of short duration (about 40 hours) significant results applicable to this design were obtained. No significant dimensional changes were found in any of the fuel rods. Only one rod, which operated at a linear heat rate of 24 kW/ft with an initial diametral gap of 0.025 in., experienced center melting. Rods which operated at 24 kW/ft with cold gaps of 0.006 in. and 0.012 in. did not exhibit center melting. On these bases, the initial gap of 0.007 in. and the maximum linear heat ratings for this design provide adequate margin against center melting, even when 112 percent overpower conditions are considered. These results also indicate that an initial diametral gap of 0.007 in. is adequate to accommodate radial thermal expansion without inducing cladding dimensional changes even at a linear heat rate of 24 kW/ft. This margin with respect to thermal expansion will be diminished with increasing burnup at a rate of 0.16 percent $\Delta V/V$ per 10^{20} fissions/cm³. However, the linear heat rating will decrease with burnup and thus limit the sum of the strains to values below the allowable.

Further substantiation of the capability of operation at maximum linear heat ratings in excess of those in this design is obtained from later irradiation tests in WTR.⁽⁵⁹⁾ Fuel rods 38 in. long and 6 in. long were irradiated at linear heat ratings of 19 kW/ft and 22.2 kW/ft to burnups of 3450 and 6250 MWd/MTU. The cold diametral gaps in these Zircaloy clad rods containing 94 percent dense UO₂ were 0.002 in., 0.006 in., and 0.012 in. The cladding t/OD was 0.064. No measurable diameter changes were noted for the 0.006 in. or 0.012 in. fuel clad gap rods. Only small changes were observed for the rods with a 0.002 in. diametral gap.

b) Shippingport Irradiation Experience

Zircaloy clad fuel rods have operated successfully (three defects have been observed which were a result of fabrication defects) in the Shippingport blanket with burnups of about 37,000 MWd/MTU and maximum linear heat ratings of about 13 kW/ft. ⁽⁵⁹⁾⁽⁶⁰⁾⁽⁶¹⁾ Although higher linear heat ratings will be experienced, swelling (primarily burnup dependent) and thermal expansion (linear heat rating dependent) provide the primary forces for fuel cladding strain at the damage limit. Thus, the Shippingport irradiations have demonstrated that Zircaloy clad rods with a cladding t/OD less than that for this plant (0.066) can successfully contain the swelling associated with 37,000 MWd/MTU burnup while at the same time containing the radial thermal expansion associated with peak linear heat ratings. Irradiation test programs in support of Shippingport in-reactor loops demonstrated successful operation at burnups of 40,000 MWd/MTU and linear heat ratings of about 11 kW/ft with cladding t/OD ratios as low as 0.053.⁽⁶²⁾

c) Saxton Irradiation Experience

→(DRN 02-1538)

Zircaloy-4 clad fuel rods containing UO₂-PuO₂ pellets of 94 percent theoretical density have been successfully irradiated in Saxton to peak burnups of 31,800 MWd/MTU at 15 kW/ft linear heat rate under USAEC Contract AT (30-1)-3385⁽⁶³⁾. The t/OD of the cladding was 0.059 which is less than that of this design. The amount of PuO₂, 6.6 percent is considered as insignificant with respect to providing any difference in performance when compared with that for UO₂. Subsequent tests on two of the above rods (18,000 MWd/MTU at 10.5 kW/ft) successfully demonstrated the capability of these rods to undergo power transients from 16.8 kW/ft to 18.7 kW/ft.

←(DRN 02-1538)

d) Vallecitos Boiling Water Reactor (VBWR) - Dresden Experience

→(DRN 02-1538)

The combined VBWR - Dresden irradiation of Zircaloy clad oxide pellets provides additional confidence with respect to the design conditions for the fuel rods for this core.⁽⁵⁵⁾⁽⁵⁷⁾⁽⁶⁴⁾ Ninety-eight rods which had been irradiated in VBWR to an average burnup of about 10,700 MWd/MTU were assembled in fuel bundles and irradiated in Dresden to a peak burnup greater than 48,000 MWd/MTU. The reported maximum heat ratings for these rods is 17.3 kW/ft which occurred in VBWR. The t/OD cladding ratio of 0.052, and the external pressure of about 1000 psia are conditions which are all in the direction of less conservatism with respect to fuel rod integrity when compared with the design values of 0.066 cladding t/OD ratio and an external pressure of 2250 psia. Ten of these VBWR - Dresden rods representing maximum combinations of burnup, linear heat rating, and pellet density have been examined in detail and found to be in satisfactory condition. The remaining 88 rods were returned to Dresden and successfully irradiated to the termination of the program.

←(DRN 02-1538)

e) Large Seed Blanket Reactor (LSBR) Rods Experience

Two rods operated in the B-4 loop at the Materials Testing Reactor (MTR) provide a very interesting simulation for current PWR designs ⁽⁶⁾⁽⁷⁾⁽⁵²⁾. Both rods were comprised of 95 percent theoretical density pellets with dished ends, clad in Zircaloy. The first of these No. 79-21, was operated successfully to a burnup of 12.41×10^{20} fission/cm³ (48,000 MWd/MTU) through several power cycles which included linear heat rates from 5.6 to 13.6 kW/ft. The second fuel pin, No. 79-25, operated successfully to 15.26×10^{20} fission/cm³ (60,000 MWd/MTU). The basic difference in this rod was the 0.028 in. wall thickness as compared to 0.016 in. (t/OD = 0.058) in the first rod. All other parameters were essentially identical.

The linear heat rating ranged from 7.1 to 16.0 kW/ft. After the seventh interim examination, the rod operated at a peak linear power of 12.9 kW/ft at a time when the peak burnup was 49,500 MWd/MTU. These high burnups were achieved with fuel elements which were assembled by shrinking the cladding onto the fuel and indicate that a comparable irradiation of the fuel elements for this reactor (cold diametral gap of 0.007 in.) would allow a considerable increase in swelling life at a given clad strain.

f) Central Melting in Big Rock Point Experience

→(DRN 00-644)

As part of a joint U.S. - Euratom Research and Development Program, Zircaloy clad UO₂ pellet rods (95 percent theoretical density) were irradiated under conditions designed to induce central melting in the Consumers Power Co. Big Rock Point Reactor⁽⁶⁵⁾. The test includes 0.7 in. diameter fuel rods (cladding t/OD = 0.057; fuel clad gap of about 0.012 in.) at maximum linear heat ratings of about 27 kW/ft and 22 kW/ft with peak burnups up to 30,000 MWd/MTU. Result of these irradiations provide a basis for incorporating linear heat ratings well in excess of those calculated for this reactor, and show that the presence of localized regions of fuel melting is not catastrophic to the fuel rod.

←(DRN 00-644)

g) KWU Irradiations-Kraftwerk Union Reactor, Obrigheim, Germany

C-E has entered into a technical agreement with Kraftwerk Union (KWU) for the complete exchange of information and technology relating to pressurized water reactor systems including fuel.

This agreement makes available to C-E the experience of eight years successful operation of the KWO reactor at Obrigheim, Germany.

→(DRN 00-644; 02-1538, R12)

In the area of nuclear fuel performance, the experience at Obrigheim has shown successful operation through seven operating cycles. Fuel batches of 95 percent TD, both pressurized and nonpressurized, have been irradiated. Substantial testing has been performed in the reactor on the load following ability of both pressurized and nonpressurized fuel rods. Selected rods were subjected to power changes from 50 to 100 percent at rates of 20 percent/min for more than 900 cycles. Peak power densities in the rods were 15 kW/ft with maximum burnups in excess of 30,000 MWD/MTU. No failures have been observed to date. This experiment demonstrates the load-following capability of a design similar to C-E's in an operating PWRs.

←(DRN 00-644; 02-1538, R12)

h) Long Term Irradiation Testing

As indicated, C-E has several self-sponsored fuel irradiation programs in progress and several cooperative fuel development programs with Kraftwerk Union as part of a technical agreement. In addition, C-E has access to all data and results of Kraftwerk Union's own fuel development programs.

→(EC-9533, R302)

i) High Burnup Combustion Engineering Operational Experience

Reference 82 presents fuel performance data obtained during poolside examinations and hot cell examinations of high burnup fuel utilizing Zircaloy-4 cladding in Combustion Engineering cores. The data demonstrates the acceptability of the fuel's performance to rod average exposures in excess of 60,000 MWD/MTU.

j) Westinghouse Experience

ZIRLO™ cladding material is in widespread use domestically in at least 38 nuclear power plants (Reference 80, Section 3.3). ZIRLO™ has been shown to have improved corrosion resistance compared to Zircaloy-4. Also, no oxide spalling has been observed in current ZIRLO™ fuel rods for normal operation.

→(LBDCR 15-035, R309)

Optimized ZIRLO™ cladding has a slightly lower allowed tin level than ZIRLO™ (lower by 0.2%) with the remainder of the material composition requirements being the same. The reduced tin level is to further enhance the corrosion resistance of the cladding. Reference 83 documents that ZIRLO™ material properties currently utilized in various models and methodologies are applicable to analyses for Optimized ZIRLO™ and shows the differences are negligible with no impact on any design or safety analyses. Reference 85 presents additional cladding corrosion data and provides updated cladding corrosion models for both ZIRLO™ and Optimized ZIRLO™ cladding. Therefore, in addition to the operational experience of Optimized ZIRLO™, the ZIRLO™ operational experience discussed above is applicable to Optimized ZIRLO™.

←(EC-9533, R302, LBDCR 15-035, R309)

4.2.3.2.12.1 Combustion Engineering Fuel Development Programs

→(DRN 02-1538, R12)

Since mid-1972, C-E has performed an extensive irradiation test program on fuel densification. When fuel densification became apparent, C-E immediately initiated an irradiation test program to determine the causes of densification and to define the specifications and processes required to limit densification of fuel. The first irradiation test program in the sequence confirmed that the phenomena is real and defined

←(DRN 02-1538, R12)

→(DRN 02-1538, R12)

the parameters important in the effect. An immediate response was a change in the C-E fuel pellet specification and a modification of the fuel fabrication process to provide densification resistant UO₂ fuel. The irradiation tests are continuing to establish conclusively that the current specification and process used is effective in minimizing densification.

←(DRN 02-1538, R12)

C-E is also a participating member of the Halden Reactor Project in Halden, Norway. The Halden project has underway a spectrum of fuel development programs from which C-E can further verify present fuel design models and continually evaluate advanced fuel design concepts.

4.2.3.2.12.2 Combustion Engineering/Kraftwerk Union Fuel Development Programs

The primary objectives of the cooperative fuel development programs are:

- a) To assess the causes of fuel densification and provide process changes which will preclude densification. Then subsequently to verify through irradiation testing that the process changes have been effective.
- b) To obtain long term data to further verify fuel performance models.
- c) To evaluate advanced fuel design concepts in-reactor.

C-E and KWU currently have three densification test programs in progress in both United States and European test reactors. In addition, C-E and KWU are participating extensively in the densification test program under primary sponsorship of the Edison Electric Institute.

4.2.3.2.12.3 Kraftwerk Union Fuel Development Programs

→(DRN 00-644)

The design of the C-E fuel rods is very similar to the KWU fuel utilized in the Obrigheim reactor. The Obrigheim core has operated with peak power densities up to 15 kW/ft with maximum burnups in excess of 46,000 MWd/MTU without observed life limiting failures. Several fuel rods, both pressurized and unpressurized, from the Obrigheim reactor have undergone detailed hot cell examination under the direction of KWU. The results of all nondestructive fuel examinations performed during shutdowns and the complete results of the hot cell program are available to C-E under the technical agreement with KWU.

←(DRN 00-644)

In addition to the programs to routinely examine high burnup standard fuel, KWU also has comprehensive fuel development programs underway which utilize special test assemblies in the Obrigheim reactor. Under this program, fuel rod design parameters have been varied over significant ranges to experimentally establish the basis for further design optimization. One assembly has been irradiated annually since October 1973. Also included in this special assembly are segmented rods or "rodlets" which are connected to form a complete fuel rod. These rodlets are preirradiated in a test reactor. The test reactor irradiations provide data on fuel rod performance under transient conditions.

In summary, C-E has in process, or in the planning stages, fuel development programs that will provide additional assurance of fuel design adequacy.

4.2.3.2.13 Temperature Transient Effects Analysis

4.2.3.2.13.1 Waterlogged Fuel

The potential for a fuel rod to become waterlogged during normal operation is discussed in Subsection 4.2.3.2.10. In the event that a fuel rod does become waterlogged at low or zero power, it is possible that a subsequent power increase could cause a buildup of hydrostatic pressure. It is unlikely that the pressure would build up to a level that could cause cladding rupture because a fuel pin with the potential for rupture requires the combination of a very small defect together with a long period of operation at low or zero power.

Tests which have been conducted using intentionally waterlogged fuel pins (capsule drive core at SPERT)(66)(67) showed that the resulting failures did eject some fuel material from the rod and greatly deformed the test specimens. However, these test rods were completely sealed, and the transient rates used were several orders of magnitude greater than those allowed in normal operation.

In those instances where waterlogged fuel rods have been observed in commercial reactors, it has not been clear that waterlogging was the cause, and not just the result, of associated cladding failures; and C-E has not observed any case in which material was expelled from waterlogged fuel rods.

It is therefore, concluded that the effect of normal power transients on waterlogged fuel rods is not likely to result in cladding rupture and even if rupture does occur it will not produce the sort of postulated burst failures which would expel fuel material or damage adjacent fuel rods or fuel assembly structural components.

4.2.3.2.13.2 Intact Fuel

The thermal effects of anticipated operational occurrences on fuel rod integrity are discussed in the following paragraphs.

- a) Fuel rod thermal transient effects are basically manifested as the change in internal pressure, the changes in clad thermal gradient and thermal stresses, and the differential thermal expansion between pellets and clad. These effects are discussed in Subsections 4.2.3.2.2 and 4.2.3.2.11.
- b) Another possible effect of transients would be to cause an axial expansion of the pellet column against a flattened (collapsed) section of the clad. However, the fuel rod design includes specific provisions to prevent clad flattening, and, therefore, such interactions will not occur.

4.2.3.2.14 Energy Release During Fuel Element Burnout

The Reactor Protection System provides fuel clad protection so that the probability of fuel element burnout during normal operation and anticipated operational occurrences is extremely low. Thus, the potential for fuel element burnout is restricted to faulted conditions. The LOCA is the limiting event since it results in the larger number of fuel rods experiencing burnout; thus the LOCA analysis, which is very conservative in predicting fuel element burnout, provides an upper limit for evaluating the consequences of burnout. The LOCA analysis explicitly accounts for the additional heat release due to the chemical reaction between the Zircaloy clad and the coolant following fuel element burnout in evaluating the consequences of this accident. LOCA analysis results are discussed in Subsection 15.6.3.

4.2.3.2.15 Energy Release on Rupture of Waterlogged Fuel Elements

A discussion of the potential for waterlogging fuel rods and for subsequent energy release is presented in Subsection 4.2.3.2.10.

4.2.3.2.16 Fuel Rod Behavior Effects from Coolant Flow Blockage

An experimental and analytical program was conducted to determine the effects of fuel assembly coolant flow maldistribution during normal reactor operation. In the experimental phase, velocity and static pressure measurements were made in cold, flowing water in an oversize model of a C-E 14 x 14 fuel assembly in order to determine the three-dimensional

flow distributions in the vicinity of several types of flow obstructions. The effects of the distributions on thermal behavior were evaluated, where necessary, with the use of a preliminary version of the TORC thermal and hydraulic code⁽⁶⁸⁾. Subjects investigated included:

- a) The assembly inlet flow maldistribution caused by blockage of a core support plate flow hole. Evaluation of the flow recovery data indicated that even the complete blockage of a core support plate flow hole would not produce a W-3, Burnout Heat Flux Correlation, DNBR of less than 1.0 even though the reactor might be operating at a power sufficient to produce a DNBR of 1.3 without the blockage.
- b) The flow maldistribution within the assembly caused by complete blockage of one to nine channels was also evaluated. Flow distributions were measured at positions upstream and downstream of a blockage one to nine channels. The influence of the blockage diminished very rapidly in the upstream direction. Analysis of the data for a single channel blockage indicated that such a blockage would not produce a W-3 DNBR of less than 1.0 downstream of the blockage even though the reactor might be operating at a power sufficient to produce a DNBR of 1.3 without the blockage.

→ (DRN 00-644)

The results presented above were obtained through flow testing an oversize model of a standard 14 x 14 fuel assembly. Because of the great similarity in design between the Waterford 3 16 x 16 assembly, and the earlier 14 x 14 array, these test results also constitute an adequate demonstration of the effects that flow blockage would have on the 16 x 16 assembly. This conclusion is also supported by the fact that the 16 x 16 assembly has been demonstrated to have a greater resistance to axial flow than the 14 x 14 assembly. The higher flow resistance of the 16 x 16 arrangement would lead to more rapid flow recovery downstream of any blockage than would occur with the 14 x 14 array. The effect of the higher flow resistance is to produce a more rapid flow recovery (i.e., more nearly uniform flow) and is analogous to the common use of flow resistance devices (screens or perforated plates) to smooth non-uniform velocity profiles in ducts or process equipment.

← (DRN 00-644)

4.2.3.2.17 Fuel Temperatures

Steady state fuel temperatures are determined by the FATES computer program. The calculational procedure considers the effect of linear heat rate, fuel relocation, fuel swelling, densification, thermal expansion, fission gas release, and clad deformations. The model for predicting fuel thermal performance is discussed in detail in Reference 14.

→ (DRN 00-644)

Two sets of burnup and axially dependent linear heat rate distributions are considered in the calculation. One is the hot rod, time averaged, distribution expected to persist during long term operation, and the other is the envelope of the maximum linear heat rate at each axial location. The long term distributions are integrated over selected time periods to determine burnup, which is in turn used for the various burnup dependent behavioral models in the FATES computer program. The envelope accounts for possible variations in the peak linear heat rate at any elevation which may occur for short periods of time and is used exclusively for fission gas release calculations.

← (DRN 00-644)

The power history used assumes continuous 100 percent power from beginning-of-cycle. Using this history, the highest fuel temperatures occur at beginning-of-life. It has been shown that fuel temperatures for a given power level and burnup are insensitive to the previous history (e.g., operating power transients, length and number of shutdowns, etc.) used to arrive at the given power level.

Fuel thermal performance parameters are calculated for the hot rod. These parameters for any other rod in the core can be obtained by using the axial location in the hot rod, whose local power and burnup corresponds to the local power and burnup in the rod being examined. This procedure will yield conservatively high stored energy in the fuel rod under consideration.

The maximum power density, including the local peaking as affected by anticipated operational occurrences, is discussed in Sections 4.3, 4.4, and Chapter 15.

4.2.3.3 Burnable Poison Rod

4.2.3.3.1 Burnable Poison Rod Internal Pressure and Cladding Stress

→(DRN 02-1538, R12; 06-1059, R15)

A poison rod cladding analysis will be performed to determine the stress and strain resulting from the various normal, upset, and emergency conditions discussed in Subsection 4.2.1.1. Specific accounting will be made for differential pressure, differential thermal expansion, cladding creep, and irradiation induced swelling of the burnable poison material. Owing to a lower linear heat generation rates in these rods, the cladding analyses can be accomplished using conventional strength of materials formula, except for determining clad collapse resistance which will be done using the CEPAN computer model⁽²²⁾.

←(DRN 06-1059, R15)

The design criteria used to evaluate the analytical results are specified in Subsection 4.2.1.3.1.

←(DRN 02-1538, R12)

4.2.3.3.2 Potential for Chemical Reaction

A discussion of possible chemical reaction between the poison material and the coolant was presented in Subsection 4.2.1.3.3.3, along with information on chemical compatibility between poison material and cladding. Since the cladding material is identical to that of the fuel rod (Subsection 4.2.1.3.2), the description of potential chemical reactions between cladding and coolant in Subsection 4.2.3.2.3 is applicable to both fuel and poison rods.

→(DRN 00-644)

The potential for waterlogging rupture in poison rods is much lower than that in fuel rods because of the smaller thermal and dimensional changes that occur in a poison rod during reactor power increases. Refer to Subsection 4.2.3.2.10 for a discussion of the potential for waterlogging rupture in fuel rods.

←(DRN 00-644)

4.2.3.4 Control Element Assembly

The CEAs are designed for 10 effective full power years based on estimates of neutron absorber burnup, allowable plastic strain of the Inconel 625 cladding and the resultant dimensional clearances of the elements within the fuel assembly guide tubes.

a) Internal Pressure

The value of internal pressure in the control element is dependent on the following parameters:

- 1) Initial fill gas pressure
- 2) Gas temperature
- 3) Helium generated and released
- 4) Available volume including B₄C porosity

→ (DRN 00-644)

Of the absorber materials utilized in the CEA design, only the B₄C contributes to the total quantity of gas which must be accommodated within the control element. The helium is produced by the nuclear reaction ${}_0n^1 + {}_5B^{10} \rightarrow {}_3Li^7 + {}_2He^4$, and the fraction of the quantity generated which is actually released to the plenum is temperature dependent and is predicted by the empirical equation discussed in Subsection 4.2.1.4.A.3. Temperatures used for release fraction calculations are the maximum predicted to occur during normal operation.

← (DRN 00-644)

b) Thermal Stability of Absorber Materials

None of the materials selected for the control elements are susceptible to thermally induced phase changes at reactor operating conditions. Linear thermal expansion, thermal conductivity, and melting points are given in Subsection 4.2.1.4.

c) Irradiation Stability of Absorber Materials

Irradiated properties of the absorber materials are discussed in Subsection 4.2.1.4. Irradiation induced chemical transmutations are produced in both the B₄C and the Ag-In-Cd. Neutron bombardment of B10 atoms results in the production of lithium and helium. The percent of helium released is given by the expression in Subsection 4.2.1.4.

Ag-In-Cd alloy, which has an initial chemical composition of 79 w/o minimum Ag, 15 ± 0.35 w/o In, 5 ± 0.35 w/o Cd and 0.2 w/o maximum impurities, is expected to undergo small changes in composition. Formation of 3 w/o tin due to the transmutation of indium and an increase in cadmium content to about 10 w/o due to the transmutation of silver is expected. These affect the thermal conductivity and linear expansion characteristics of the alloy and are accounted for in the design of the control elements.

Irradiation enhanced swelling characteristics of the absorber materials are given in Subsection 4.2.1.4. Accommodations for swelling of the absorbers have been incorporated in the design of the control elements and include the following measures:

- 1) All B₄C pellets have chamfered edges to promote sliding of the pellets in the cladding due to differential thermal expansion and irradiation enhanced swelling.
- 2) Dimensionally stable Type 304 stainless steel spacers are located at the bottom of all absorber stacks adjacent to the nose cap to minimize strain at the weld joint.
- 3) A hole is provided in the center of the Ag-In-Cd cylinder to accommodate swelling in excess of the amount expected over the life of the control element.

d) Potential for and Consequences of CEA Functional Failure

The probability for a functional failure of the CEA is considered to be very small. This conclusion is based on the conservatism used in the design, the quality control procedures used during manufacturing and on testing of similar full size CEA/CEDM combinations under simulated reactor conditions for lengths of travel and numbers of trips greater than that expected to occur during the Waterford 3 design life. The consequences of CEA/CEDM functional failure are discussed in Chapter 15.

→ (DRN 00-644)

A postulated CEA failure mode is cladding failure. In the event that an element is assumed to partially fill with water under low or zero power conditions, the possibility exists that upon returning to power, the path of the water to the outside could be blocked. The expansion of the entrapped water could cause the element to swell. In tests, specimens of CEA cladding were filled with a spacer representing the poison material. All but nine percent of the remaining volume was filled with water. The sealed assembly was then subjected to a temperature of 650°F and an external pressure of 2,250 psia followed by a rapid removal of the external pressure. The resulting diametral increases of the cladding were on the order of 15 to 25 mils and were not sufficient to impair axial motion of the CEA, which has a 0.084 in. diametral clearance with the fuel assembly guide tubes. This test result, coupled with the low probability of a cladding failure leading to a waterlogged rod, demonstrates that the probability for a CEA functional failure from this cause is low.

← (DRN 00-644)

Another possible consequence of failed cladding is the release of small quantities of CEA filler materials, and helium and lithium (from the neutron-boron reactions). However, the amounts which would be released are too small to have significant effects on coolant chemistry or rod worth.

4.2.4 TESTING AND INSPECTION PLAN

Fuel bundle assembly and control element assembly quality assurance is attained by adherence to the ANS Quality Assurance Program Requirements for Nuclear Power Plants, ANSI N45.2-1971.

Vendor product certifications, process surveillance, inspections, tests, and material check analyses are performed to ensure conformity of all fuel assembly and control element assembly components to the design requirements from material procurement through receiving inspection at the plant site. The following are basic quality assurance measures which are performed.

4.2.4.1 Fuel Assembly

A comprehensive quality control plan is established to ensure that dimensional requirements of the drawings are met. In those cases where a large number of measurements are required and 100 percent inspection is impractical, these plans shall ensure with 95 percent confidence that 95 percent of these dimensions are within tolerance. Sensitivity and accuracy of all measuring devices are within ± 10 percent of the dimensioned tolerance. The basic quality assurance measures which are performed in addition to dimensional inspections and material verifications are described in the following sections.

4.2.4.1.1 Weld Quality Assurance Measures

The welded joints used in the fuel assembly design are listed below in a series of paragraphs which describe the type and function of each weld, and include a brief description of the testing (both destructive and non-destructive) performed to ensure the structural integrity of the joints. The welds are listed from top to bottom in the fuel assembly.

The CEA guide tube joints (between the tube and threaded upper and lower ends) are butt welds between the two Zircaloy subcomponents. The welds are required to be full penetration welds and must not cause violation of dimensional or corrosion resistance standards.

The upper end fitting center guide post to lower cast flow plate joint has a threaded connection which is prevented from unthreading by tack welding the center guide post to the bottom of the lower cast plate using the gas tungsten arc (GTA) process. Each weld is inspected for compliance with a visual standard.

→(DRN 02-1538, R12)

The spacer grid welds at the intersection of perpendicular Zircaloy-4 grid strips are made by the laser processes. Each intersection is welded at the top and at the bottom, and each weld is inspected by comparison with a visual standard.

←(DRN 02-1538, R12)

For the spacer grid to CEA guide tube weld (both components Zircaloy-4), each grid is welded to each guide tube with eight small welds, evenly divided between the upper and lower faces of the grid. Each weld is required to be free of cracks and burnthrough and each weld is inspected by comparison to a visual standard. Also, sufficient testing of sample welds is required to establish acceptable corrosion resistance of the weld region. Each guide tube is inspected after welding to ensure that welding has not affected clearance for CEA motion.

The bottom spacer grid welds at spacer strip intersections and between spacer and perimeter strips (all components Inconel 625) have the same configuration as for the Zircaloy and are all inspected for compliance with appropriate visual standards.

→(DRN 02-1538, R12; EC-9533, R302)

The bottom spacer grid (Inconel 625) to Inconel skirt weld was made using the GTA process. Each weld was inspected to ensure compliance with a visual standard. The debris-filtering bottom spacer grid has eliminated this weldment.

←(DRN 02-1538, R12; EC-9533, R302)

→(LBDCR 15-025, R309)

The Inconel skirt to lower end fitting (stainless steel) weld is made using the GTA process and each weld is inspected to ensure compliance with a visual standard.

←(LBDCR 15-025, R309)

The lower end fitting is fastened to the Zircaloy guide tubes using threaded connections. The connections are prevented from unthreading by stainless steel locking rings which are welded to the lower end fitting. Each ring is tack welded to the end fitting in four places using the GTA process, and each weld is inspected for compliance with a visual standard. The inspection requirements and acceptance standards for each of the welds are established on the basis of providing adequate assurance that the connections will perform their required functions.

→(EC-9533, R302)

The implementation of the NGF design eliminates four weld types while introducing three new weld types. As discussed in Section 4.2.2.1, the welds between the flange and the CEA guide tubes, between the Zircaloy-4 spacer grids and the guide tubes, between the bottom grid and the lower end fitting, and between the locking disc and the lower end fitting have all been eliminated. The three new weld types are discussed below:

- The Inconel top grid is a brazed design composed of Inconel-718 inner and outer straps and stainless steel sleeves. The braze joints are inspected for length and the absence of cracks.
- ZIRLO™ sleeves are laser welded to the Optimized ZIRLO™ inner straps of the mids grids and the IFMs. The welds are inspected for length and the absence of cracks.
- Stainless steel inserts are laser welded to the Inconel inner straps of the bottom grid. The welds are inspected by comparison to a visual standard and the absence of cracks.

←(EC-9533, R302)

4.2.4.1.2 Other Quality Assurance Measures

All guide tubes are internally gaged ensuring free passage within the tubes including the reduced diameter buffer region.

Each upper end fitting post to guide tube joint is inspected for compliance with a visual standard.

The spacer grid to fuel rod relationship is carefully examined at each grid location.

Stainless steel inserts are laser welded to the Inconel inner straps of the bottom grid. The welds are inspected by comparison to a visual standard and the absence of cracks.

→(EC-9533, R302)

For NGF assemblies, inspections of the bulges are performed for size, location, and absence of cracks.

←(EC-9533, R302)

→(DRN 06-895, R15)

Each completed fuel assembly is inspected for cleanliness, wrapped to preserve its cleanliness and loaded within shipping containers.

←(DRN 06-895, R15)

Visual inspection of the conveyance vehicle, shipping container, and fuel assembly are performed at the reactor site. Approved procedures are provided for unloading the fuel assemblies. Following unloading, exterior portions of the fuel assembly components are inspected for shipping damage and cleanliness. If damage is detected, the assembly may be repaired onsite or returned to the manufacturing facility for repair. In the event the repair process were other than one normally used by the manufacturing facility, or that the repaired assembly did not meet the standard requirements for new fuel, the specific process or assembly would be reviewed by the appropriate design department before the process or assembly would be accepted.

4.2.4.2 Fuel Rod

4.2.4.2.1 Fuel Pellets

→(DRN 00-644; 02-1538, R12)

Beginning with Batch U, all uranium fuel pellets will be fabricated at the Columbia, SC, manufacturing facility.

←(DRN 00-644; 02-1538, R12)

→(DRN 00-644; 02-1538, R12)

During the conversion of source material to ceramic grade uranium dioxide powder, the UO₂ powder is divided into lots blended to form uniform isotopic, chemical and physical characteristics. Samples are tested from each powder blend to verify compliance with the specification limits for the blend. Additional finished pellets are tested for the final enrichment certification of the pellets.

Pellets are divided into lots during fabrication with all pellets within the lot being processed under the same conditions, as defined per the pellet specification. Representative samples are obtained from each lot for product acceptance tests. Hydrogen content of the finished ground pellets is restricted. The pellets' diameters are inspected and certified to meet the design tolerance requirements at a 95/99 confidence level. All other pellet dimensions meet a 90/90 confidence level. Density requirements of the sintered pellets must meet a 95/95 confidence level. Sample pellets from each pellet lot are prepared for metallographic examination to ensure conformance to microstructural requirements. Surface finish of ground pellets is restricted and meets a 90/90 confidence level. Pellet surfaces are inspected for chips, cracks, and fissures in accordance with approved standards.

←(DRN 00-644; 02-1538, R12)

→(DRN 02-1538, R12)

←(DRN 02-1538, R12)

4.2.4.2.2 Cladding

→(DRN 02-1538, R12)

Lots are formed from tubing produced from the same ingot, annealed in the same final vacuum annealing charge and fabricated using the same procedures. Samples randomly selected from each lot of finished tubing are chemically analyzed to ensure conformance to specified chemical requirements, and to verify tensile properties and hydride orientation. Samples from each lot are also used for metallographic tests, and burst tests. Each finished tube is ultrasonically tested for internal soundness; visually inspected for cleanliness and the absence of acid stains, surface defects, and deformation; and inspected for inside dimension and wall thickness. The following summarizes the test requirements:

←(DRN 02-1538, R12)

a) Test (refer to Subsection 4.2.1.2.2)

1) Chemical Analysis

→(DRN 02-1538, R12)

Ingot analysis is required for top, middle, and bottom of each ingot. Finished intermediate TREX or finished tube product is tested for hydrogen, nitrogen, and oxygen per ASTM E353.

←(DRN 02-1538, R12)

2) Tensile Test at Room Temperature (ASTM E8-69)

3) Corrosion Resistance Test (ASTM G2-67)

4) Grain Size (ASTM E112-63)

→(DRN 02-1538, R12)

5) Deleted

←(DRN 02-1538, R12)

6) Surface Roughness

7) Visual Examination

- 8) Ultrasonic Test
- 9) Wall Thickness
- 10) Straightness
- 11) Inside Diameter

4.2.4.2.3 Fuel Rod Assembly

→(DRN 02-1538, R12)

Immediately prior to loading pellets must be capable of passing approved visual standards. Each fuel pellet stack is weighed to within 0.1 percent accuracy. The loading process is such that cleanliness and dryness of all internal fuel rod components are maintained until after the final end cap weld is completed. Loading and handling of pellets is carefully controlled to minimize chipping of pellets.

←(DRN 02-1538, R12)

The following procedures are used during fabrication to assure that there are no axial gaps in fuel rods.

4.2.4.2.3.1 Stack Length Gage

→(DRN 02-1538, R12)

The pellet stacks for Batches A through T were preassembled in "V" troughs that had been gauge marked to the proper length. They were then pushed into cladding tubes and the distance from the end of the tube to the end of the pellet stack checked with a gauge. The rods for Batches U and later are fabricated at the Columbia facility, which builds its pellet stacks directly in the cladding tubes. Their stacks are built up, 25 at a time, from a series of shorter preassembled segments that are fed into a like number of tubes by a vibratory feeder. Before feeding the last row of segments into the tubes, the distance from the end of the tube to the end of the pellet stack is checked with a gauge. If necessary, an appropriate number of pellets are added to or removed from each segment in the row. As before, the distance from the end of the tube to the end of the pellet stack is then checked with a gauge.

4.2.4.2.3.2 Rod Scanner

Before being loaded into bundle assemblies, the finished fuel rods are gamma scanned to ensure that no gaps exist within them.

Loaded fuel rods are pressurized with helium to a prescribed pressure as determined for the fuel batch. Impurity content of the fill gas shall not exceed 0.5 percent.

In Batches A through T, the fuel rod upper end cap to cladding tube weld is a Magnetic Force (i.e., resistance) Weld whose outer surface is subsequently machined (i.e., deflashed). Beginning with Batch U, the joint was converted to Tungsten Inert Gas (TIG) welding. The latter also utilizes a separate (TIG) seal weld to close the opening through which the rod is pressurized. Quality assurance on the end cap weld is as follows:

→(DRN 04-502, R13)

a) Non-destructive examination in accordance with approved procedures of all end cap welds (Batches U and later only) to certify bond length and to detect porosity or undercut.

←(DRN 04-502, R13)

b) Visual examination of all end cap welds to establish freedom from cracks, seams, inclusions and foreign particles (Note: In Batches A through T, this examination was performed after final machining of the weld).

c) Destructive examination of a sufficient number of weld samples to establish that the allowable percent of unbonded wall thickness and the maximum allowable continuous unbonded region are satisfied.

←(DRN 02-1538, R12)

→(DRN 02-1538)

- d) Helium Leak checking of all end cap welds to establish that no leak rate greater than $10^{-8}\text{cc}/\text{sec}$ is present.
- e) Corrosion testing of a sufficient number of samples to establish that weld zones do not exhibit excessive corrosion compared to a visual standard.

←(DRN 02-1538)

All finished fuel rods are visually inspected to ensure a proper surface finish (scratches that measure greater than 0.001 in. depth, cracks, slivers and other similar defects are not acceptable).

Each fuel rod is marked to provide a means of identification.

4.2.4.3 Burnable Poison Rod

4.2.4.3.1 Burnable Poison Pellets

B₄C powder is sampled to verify particle size and w/o boron requirements prior to its use in pellet production. Finished pellets are 100 percent inspected for diameter and must satisfy a 90/90 confidence level on other dimensions. Samples are taken from each of the pellet lots and examined for uniform dispersion of the B₄C in A1₂O₃. Conformance with density range requirements is demonstrated at a 95/95 confidence level and with B₄C loading requirements at a 90/90 level. Samples are drawn from each lot to verify acceptable impurity levels. Finally, all pellets are inspected for conformance with surface chip and crack standards.

4.2.4.3.2 Cladding

The testing and inspection plan for burnable poison rod cladding is identical to that for fuel rod cladding (Subsection 4.2.4.2.2).

4.2.4.3.3 Burnable Poison Rod Assembly

The moisture content of poison pellets prior to loading is limited. The loading process is such that cleanliness and dryness of all internal poison rod components are maintained until the final end cap weld is completed.

The following procedure is used during fabrication to assure that there are no axial gaps in poison rods:

The operator stacks pellets onto V troughs that are gage marked to the proper column height. When pellet stacking is completed, all column heights are checked by Quality Control. The pellets are subsequently loaded into tubes. After loading, the distance from the end of the tube to the end of the pellet column is checked with a gage.

Loaded poison rods are evacuated and backfilled with helium to a prescribed level. Impurity content of the fill gas must not exceed 0.5 percent.

→(DRN 02-1538)

End cap weld integrity and corrosion resistance is ensured by a Quality Control plan identical to that used in fuel rod fabrication (Subsection 4.2.4.2.3).

←(DRN 02-1538)

All finished rods are visually inspected to ensure a proper surface finish (scratches greater than 0.001 in. in depth, cracks, slivers, and other similar defects are not acceptable).

4.2.4.4 Control Element Assemblies

The CEAs are subjected to numerous inspections and tests during manufacturing and after installation in the reactor. A general product specification controls the fabrication, inspection, assembly, cleaning, packaging, and shipping of CEAS. All materials are procured to AMS, ASTM or C-E specifications. In addition, various CEA hardware tests have been conducted or are in progress.

During manufacturing, the following inspections and tests are performed:

→(DRN 01-1103; 02-1477)

- a) The loading of each control element is carefully controlled to obtain the proper amounts and types of filler materials.

←(DRN 01-1103; 02-1477)

- b) All end cap welds are liquid penetrant examined and helium leak tested. A sampling plan is used to section and examine end cap welds.

→(DRN 02-1477)

- c) Deleted.

- d) Each CEA has unique serialization on the spider. See Figures 4.2-5.

←(DRN 02-1477)

→(DRN 00-644)

- e) Fully assembled CEAs are checked for proper alignment of the neutron absorber elements using a special fixture. The alignment check ensures that the frictional force that could result from adverse tolerances is below the force which could significantly increase trip time.

←(DRN 00-644)

In addition to the basic measurements discussed above, the manufacturing process includes numerous other quality control steps for ensuring that the individual CEA components satisfy design requirements for material quality, detail dimensions, and process control.

After installation in the reactor, but prior to criticality, each CEA is traversed through its full stroke and tripped. A similar procedure will also be conducted at refueling intervals.

The integrity of each CEA will be tested at the beginning of the initial fuel cycle by performing a CEA symmetry test as part of the low power physics testing. The CEA symmetry test will determine whether the reactivities of symmetric CEAs are equal within the measurement limitation. The successful completion of these tests will demonstrate that no core loading or fabrication errors or loss in rod integrity exist that are sufficient to result in measurable CEA asymmetries. A CEA symmetry test will also be performed at the beginning of each subsequent fuel cycle, as a minimum, on an abbreviated number of CEAS.

Hardware tests to date have been performed using CEA components developed primarily for CE 800 MWe class reactors which use 14 x 14 fuel assemblies.

→(DRN 01-1103, R12; 02-1477, R12)

CEAs used in the Waterford 3 reactor are essentially similar in design and construction to the 800 MWe class CEA. The CEA spider arms are shorter and the neutron absorber elements are smaller in diameter for compatibility with the 16 x 16 fuel assembly guide tube dimensions employed in Waterford 3.

←(DRN 01-1103, R12)

→(LBDCR 15-039, R309)

Safety analyses assume the average CEA position is at least 90% inserted at 3.2 seconds after trip breakers open. CEAs meet the 3.2 second average even under worst case conditions to reach 90 percent insertion in 3.2 seconds to agree with assumptions in Section 15.0.2.

←(DRN 02-1477, R12)

The reactivity worth of a CEA depends on the power (i.e., neutron flux) surrounding the CEA. During a reactor trip faster CEAs move into higher flux regions sooner and, thus, add more negative reactivity than slower CEAs. Note, CEAs do not necessarily fall with the same insertion times or at the same rate during a reactor trip. Therefore, the amount of negative reactivity inserted correlates to the average CEA insertion rate rather than the slowest CEA insertion rate. This relation between CEA insertion and reactivity insertion is cycle independent if the mechanical design, CEDM design, plus core physics and core thermohydraulics (pertinent to the CEAs) remain unchanged.

→(DRN 02-1477, R12)

CE performed three-dimensional space-time calculations with the NRC approved HERMITE computer program. The calculations adequately cover possible operating conditions and limits on the as-measured CEA distributions (Safety Evaluation Report for Amendment 58, dated October 31, 1989). The calculations show that for any reasonable distribution around an average CEA position during a trip, CEAs add negative reactivity at a rate directly related to the average CEA position. Thus, Technical Specification limits should exist for the average CEA position. Thus, Technical Specification limits should exist for the average CEA drop time and Safety Analysis should assume that all CEAs fall in a "window shade" pattern with the average CEA drop time. However, if the time between the fastest and slowest CEA becomes too large, or the CEA distribution deviates from the one modeled by CE, then the "window shade" may not necessarily represent the time dependent negative reactivity insertion. Therefore, besides the 3.2 second average insertion time limit, the Technical Specifications limit the maximum drop time for the slowest CEA to 3.5 seconds.

←(DRN 02-1477, R12, LBDCR 15-039, R309)

SECTION 4.2: REFERENCES

1. Timoshenko, S., Strength of Materials, Part II Chapter IX, D. Van Nostrand Co., Inc., New York, 1956.
2. "High Temperature Properties of Zircaloy and UO₂ for use in LOCA Evaluation Models," Combustion Engineering, Inc., CENPD-136 (Proprietary).
3. "Zircaloy Growth-In-Reactor Dimensional Changes in Zircaloy-4 Fuel Assemblies." Combustion Engineering, Inc., CENPD-198P (Proprietary), December 1975.
4. O'Donnell, W.J., "Fracture of Cylindrical Fuel Rod Cladding due to Plastic Instability," WAPD-TM-651, April 1967.
5. Weber, J.M., "Plastic Stability of Zr-2 Fuel Cladding, Effects of Radiation on Structural Metals," ASTM STP 426, AM. Soc. Testing Mats., pp 653-669, 1967.
6. Engle, J.T. and Meieran, H.B., "Performance of Fuel Rods Having 97 Percent Theoretical Density UO₂ Pellets Sheathed in Zircaloy-4 and Irradiated at Low Thermal Ratings," WAPD-TM-631, July 1968.
7. Duncombe, E., Meyer, J.E., and Coffman, W.A., "Comparisons with Experiment of Calculated Dimensional Changes and Failure Analysis of Irradiated Bulk Oxide Fuel Test Rods Using the CYGRO-1 Computer Program," WAPD-TM-583, December 1966.
8. McCauley, J.E., et al., "Evaluation of the Irradiation Performance of Zircaloy-4 Clad Test Rod Containing Annular UO₂ Fuel Pellets (Rod 79-19)," WAPD-TM-595, December 1966.
9. Notley, M.J.F., Bain, A.S., and Robertson, J.A.L., "The Longitudinal and Diametral Expansion of UO₂ Fuel Elements," AECL-2143, November 1964.
10. Notley, M.J.F., "The Thermal Conductivity of Columnar Grains in Irradiated UO₂ Fuel Elements," AECL-1822 July 1962.
11. Manson, S.S., "Fatigue: A Complex Subject - Some Simple Approximations," Experimental Mechanics, Vol. 22, No. 2, pp 193-226, July 1965.
12. O'Donnell, W.J. and Langer, B.F., "Fatigue Design Basis for Zircaloy Components," Nuc. Sci. Eng., Vol. 20, pp 1-12, 1964.
13. CESSAR Proprietary Appendix, Docket 50-470.
14. "C-E Fuel Evaluation Model Topical Report," Combustion Engineering, Inc., CENPD-139 (Proprietary), CENPD-139 Rev. 01 (Non-Proprietary) CENPD-139 Supplement 1 (Proprietary), CENPD-139 Supplement 1, Rev. 01 (Non-Proprietary), July 1974.

SECTION 4.2: REFERENCES (Cont'd)

15. Conway, J.B., "The Thermal Expansion and Heat Capacity of UO_2 to 2200°C", GE-NMPD-TM-63-6-6.
16. Christensen, J.A., "Thermal Expansion of UO_2 ", HW-75148, 1962.
17. Jones, J.M., et. al., "Optical Properties of Uranium Oxides," Nature, 205, 663-65, 1965.
18. Cabannes, F. and Stora, J.P., "Reflection and Emission Factors of UO_2 at High Temperatures", C.R. Acad. Sci., Paris, Ser. B. 264 (1) 45-48, 1967.
19. Held, P.C. and Wilder, D.R., "High Temperature Hemispherical Spectral Emittance of Uranium Dioxide at 0.65 and 0.70 μ m," J.Am. Cer. Soc., Vol. 52, No. 4, 1969.
20. Brassfield, M.C., "Recommended Property and Reaction Kinetics Data for Use in Evaluating a Light Water Cooled Reactor Loss-of-Coolant Incident Involving Zircaloy-4 or 324-53 Clad UO_2 ," GEMP-482, 1968.
21. "C-E Thermo-Structural Fuel Evaluation Method," Combustion Engineering, Inc., CENPD-179, April 1976.
22. "CEPAN, Method of Analyzing Creep Collapse of Oval Cladding," Combustion Engineering, Inc. CENPD-179, April 1976.
23. "STRIKIN-II, A Cylindrical Geometry Fuel Rod Heat Transfer Program," Combustion Engineering, Inc., CENPD-135P (Proprietary), CENPD-135 (Non-Proprietary), August 1974.
24. Deverall, J.E., LA-2669 USAEC, Vol. 62, 1954.
25. Rudkin, R.L., Parker, J.W., and Jenkins, R.J., ASD-TDR-62-24, Vol. 1, p. 20, 1963.
26. Thorne, R.P. and Howard, V.C. "Changes in Polycrystalline Alumina by Fast Neutron Irradiation," p. 415, Proceedings, of the British Ceramic Society, No. 7, February 1967.
27. Simnad, M.T. and Meyer, R.S., "BeO Review of Properties for Nuclear Reactor Applications," Proceedings of the Conference on Nuclear Applications of Nonfissionable Ceramics, p 209-210, May 9-11, 1966.
28. Rason, N.S. and Smith, A.W., "NAA-SR-862", Vol. 37 (AD85006), 1954.
29. Saba, W.G. and Sterret, K.F., "J. Am. Chem. Soc." Vol. 79, pp 3637-38.
30. "Fuels and Materials Development Quarterly Progress Report," pp 38-58, ONRL-TM-3703, December 31, 1971.

SECTION 4.2: REFERENCES (Cont'd)

31. Kingery, W.D., "Introduction to Ceramics." John Wiley & Sons, pp 486-504.
32. Toulookan, Y.S., "Thermophysical Properties of High Temperature Solid Materials," Vol. 4 and 5, MacMillan.
33. Moore, G.E. and Kelley, K.K. , "J. Am. Chem. Soc.", Vol. 69, pp 309-16, 1947.
34. Keilholtz, G.W. Moore, R.E., and Robitson, M.E., "Effects of Fast Neutrons on Polycrystalline Alumina and Other Electric Insulators at Temperatures From 60C-1230C" ORNL 4678, May 1971.
35. Burian, R.J., Fromm, E.O., and Gates, J.E, "Effect of High Boron Burnups on B₄C and ZrB Dispersions in A1₂O₃ and Zircaloy-2," BM1-1627, April 24, 1963.
36. Cunningham, G.W., "Compatibility of Metals and Ceramics, "Proceedings of Nuclear Applications of Nonfissionable Ceramics, pp 279-289, May 1966.
37. Graber, M.J., "A Metallurgical Evaluation of Simulated BWR Emergency Core Cooling Tests,' Idaho Nuclear Corporation, IN-1453, March 1971.
38. Pitner, A.L., "The WDC -1-1 Instrumental Irradiation of Boron Carbide in a Spectrum-Hardened ETR Flux" HEDL-TME-73-38, April 1973.
39. Gray, R.G. and Lynam, L.R., "Irradiation Behavior of Bulk B₄C and B₄C-SiC Burnable Poison Plates," WAPD-261, October 1963.
40. "HEDL Quarterly Technical Report for October, November, and December 1974," Vol. 1, HEDL-TME-74-4, pp A-51 to A-53, January 1975.
41. Mahagan, D.E., "Boron Carbide Thermal Conductivity," HEDL-TME-73-78, September 1973.
42. Homan, F.J., "Performance Modeling of Neutron Absorbers," Nuclear Technology, Vol. 16, pp 216-225, October 1972.
43. Pitner, A.L. and Russcher, G.E., Irradiation of Boron Carbide Pellets and Powders in Hanford Thermal Reactors," WHAN-FR-24, December 1970.
44. Pitner, A.L. and Russcher, G.E., "A Function of Predict LMFBR Helium Release Bound on Boron Carbide Irradiation Data from Thermal Reactors," HEDL-TME-71-127, September 30, 1971.
45. HEDL-73-6, "Materials Technology Program Report for October, November, and December 1973," pp A-69 to A-72.

SECTION 4.2: REFERENCES (Cont'd)

46. Cohen, I., "Development and Properties of Silver-Base Alloys as Control Rod Materials for Pressurized Water Reactors," WAPD-214, December 1959.
47. Tipton, C.R., "Reactor Handbook," Vol. 1, Materials, Interscience, p 827, 1960.
48. "National Alloy Development Program Information Meeting," pp 39-63, TC-291, May 22, 1975.
49. "Quarterly Progress Report - Irradiation Effects on Structural Materials," HEDL-TME-161, pp GE-5 - GE-10.
50. "Structural Analysis of Fuel Assemblies for Combined Seismic and Loss of Coolant Accident Loadings," Combustion Engineering, Inc., CENPD-178, August 1976.
51. "Joint C-E/EPRI Fuel Performance Evaluation Program, Task C, Evaluation of Fuel Rod Performance on Maine-Yankee Core I," Combustion Engineering, Inc., CENPD-221, December 1975.
52. "Pressurized Water Reactor Project Period January 24, 1964 to April 23, 1964," WAPD-MRP-108.
53. "Fuel and Poison Rod Bowing," Combustion Engineering, Inc., CENPD-225-P (Proprietary), October 1976.
54. Caye, T.E., "Saxton Plutonium Project, Quarterly Progress Report for the Period Ending March 31, 1972," WCAP-3385-31, November 1972.
55. Berman, R.M., Meieran, H.B., and Patterson, P., "Irradiation Behavior of Zircaloy-Clad Fuel Rods Containing Dished End UO₂ Pellets," (LWBR-LSBR Development Program), WAPD-TM-629, July 1967.
56. Baroch, S.J., et al., "Comparative Performance of Zircaloy and Stainless Steel Clad Fuel Rods Operated to 10,000 MWd/MTU in the VBWR," GEAP-4849, April 1966.
57. Megerth, F.H., "Zircaloy-Clad UO₂ Fuel Rod Evaluation Program," Quarterly Progress Report No. 8, August 1969-October 1969. GEAP-10121, November 1969.
58. Megerth, F.H., "Zircaloy-Clad UO₂ Fuel Rod Evaluation Program," Quarterly Progress Report No. 1, November 1967-January 1968, GEAP-5598, March 1968.
59. Indian Point Nuclear Generating Unit No. 2, Preliminary Safety Analysis Report - Appendix A, Docket No. 50-247.
60. Stiefel, J.T., Feinroth, H., and Oldham, G.M., "Shippingport Atomic Power Station Operating Experience, Developments and Future Plans," WAPD-TM-390, April, 1963.

SECTION 4.2: REFERENCES (Cont'd)

61. Question V.B. 2, Prairie Island Nuclear Generating Plant, Preliminary Safety Analysis Report, Docket No. 50-306.
62. Anderson, T.D., "Effects of High Burnup on Bulk UO₂ Fuel Elements," Nuclear Safety Vol. 6, No. 2, Winter 1964-65 pp 164-169.
63. Miller, R.S., et.al., "Operating Experience with the Saxton Reactor Partial Plutonium Core - II," paper presented at AEC Plutonium Meeting in Phoenix, August, 1967.
64. Megerth, F.H., "Zircaloy-Clad UO₂ Fuel Rod Evaluation Program," Quarterly Progress Report No. 2, February 1968 April 1968, CEAP-5624, May, 1968.
65. Blakely, J.P., "Action on Reactor and Other Projects Undergoing Regulatory Review of Consideration," Nuclear Safety, Vol. 9, No. 4, p 326, July-August, 1968.
66. Stephan, L.A., "The Response of Waterlogged UO₂ Fuel Rods to Power Bursts," IDO-ITR-105, April, 1969.
67. Stephan, L.A., "The Effects of Cladding Material and Heat Treatment on the Response of Waterlogged UO₂ Fuel Rods to Power Burst," IM-ITR-111, January, 1970.
68. "TORC Code: A Computer Code for Determining the Thermal Margin of a Reactor Core," Combustion Engineering, Inc., CENPD-161-P, (Proprietary) July 1, 1975.
69. Sandler, Y.L., "Structure of PWR Primary Corrosion Products," presented during NACE Corrosion/78, March, 1978, Houston, Texas. Published in NACE-CORROSION, Vol. 35, No. 5, May, 1979.
70. Lister, D.H., "The Accumulation of Radioactive Corrosion Products in Nuclear Steam Generators," presented during NACE Corrosion/76, March, 1976, Houston, Texas.
71. Yankee Core Evaluation Program,-Final Report, WCAP-3017-6094, 1971.
72. Solomon, Y., Roesmer, T., "Measurement of Fuel Element Crud Deposits in Pressurized Water Reactors," Nuclear Technology, Vol 29, May, 1976, pp 166-173.
73. Bessette, D.E., et al., CE/EPRI Fuel Performance Evaluation Program, RP-586-1, Task A, Examination of Calvert Cliffs I Test Fuel Assemblies at End of Cycles 1 and 2, September, 1978.
74. Hillner, E., "Corrosion of Zirconium Base Alloys - An Overview," Zirconium in the Nuclear Industry, ASTM STP 633, pp.211-235, 1977.
75. "Fuel and Poison Rod Bowing," Combustion Engineering, Inc., CENPD--225-P, Supplement 3-P (Proprietary), August 1979.

SECTION 4.2: REFERENCES (Cont'd)

76. J.A. Christensen, et. al., "Melting Point of Irradiated Uranium Dioxide," ANS Transactions, Volume 7:2, November 1964, p 390.
77. Final Safety Analysis Report, San Onofre Nuclear Generating Station Units 2 and 3, NRC Docket Nos. 50-361 and 50-362, Response to NRC Question 231.26.
78. CEN-382-P-A, "Methodology for Core Designs Containing Erbium Burnable Absorbers," ABB Combustion Engineering Nuclear Fuel, August 1993.
- (DRN 03-1821, R13)
79. "Fuel Rod Maximum Allowable Gas Pressure," CEN-372-P-A, May 1990.
←(DRN 03-1821, R13)
- (DRN 06-1059, R15)
80. CENPD-404-P-A, "Implementation of ZIRLO™ Material Cladding in CE Nuclear Power Fuel Assembly Designs," November 2001.
81. WCAP-16072-P-A, "Implementation of Zirconium Diboride Burnable Absorber Coatings in CE Nuclear Power Fuel Assembly Designs," August 2004.
←(DRN 06-1059, R15)
→(EC-9533, R302)
82. CEN-386-P-A, "Verification of the Acceptability of a 1-Pin Burnup limit of 60 MWD/kg for Combustion Engineering 16x16 PWR Fuel", August 1992.
83. WCAP-12610-P-A and CENPD-404-P-A Addendum 1-A, "Optimized ZIRLO™", July 2006.
84. WCAP-16500-P-A, "CE 16x16 Next Generation Fuel Core Reference Report", August 2007.
←(EC-9533, R302)
→(LBDCR 15-035, R309)
85. WCAP-12610-P-A and CENPD-404-P-A Addendum 2-A, "Westinghouse Clad Corrosion Model for ZIRLO™ and Optimized ZIRLO™," October 2013.
←(LBDCR 15-035, R309)

WSES-FSAR-UNIT-3

TABLE 4.2-1 (Sheet 1 of 4)

Revision 302 (12/08)

MECHANICAL DESIGN PARAMETERS

Core Arrangement

→(EC-9533, R302)

NGF

Number of fuel assemblies in core, total	217	
→(DRN 01-1103, R12)		
Number of CEAs	87	
←(DRN 01-1103, R12)		
Number of fuel rod locations	51,212	
Spacing between fuel assemblies, fuel rod surface to surface, in.	0.208	0.216
Spacing, outer fuel rod surface to core shroud, in.	0.214	0.218
Hydraulic diameter, nominal channel, ft.	0.0394	0.0415
Total flow area (excluding guide tubes), ft ²	54.8	56.5
Total core area, ft ²	101.1	
Core equivalent diameter, in.	136	
Core circumscribed diameter, in.	143	
Total fuel loading, Kg U	90 x 10 ³	93x10 ³
Total fuel weight, lbm. UO ₂	224 x 10 ³	234x10 ³
Total weight of Zircaloy, lbm.	64,092	61,385
Fuel volume (including dishes), ft ³	356	359
Fuel Rod Array, square	16 x 16	
Fuel Rod Pitch, in.	0.506	
←(EC-9533, R302)		

Fuel Assemblies (Cont'd)

→(EC-9533, R302)			
Spacer Grid			<u>NGF</u>
Type – HID-1L	Cantilever Spring		
Material	Zircaloy-4		
→(DRN 02-1538, R12)			
Number per assembly	11		
←(DRN 02-1538, R12)			
Weight each, lb	1.7		
→(DRN 02-1538, R12; 06-1059, R15)			
←(DRN 02-1538, R12; 06-1059, R15)			
Type	Cantilever Spring	Vertical Spring	
Material	Inconel 625	Inconel-718	
Number per assembly	1*	1	
Weight each, lb	2.3	1.5	
Type – Vaned Mid Grid			I-Spring
Material			Optimized ZIRLO™
Number per Assembly			6
Weight, each, lb			2.8
Type – Unvaned Mid Grid			I-Spring
Material			Optimized ZIRLO™
Number per Assembly			3
Weight, each, lb			2.7
Type – IFM Grid			Co-planar Dimples
Material			Optimized ZIRLO™
Number per Assembly			2
Weight, each, lb			1.1
Type – Inconel Bottom Grid	Cantilever Spring		Cantilever Spring
Material	Inconel-625		Inconel-625
Number per Assembly	1		1
Weight, each, lb	2.6		2.3
Weight of fuel assembly, lbm.	1,435		1,416
Outside Dimensions			
Fuel rod to fuel rod, in.	7.972 x 7.972		7.96x7.964
Fuel Rod			
Fuel rod material (sintered pellet)	UO ₂		
→(DRN 06-1059, R15)			
Pellet diameter, in., OD (annular ID)	0.325 (0.1625)		0.3225 (0.1550)
Pellet length, in., solid (annular)	0.390 (0.500)		0.387 (0.500)
Pellet density, g/cm ³	10.44		
←(DRN 06-1059, R15)			
Pellet theoretical density, g/cm ³	10.96		
→(DRN 06-1059, R15)			
Pellet density (% theoretical)	95.25		
Stack density, g/cm ³ , solid (annular)	10.11 (7.80)		(10.31 (8.00))
Clad material	Zircaloy-4, ZIRLO™		Optimized ZIRLO™
←(DRN 06-1059, R15)			
Clad ID, in.	0.332		0.329
Clad OD, (nominal), in.	0.382		0.374
→(DRN 06-1059, R15)			

* some fuel assemblies in Batch U; all fuel assemblies beginning w/ Batch W

←(DRN 06-1059, R15)

WSES-FSAR-UNIT-3

TABLE 4.2-1 (Sheet 3 of 4)

Revision 302 (12/08)

Fuel Assemblies (Cont'd)

→(EC-9533, R302)

NGF

Clad thickness, (nominal), in.	0.025	0.0225
Diametral gap, (cold, nominal), in.	0.007	0.0065
Active length, in.	150	
→(DRN 02-1477, R12; 04-502, R13)		
Plenum length, in.	8.888 (Batch T) 9.138 (Batches U&W)	10.013
→(DRN 06-992, R15)		
Uranium weight (nominal) grams	1830	1825
←(DRN 04-502, R13; 06-992, R15; EC-9533, R302)		

Control Element (CEA)

←(DRN 02-1477, R12)

→(DRN 01-1103, R12)

Number	87
Absorber elements, No. per assy.	5
Type	Cylindrical rods
Clad material	Inconel 625
Clad thickness, in.	0.035
Clad OD, in.	0.816
Diametral gap, in.	0.009
Outside elements	
Poison material	B ₄ C/Ag-In-CD
Poison length, in.	135.5/12.5
B ₄ C Pellet	
Diameter, in.	0.737
Density, % of theoretical density of 2.52 g/cm ³	73
Weight % boron, minimum	77.5

←(DRN 01-1103, R12)

TABLE 4.2-1 (Sheet 4 of 4)

Burnable Poison Rod

Absorber material	A1 ₂ O ₃ -B ₄ C
Pellet diameter	.307
Pellet length, min.	1.000
Pellet density, (% theoretical), min.	93
Theoretical density, A1 ₂ O ₃ , g/cm ³	3.94
Theoretical density, B ₄ C, g/cm ³	2.52
Clad material	Zircaloy-4
Clad ID, in.	0.332
Clad OD, in.	0.382
Clad thickness, (nominal), in.	0.025
Diametral gap, (cold, nominal), in.	.025
Active length, in.	136.0
Plenum length, in.	11.090

TABLE 4.2-2

TENSILE TEST RESULTS ON IRRADIATEDSAXTON CORE III CLADDING (54)Fluence (1 MeV) 4.7×10^{21} n/cm² (estimated)

Rod	Location From Bottom	Testing Temp	0.2% Yield Stress	Ultimate Tensile Strength	Uniform Strain In 2 in. Gage Length	Total Strain In 2 in. Gage
<u>ID</u>	<u>(in.)</u>	<u>(F)</u>	<u>(psi x 103)</u>	<u>(psi x 103)</u>	<u>(%)</u>	<u>Length</u>
BO	11-17	650	61.4	65.6	2.2	6.8
BO	26-32	650	58.1	68.9	2.4	11.3
RD	3-9	650	62.2	70.0	2.0	4.2
RD	12-18	650	60.5	65.4	1.7	5.8
MQ	12-18	675	70.4	77.4	1.9	6.1
MQ	28-34	675	66.0	75.1	1.6	6.2
FS	28-34	675	57.2	71.4	3.9	12.9
GL	12-18	675	60.5	71.5	2.4	9.3